

INVERSE PROBLEM FOR STRESS IN THE EARTH  
BASED ON GEODETIC DATA

BY

KEIICHIRO IKEDA

//

B.S. University of Tokyo (1974)

M. Eng. University of Tokyo (1976)

M.S. Massachusetts Institute of Technology (1980)

SUBMITTED IN PARTIAL FULFILLMENT  
OF THE REQUIREMENTS OF  
THE DEGREE OF DOCTOR OF PHILOSOPHY

AT THE

MASSACHUSETTS INSTITUTE OF TECHNOLOGY

June 1981

© Massachusetts Institute of Technology

---

Signature of Author: Department of Earth & Planetary  
Sciences  
June 16, 1981

---

Certified by: Keiiti Aki  
Thesis Supervisor

---

Accepted by: Theodore R. Madden  
Chairman, Departmental Graduate  
Committee

ARCHIVES  
MASSACHUSETTS INSTITUTE  
OF TECHNOLOGY

AUG 26 1981

LIBRARIES

## INVERSE PROBLEM FOR STRESS IN THE EARTH

BASED ON GEODETIC DATA

by

KEIICHIRO IKEDA

Submitted to the  
Department of Earth and Planetary Sciences  
on June 15, 1981, in partial fulfillment of the  
requirements for the degree of  
Doctor of Philosophy

## ABSTRACT

Mathematical formulations for an elastostatic inverse problem to determine incremental stresses in the earth were recognized as a Cauchy problem for elliptic equations and the uniqueness and stability of solutions were investigated. A general approach for this inverse problem is (1) to define a body (domain) under the earth beneath an area over which displacements are known, (2) to apply eigenfunction expansions to operators, (3) to reduce the problem to ordinary differential equations, and (4) to convert two point boundary value problems into initial value problems as is done in a shooting method for ordinary differential equations. The necessary initial values, i.e. the Cauchy data are obtained from stress free conditions at the surface and displacements measured on the surface by means geodimeter networks and levelling surveys.

The solution for the two-dimensional elastostatic inverse problem is obtained by expanding Airy's stress function into polynomials along a horizontal axis and by imposing stress free conditions to determine coefficients of the reduced system of linear equations. Remaining coefficients are determined by matching the displacements expanded into polynomials on the surface with an integrated form of the stress function. For the three dimensional inverse elastostatic problem the solution is obtained via the Galerkin vector instead of Airy's stress function. By expanding the Galerkin vector into polynomials, we obtain a system of linear equations, which can be solved by imposing stress free conditions and known displacements on the surface.

The uniqueness of these solutions within a domain in which we seek solutions is assured by repeated applications of the Cauchy-Kowalewsky theorem which states that analytic Cauchy data can be continued locally into the domain. The stability of solutions depend on the horizontal wave number exponentially and therefore become unstable unless data with short wavelengths decrease exponentially with the wave number.

In the case of elastostatic inverse problems this condition is always satisfied due to the elliptic nature of the Navier's equation which governs the problem. Therefore, if data are due to a source located outside the domain in which we seek the solution, the solution is stable.

A numerical solution for the three dimensional elastostatic inverse problem is also obtained by discretizing a variational form of Navier's equation using the finite element method. The resultant linear matrix equation is then re-assembled to impose the stress free conditions and displacements on the surface nodes. Even though the original matrix is positive definite and thus well conditioned, the resultant matrix for the inverse problem is very ill-conditioned and thus special care is taken about the mesh configurations to obtain an appropriate solution. These two methods of inversion are tested by using artificial data generated by a buried point force and a buried strip of dislocation. The distribution of errors as a function of depths of sources show that if the source is deep or is distributed over broad areas as in the case of the strip of dislocation, the analytic method of inversion gives superior results than the finite element inversion. Considering that it is in principle easier in the finite element method to improve the order of accuracy than in the analytic method, it is recommended that these two methods should be used to complement each other. Large-scale smoother variation can be handled effectively by the analytic method while detailed analysis of localized stress field can be done by the finite element method.

The analytic method of inversion is then applied to the geodetic data obtained in southern California where anomalous uplift called Palmdale bulge has been observed between 1959 to 1974 along the San Andreas fault. Results of inversion for stress show that the principal stresses at 10km depth have significantly different patterns from the horizontal stresses obtained at the surface. At the surface the principal stresses are the nearly N-S horizontal compression of 3.5 to 4.5 bar, the nearly E-W horizontal compression of 0.0 to 0.1 bar and vertical stress of zero magnitude. At 10km depth the nearly N-S compression reaches to 12 bars and the nearly E-W compression reaches to 6 bars under the central region of the Palmdale Bulge. Thus the incremental shear stress along the fault at 10km depth near Palmdale is only slightly greater than at the surface, but the incremental normal compressional stress increases with depth considerably, suggesting a locking mechanism on the San Andreas fault during the period of Palmdale uplift. This result is consistent with the swarm of microearthquakes which occurred in this area during 1977 to 1978 after the uplift stopped and then turned to downwarp. It is shown that while our method of inversion is quite useful in earthquake prediction researches, currently obtainable geodetic data are not satisfactory for our inversion scheme.

We need a matched data on vertical and horizontal components of displacement vector at the same points, but the current geodetic measurements are independent and unmatched between the vertical and horizontal components. The use of new methods based on space technology such as VLBI, ARIES and GPS which enable matched 3-component measurements at all points is required for an adequate application of our inversion method to the determination of the incremental stress in the Earth.

Thesis Supervisor: Dr. Keiiti Aki

Title: Professor of Geophysics

## Acknowledgement

I would like to express my deepest gratitude to Professor Keiiti Aki for his continuous guidance, encouragement, and support throughout my stay at M.I.T. It has been a great experience for me to have him as my advisor.

I also would like to thank Ms. Dorothy Frank for her beautiful typing work and Ms. Judy Roos for her assistance in preparing the manuscript.

Finally I would like to thank my family, Ayako and Issey, for their continuous assistance and sacrifices they have made in the last stage of preparing this thesis.

This research was supported by U.S. Geological Surveys under contract number 14-08-0001-18205.

## Table of Contents

	Page
Abstract.....	2
Acknowledgement.....	5
Chapter 1. Introduction.....	7
Chapter 2. Cauchy's problem for the Laplace equation.....	13
2.1 Ill-posed problems.....	13
2.2 Methods for inverse problems.....	16
2.3 Eigenfunction expansion method.....	18
Chapter 3. Inverse elastostatic problem.....	26
3.1 Inverse elastostatic problem.....	26
3.2 Inverse elastostatic problem in two dimensions.....	27
3.3 Inverse elastostatic problem in three dimensions...	35
3.4 Inversion by finite element method.....	73
Chapter 4. Error analysis.....	86
4.1 Exactness and uniqueness of solutions.....	86
4.2 Geodetic network.....	87
4.3 Testing with artificial data.....	90
4.4 Theoretical error estimate.....	94
Chapter 5. Palmdale uplift.....	113
5.1 Geodetic data.....	113
5.2 Inversion.....	115
5.3 Error estimate in the Palmdale network.....	118
Chapter 6. Conclusion.....	161
References.....	165

## CHAPTER 1. INTRODUCTION

In order to put the earthquake prediction research on a firm ground of quantitative science it is necessary to obtain a precise knowledge of the state of stress in the earth in a seismically active region because the stress is believed to be the cause of an earthquake, and all precursors will depend on the stress. Reflecting the importance of this subject, many studies have been done to infer the state of stress in the earth. Laboratory studies suggest high shear stress up to 2kb along the San Andreas fault (Stesky and Brace, 1973, Stesky, 1975), while heat flow studies give low upper limit around 250 bar for possible shear stress there (Brune et al., 1969, Lachenbruch and Sass, 1973). This low shear stress is consistent with the value suggested from the studies of driving force for plate tectonics (Forsyth and Uyeda, 1975, Richardson and Solomon, 1977, Richardson, 1978), and seismic studies on stress drop (Aki, 1966, Wyss, 1970, Wyss and Molnar, 1972), although recent discussion on plate tectonics and earthquake stress-drop (Hanks, 1977) suggests high shear stress of the order of a kilobar.

The lack of agreements among these studies show a fundamental difficulty to know the state of stress in the lithosphere precisely. On the other hand the stress increment in the earth may be easier to estimate than the absolute stress since the incremental stress changes are directly related to the incremental changes of displacements which can be measured by repeated geodetic measurements on the surface of the earth.

If we can determine the incremental stress in the earth, we may be able to understand various earthquake precursors that are supposedly caused by the stress increase. Sassa and Nishimura (1956) reported rapid tilt changes in which so-called S-shaped changes in the tilt-vector diagram were observed to occur a few hours prior to the Nanki earthquake of 1950. The magnitude of tilt was of the order of 0.1" at a distance of 100 km from the epicenter. They observed similar tilt changes prior to some other earthquakes. Tilt changes before earthquake have been widely reported. Alewine and Heaton (1973) reported rapid tilt changes before Pt. Mugu earthquake of 1973 and similar changes were reported before Hai-Cheng earthquake of 1975. Even though they do not give systematic variations that allow quantitative analysis, tilt vectors are considered to be very effective precursors because of its simplicity of obtaining measurements continuously in comparison with other measurement such as levellings and triangulations. There have been many precursory anomalous changes in land level such as reported for the Niigata earthquake of 1964 (Danbara, 1973). Castle et al., (1974) studied levelling data near San Fernando and found that anomalous level changes with the maximum value of 200 mm had taken place in a few years preceding the San Fernando earthquake of 1971. An aseismic creep along the fault at depth or a dilatancy was considered as causing these land deformations prior to the occurrence of this earthquake (Wyss, 1977, Thatcher, 1976). These land deformations are believed to be one of the most promising precursors for earthquakes



because they have been frequently observed prior to many shallow earthquakes such as near Izu-Oshima island earthquake of 1978 (Tsumura, 1976, Rikitake, 1979) and Hai-Cheng earthquake of 1975 (Raleigh et al., 1977).

The determination of incremental stress in the earth may throw a new light on the reality of other precursors such as changes in  $V_p/V_s$ , resistivity and geomagnetic field that were once considered very promising precursors, in view of the dilatancy-diffusion hypothesis (Nur, 1969). Semenov's (1969) observation that the ratios of travel times of P and S waves significantly varied prior to earthquakes in the Garm region, USSR has been followed by both verifications and contradictions. For example Whitcomb et al. (1973) reported 10% change in  $V_p/V_s$  over the three years prior to the San Fernando earthquake of 1971 and Stewart (1973) showed a  $V_p$  decrease by 20% prior to the Pt. Mugu earthquake of 1973 while no change in  $V_p/V_s$  was observed in the Bear Valley earthquake of 1972 (Bakun et al., 1973). Bakun et al. attributed their negative results to the stress level at shallow depths which might be too low for dilatancy to take place. The laboratory experiments showed that the stress needed to produce the observed large  $V_p/V_s$  anomaly was much greater than the stress level expected in the Bear Valley (Hadley, 1975). The above discrepancies suggest that the effective prediction based on the  $V_p/V_s$  anomaly may require an identification of the region of high stress concentration.

Electrical resistivity change up to 24% was observed two months before the Bear Valley earthquake of 1972 by Mazzella and Morrison (1974). Laboratory experiments showed dramatic changes in the electrical properties of rock prior to failure (Brace and Orange, 1968) in agreement with some field observations. On the other hand, a theoretical study of resistivity change based on a model of strike slip fault showed that the observed resistivity changes were several orders of magnitude larger than predicted for the expected stress change.

The geomagnetic change due to the piezomagnetic property of rock under incremental stress is known to be very effective as a precursor as well as an indirect way to estimate the incremental stress at depth. Theoretical studies show, assuming optimal material constants, that is, highest possible magnetization and highest possible stress sensitivity, the stress change caused by slip on a fault at shallow depth is sufficient to produce observable geomagnetic field change on the surface (Johnston, 1978, Johnston et al., 1979).

Some of the discrepancies between the laboratory results on stress-induced precursors and actual phenomena observed in the field may be attributed to the scale effect of specimen as well as our uncertainty about the state of incremental stress at depth. The purpose of this thesis is to investigate the incremental stresses in the earth as an inverse problem in elasticity and to develop an inversion

method which uses geodetic data (three-component displacement vector) obtained on the earth's surface to obtain the distribution of incremental stresses at depths in the seismically active region.

In the above inverse problem, we want to calculate the stress and displacement inside the earth without specifying anything on the internal boundary inside the earth. The only boundary conditions available to us are displacements and free surface conditions on the surface boundary. Since a problem in elasticity is reduced to a system of elliptic equations in static case (Fung, 1965, Sokolnikoff, 1956), mathematically our inverse problem is equivalent to so-called Cauchy's problem for elliptic equations which is known to result generally in unstable solutions unless special conditions are met (Morse and Feshbach, 1953, Garabedian, 1968, Lieberstein, 1972).

In subsequent chapters we shall study theoretical aspects of the above inverse problem. We start with the simplest problem of all, i.e. Cauchy's problem for the Laplace equation and then proceed to two and three dimensional elastostatic inverse problems, for which we obtain exact solutions based on a simultaneous use of an eigenfunction expansion method and a shooting method. We shall compare the method with a numerical technique based on a finite element method which is more flexible but costly for a given accuracy. Finally, we shall apply the inversion method to southern California where an anomalous uplift known as the Palmdale bulge was discovered

over a large area along the San Andreas fault in 1975 and extensive geodetic measurements have been conducted since then. The resultant three-dimensional distribution of incremental stress at depths is considerably different from the horizontal stress determined from the horizontal displacement at the surface and shows an interesting systematic variation in relation to the Palmdale bulge.

## CHAPTER 2. CAUCHY'S PROBLEM FOR THE LAPLACE EQUATION

2.1 Ill-posed Problems

Since a problem in elasticity can be reduced to a problem of a system of elliptic equations in a static case (Fung, 1965, Sokolinikoff, 1956), we can obtain many basic properties of a solution for the problem in elasticity by studying the Laplace equation with appropriate boundary conditions. Therefore to study an inverse boundary value problem in elasticity, we shall start with the study of the Laplace equation with Cauchy's boundary condition, i.e. Dirichlet's condition and Neumann's condition specified on a part of the boundary simultaneously.

Hadamard showed in his famous treatise on hyperbolic partial differential equations that Cauchy's problem for the Laplace equation is ill-posed because the solution does not depend on data continuously (Hadamard, 1953). His example was the Laplace equation

$$\frac{\partial^2 \phi}{\partial x^2} + \frac{\partial^2 \phi}{\partial y^2} = 0 \quad (1)$$

with boundary conditions at  $y=0$  as

$$\phi|_{y=0} = 0 \quad (2)$$

$$\frac{\partial \phi}{\partial y}|_{y=0} = \frac{1}{n} \sin nx \quad (3)$$

The coordinate system is shown in Fig. 1.

The solution of this problem is given by

$$\phi = \frac{1}{n^2} \sin nx \sinh ny. \quad (4)$$

Since this solution becomes infinitely large if we make  $n$  infinitely large while the boundary value becomes infinitely close to zero, it does not depend on the boundary data continuously and therefore the problem is ill-posed.

Though the problem is ill-posed, the uniqueness of the solution i.e. eq. (4) can be shown by the Cauchy-Kowalewsky theorem which states that a system of partial differential equations with analytic coefficients has at most one solution in the neighborhood of non-characteristic boundaries if the Cauchy data specified on this boundary are analytic. Although this theorem uses a method of majorants to prove the existence of solutions and therefore is very complicated (Treves, 1975, Courant and Hilbert, 1963), we do not have to use the method of majorants because all that we need to prove here is the uniqueness of solution.

By expanding  $\phi$  in the neighborhood of a line  $y=0$  with a Taylor series, we have

$$\phi(x, \Delta y) = \phi(x, 0) + \frac{\partial \phi(x, 0)}{\partial y} \Delta y + \frac{\partial^2 \phi(x, 0)}{2 \partial y^2} \Delta y^2 + \dots \quad (5)$$

where  $\Delta y$  denotes a small increment in  $y$  direction. Since we have first two terms in R.H.S. of eq. (5) as boundary conditions, i.e.

$$\phi|_{y=0} = 0 \quad (6)$$

$$\frac{\partial \phi}{\partial y}|_{y=0} = \frac{1}{n} \sin nx \quad (7)$$

we can determine remaining terms from the Laplace equation.

That is,

$$\frac{\partial^2 \phi}{\partial y^2} = - \frac{\partial^2 \phi}{\partial x^2} \quad (8)$$

$$\frac{\partial^3 \phi}{\partial y^3} = \frac{\partial}{\partial y} \left( - \frac{\partial^2 \phi}{\partial x^2} \right) = - \frac{\partial^2}{\partial x^2} \left( \frac{\partial \phi}{\partial y} \right) \quad (9)$$

$$\frac{\partial^4 \phi}{\partial y^4} = \frac{\partial}{\partial y} \left( \frac{\partial^3 \phi}{\partial y^3} \right) = \frac{\partial}{\partial y} \left( - \frac{\partial^2}{\partial x^2} \left( \frac{\partial \phi}{\partial y} \right) \right) = - \frac{\partial^2}{\partial x^2} \left( \frac{\partial^2 \phi}{\partial y^2} \right), \text{ etc.} \quad (10)$$

It is apparent that if we have vanishing Cauchy's boundary conditions, i.e.

$$\phi|_{y=0} = 0 \quad (11)$$

$$\frac{\partial \phi}{\partial y}|_{y=0} = 0 \quad (12)$$

all terms in R.H.S. of eq. (5) also vanish. By repeating this procedure from  $k\Delta y$  to  $(k+1)\Delta y$ , the uniqueness of the solution in the whole domain can be proved by a mathematical induction.

The above example of the Cauchy problem for the Laplace equation shows that while the solution is unique

mathematically, in practice we cannot avoid the possibility of a highly oscillating solution because of the error in the boundary data (Atkinson, 1978). On the other hand if we know beforehand that the solution should be fairly smooth and that there is no highly oscillating solutions, we can obtain the solution in a unique manner. This situation is similar to a discrete inverse problem in which one is often forced to use a damped least squares method (Levenberg, 1944) or a stochastic inverse (Franklin, 1970) to eliminate unwanted oscillations due to small eigenvalues of matrices governing the corresponding forward problem.

## 2.2 Methods for Inverse Problems

There have been many methods presented for solving the Cauchy problem for elliptic equations both analytically and numerically. Garabedian (1960) showed that the problem can be solved by introducing auxiliary complex variables and then continuing boundary conditions into a complex domain in which the elliptic equation is converted to a hyperbolic equation. Garabedian and Lieberstein (1958) used a finite difference analogue of this technique to solve an inverse problem relating to two-dimensional detached shock waves due to a blunt bow in aerodynamics successfully. Though their method gives a very flexible and general way to solve inverse problems numerically, a computational labour may become prohibitively large in case of higher dimensional problems because that additional numbers of dimensions must be introduced to continue solutions into the complex domain. The quasi-reversibility method which was



introduced by Lattece and Lions (1969) gives another numerical method for the problem. It uses an auxiliary biharmonic term as a perturbation factor of the original equation and then solving this perturbed but now well-posed problem. The solution of the original equation can be obtained by diminishing the perturbation term and taking a limit. The difficulty associated with their method is that it does not assure an unique solution at all even in the sense discussed in the previous section. The regularization method of Tikonov (1963) gives another very general and stable method for solving the problem and it gives essentially a similar solutions to the damped least squares method (Levenberg, 1944) if it is applied to discrete problems.

Contrary to these numerical methods for the Cauchy problem for elliptic equations, analytic methods are studied only in formal ways and very little application appears in literature. Lavrentiev's (1967) work using Carlman function, which is a kind of modified Green's function, and logarithmic convexity method (Knops, 1973, Payne, 1975) are among them. Although these methods give formally acceptable solutions, we need to see more applications to find their effectiveness.

In case that the problem is governed by ordinary differential equations, there is one group of methods that provides very powerful solutions to both forward and inverse problems. They are known as shooting method and dynamic programming method. The former is a technique in which one converts a two point boundary value problem to an initial value problem and solves the problem by forward integrations

while arranging initial values to satisfy all boundary values (Keller, 1968, Meyer, 1973). The latter is a technique in which one converts a two point boundary value problem into an initial value problem governed by a set of first order partial differential equations and then solves the problem by integrating equations along characteristic lines (Bellman, 1957, Bellman and Kalaba, 1965). This method was applied to an inverse problem relating to a transport phenomena successfully and is called sometimes Bellman-Kagiwada-Kalaba method (Bellman, Kagiwada, Kalaba, 1967, Scott, 1973).

### 2.3 Eigenfunction Expansion Method

Eigenfunction expansions are commonly used when we are seeking solutions for a boundary value problem governed by partial differential equations with finite ranges of independent variable, i.e. within a finite domain, to reduce the problem to the two point boundary value problem governed by ordinary differential equations (Sommerfeld, 1949, Morse and Feshbach, 1953). Power polynomials and the Fourier series are used as eigenfunctions if the domain is rectangular or cubic while Legendre functions and Bessel functions are used for spherical and cylindrical domains respectively. The counterpart of the above method is, of course, integral transform methods for infinite domains. The Fourier transform and the Hankel transform are commonly used methods for the infinite domain with rectangular and cylindrical coordinates respectively.

Since these eigenfunction expansions of partial differential equations leave us with two point boundary value problems, we have usually two options to choose to solve the forward problem, i.e. option (1) solve the resultant two point boundary value problem directly, or option (2) solve the resultant two point boundary value problem by shooting method, i.e. by converting it to the initial value problem and then arranging the initial value to satisfy all boundary conditions. If the two point boundary value problem is linear, these two choices are merely matter of taste and they give identical answers. If the two point boundary value problem is non-linear, however, the choice between option (1) and option (2) must be made while considering a stability and complexity of solution procedures because we usually are forced to resort to a numerical technique to solve the problem. In most cases the option (2) is preferable and gives stable solutions (Collatz, 1966, Meyer, 1973).

If we are dealing with an inverse boundary value problem, we do not have any choice but to choose option (2) because all that we have are initial values on a part of the boundary and we do not have any conditions to specify boundary values in remaining part of the boundary. The main difference between the forward problem and the inverse problem in choosing option (2) is that while the initial values are tentative and must be arranged to satisfy all boundary conditions in the former, the initial values are a part of the problem and

determined initially and therefore they do not have to be varied to satisfy boundary conditions in the latter. Since solutions obtained by these two methods coincide with each other when the problem is linear, it is concluded that we can obtain exact solutions for the inverse problem by using option (2) if we have initial values that are given as a consequence of the forward problem. We shall show this by using the Cauchy problem for the Laplace equation as an example.

First we set up the forward problem for the Laplace equation in a two-dimensional rectangular coordinate system as shown in Fig. 1. The equation is

$$\frac{\partial^2 \phi}{\partial x^2} + \frac{\partial^2 \phi}{\partial y^2} = 0 \quad (13)$$

with boundary conditions as

$$\phi|_{y=b} = f(x) \quad (14)$$

$$\frac{\partial \phi}{\partial y}|_{y=0} = 0. \quad (15)$$

The solution is obtained by expanding the equation into a Fourier series. That is

$$\phi = \sum_{m=1}^{\infty} \frac{\cosh \lambda y}{\cosh \lambda b} (A_m \sin \lambda x + B_m \cos \lambda x) \quad (16)$$

where  $\lambda$ ,  $A_m$ ,  $B_m$  are

$$\lambda = \frac{2m\pi}{a} \quad (17)$$

$$A_m = \frac{1}{2a} \int_0^a f(x) \sin \lambda x \, dx \quad (18)$$

$$B_m = \frac{1}{2a} \int_0^a f(x) \cos \lambda x \, dx. \quad (19)$$

At  $y=0$  the solution becomes

$$\phi|_{y=0} = \sum_{m=1}^{\infty} \frac{1}{\cosh \lambda b} [A_m \sin \lambda x + B_m \cos \lambda x], \quad (20)$$

which shows that if  $f(x)$  is a well-behaved function, say in  $L^2$  class, the solution of the Laplace equation at  $y=0$  is exponentially decaying as a function of  $\lambda$ .

The inverse problem is set up as the Cauchy problem for the Laplace equation in the same coordinate system as before. That is

$$\frac{\partial^2 \phi}{\partial x^2} + \frac{\partial^2 \phi}{\partial y^2} = 0 \quad (21)$$

with boundary conditions as

$$\phi|_{y=0} = g(x) \quad (22)$$

$$\frac{\partial \phi}{\partial y}|_{y=0} = 0. \quad (23)$$

By using Fourier series expansion, we obtain the solution as

$$\phi = \sum_{m=0}^{\infty} \cosh \lambda y (C_m \sin \lambda x + D_m \cos \lambda x) \quad (24)$$

where  $C_m, D_m$  are

$$C_m = \frac{1}{2a} \int_0^a g(x) \sin \lambda x \, dx \quad (25)$$

$$D_m = \frac{1}{2a} \int_0^a g(x) \cos \lambda x \, dx. \quad (26)$$

This solution becomes highly oscillatory when  $\lambda$  becomes large unless coefficients  $C_m$  and  $D_m$  are exponentially decaying functions of  $\lambda$ . For a general setting of the Cauchy problem for the Laplace equation with arbitrary initial values, this is a very restrictive condition and makes the whole problem impractical. For the inverse problem, however, the initial value  $g(x)$  is always a consequence of boundary conditions on the other side of boundaries, i.e.  $f(x)$  and is given by eq. (20) which is an exponentially decaying function of  $\lambda$ .

Therefore in the case of inverse boundary value problems we can

solve the problem by expanding the equation by suitable eigenfunctions and then solving the resultant two point boundary value problem by the shooting method. Inserting (18) and (19) into (20), and replacing (22) by (20), we obtain

$$\phi = \sum_{m=0}^{\infty} \frac{\cosh \lambda y}{\cosh \lambda b} (C_m^* \sin \lambda x + D_m^* \cos \lambda x) \quad (27)$$

where  $C_m^*$  and  $D_m^*$  are

$$C_m^* = \frac{A_m}{4a^2} \frac{a}{\int_0^a f(x) \sin \lambda x \, dx} \frac{a}{\int_0^a \sin^2 \lambda x \, dx} \quad (28)$$

$$D_m^* = \frac{B_m}{4a^2} \frac{a}{\int_0^a f(x) \cos \lambda x \, dx} \frac{a}{\int_0^a \cos^2 \lambda x \, dx} \quad (29)$$

which gives a stable and well-defined solution for our inverse problem.

Figure Captions for Chapter 2

Fig. 1. Coordinate system used for the Laplace equation.



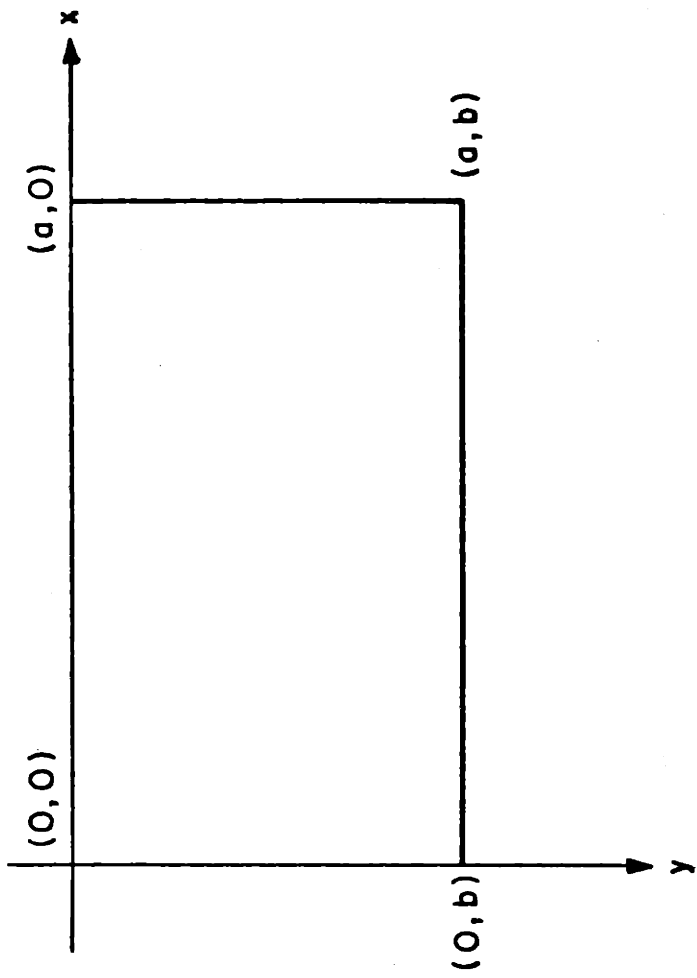


FIG. 1

## CHAPTER 3. INVERSE ELASTOSTATIC PROBLEM

3.1 Inverse Elastostatic Problem

Our inverse elastostatic problem, is to find a solution in a domain  $B$  when displacement (Dirichlet's boundary condition), and traction (Neumann's boundary condition), are both given only on  $\partial B^*$  which is a part of the boundary  $\partial B$  but no condition is given on the remaining part of the boundary, i.e.  $\partial B - \partial B^*$ . This problem is a natural extension of the Cauchy problem for the Laplace equation studied in the preceding chapter and the only difference is that we have to deal with a system of elliptic equations in elastostatic inverse problems.

Comparing with the amount of works relating to inverse problems for the Laplace equation, the inverse elastostatic problem has been studied very little. Most of works seen in literature are on earthquake problems and are concerned with surface deformations associated with a dislocation source. The inversion for displacement due to a dislocation source and associated stress change in the earth based on surface displacement using two-dimensional finite element method (McCowan et al., 1977, Jungles and Frazier, 1973), three-dimensional dislocation source using the generalized inverse method (Alewine and Jordan 1973, Matsu'ura 1977), visco-elastic two-dimensional finite element model inversion with generalized inverse method (Smith, 1974) are among them. Although these works gave more or less acceptable state of stress associated with observed surface displacement on the earth, they have a shortcoming in common. These

methods are highly model dependent and solutions are variable with respect to small change of model parameters, especially the geometry and configuration of dislocation sources. Our inverse method is an attempt to remedy this shortcoming by less restrictive assumptions about the source that generated surface displacements. In the following sections we only assume that the source is located outside the domain in which we seek a solution and we make no assumption about the nature of the source, i.e. it can be a dilatancy source, a dislocation source, an explosive source, or anything else as long as they are located outside.

As is mentioned before our inverse problem is Cauchy's problem for a system of elliptic equations, and therefore the same general line of attacking the problem as used for the Laplace equation, i.e. eigenfunction expansion - shooting method technique can be used. This method is in a sense similar to well-known semi-inverse method of Saint Venant in which one starts with a trial solution which satisfies a part of the boundary condition and then modify it to satisfy remaining boundary conditions (Fung, 1965). Our trial solution is provided by the eigenfunction expansion.

### 3.2 Inverse Elastostatic Problem in Two Dimensions

It is well-known that in two-dimensional elasticity, Airy's stress function simplifies the problem considerably and one has to only solve one biharmonic equation (Fung, 1965, Timoshenko and Goodier, 1951, Sokolinikof 1956).

Denoting Airy's stress function by  $\phi$ , we have

$$\nabla^4 \phi = 0 \quad (30)$$

where  $\nabla^4$  denotes a biharmonic operator. Stress components are expressed as

$$\sigma_{xx} = \frac{\partial^2 \phi}{\partial y^2} \quad (31)$$

$$\sigma_{yy} = \frac{\partial^2 \phi}{\partial x^2} \quad (32)$$

$$\sigma_{xy} = - \frac{\partial^2 \phi}{\partial x \partial y} \quad (33)$$

where  $\sigma_{xx}$ ,  $\sigma_{yy}$ ,  $\sigma_{xy}$  are components of a stress tensor. We shall start with the simplest inverse problem which has a configuration of domain and boundary conditions as shown in Fig. 2. This configuration will be used for all two-dimensional problems in this chapter. We have boundary conditions at  $y=0$  as

$$u = x \quad (34)$$

$$v = \nu \quad (35)$$

$$\sigma_{yy} = 0 \quad (36)$$

$$\sigma_{xy} = 0 \quad (37)$$

where  $u$ ,  $v$ , are  $x, y$  components of displacement,  $\nu$  is Poisson's ratio and  $\sigma_{xx}$ ,  $\sigma_{xy}$  are components of stress tensor. In a geodetic inverse problem these boundary

conditions correspond to the case in which we have uniform vertical displacements and lateral extensions on the surface of the earth.

We shall expand Airy's stress function  $\phi$  into a second order polynomial that is

$$\phi = Ax^2 + Bxy + Cy^2 \quad (38)$$

where A,B,C, are constants. Substituting this into eq. (31) through (33) we have

$$\sigma_{xy} = -B \quad (39)$$

$$\sigma_{yy} = 2A \quad (40)$$

$$\sigma_{xx} = 2C. \quad (41)$$

Using stress boundary condition i.e. eq. (36) and eq. (37), we determine these coefficients as

$$A = 0 \quad (42)$$

$$B = 0. \quad (43)$$

Thus Airy's stress function becomes

$$\phi = Cy^2. \quad (44)$$

To obtain displacements we have to integrate stress components using formulas as

$$u = \int \epsilon_{xx} dx = \frac{1}{E} \int (\sigma_{xx} - \nu \sigma_{yy}) dx \quad (45)$$

$$v = \int \epsilon_{yy} dy = \frac{1}{E} \int (\sigma_{yy} - \nu \sigma_{xx}) dy \quad (46)$$

where  $\sigma_{xx}$ ,  $\sigma_{yy}$  are components of a strain tensor and E is Young's modulus. Performing integrations we have

$$u = \frac{2C}{E} x + f(y) \quad (47)$$

$$v = -\frac{2\nu}{E} y + g(x) \quad (48)$$

where  $f(y)$  and  $g(x)$  are a function that only depends on  $y$  or  $x$  respectively. Noting that  $\sigma_{xy}$  vanishes on the boundary i.e. at  $y = 0$ , we have

$$\frac{df}{dy} + \frac{dg}{dx} = 0 \quad (49)$$

at  $y=0$ . Since  $f(y)$  and  $g(x)$  should be at most first order, we have

$$f(y) = Dy + F \quad (50)$$

$$g(x) = Gx + H \quad (51)$$

$$D + G = 0 \quad (52)$$

where  $D, F, G, H$  are constants. We obtain equations to be solved for coefficients  $C, D, F, G, H$ , as

$$u = \frac{2C}{E}x + Dy + F \quad (53)$$

$$v = -\frac{2\nu C}{E}y + Gx + H \quad (54)$$

$$D + G = 0. \quad (55)$$

Applying displacements boundary conditions at  $y = 0$ , i.e. eq. (34) and eq. (35), these coefficients are determined as

$$C = \frac{E}{2} \quad (56)$$

$$F = 0 \quad (57)$$

$$G = 0 \quad (58)$$

$$H = \nu \quad (59)$$

$$D = 0. \quad (60)$$

Solutions for the inverse problem are,

$$u = x \quad (61)$$

$$v = \nu(1-y) \quad (62)$$

$$\sigma_{xx} = E \quad (63)$$

$$\sigma_{xy} = 0 \quad (64)$$

$$\sigma_{yy} = 0 \quad (65)$$

Thus we obtained an expected result that shows a pure tension in the x direction in the domain under the surface. The above simplest case illustrates the essence of our method of the eigenfunction expansion and the shooting to satisfy the boundary conditions.

If data on the surface are given by not only linear terms but also quadratic terms in x we should expand Airy's stress function into a polynomial of the third order, that is

$$\phi = Ax^3 + Bx^2y + Cxy^2 + Dy^3 \quad (66)$$

Substituting this into eq. (31) through (33), we have

$$\sigma_{xx} = 2cx + 6Dy \quad (67)$$

$$\sigma_{yy} = 6Ax + 2By \quad (68)$$

$$\sigma_{xy} = -2Bx - 2Cy. \quad (69)$$

Using the stress free condition at  $y=0$ , we have

$$B = 0 \quad (70)$$

$$A = 0. \quad (71)$$

Displacement components can be obtained by integrations as before. They are

$$u = \frac{1}{E} (Cx^2 + 6Dxy) + f(y) \quad (72)$$

$$v = -\frac{\nu}{E} (2Cxy + 3Dy^2) + g(x) \quad (73)$$



$f(y)$  and  $g(x)$  can be determined by using the relation

$$\sigma_{xy} = \mu \left( \frac{\partial v}{\partial x} + \frac{\partial u}{\partial y} \right) \quad (74)$$

where  $\mu$  is a rigidity. This gives an equation

$$-\frac{2\nu}{E} Cy + \frac{dg}{dx} + \frac{6}{E} D + \frac{df}{dy} = -\frac{4(1+\nu)}{E} Cy. \quad (75)$$

Remembering  $g$  and  $f$  are functions only depending on  $x$  and  $y$  respectively, we have

$$\frac{dg}{dx} = -\frac{6D}{E} \quad (76)$$

$$\frac{df}{dy} = -\frac{2(\nu-2)C}{E} y. \quad (77)$$

Assuming  $g$  and  $f$  to be at most second order integrations of these equations give  $g$  and  $f$  as

$$g(x) = -\frac{3D}{E} x^2 + F \quad (78)$$

$$f(y) = -\frac{(2-\nu)C}{E} y^2 + G. \quad (79)$$

Therefore displacements are

$$u = \frac{1}{E} [Cx^2 + 6Dxy + (2-\nu)Cy^2] + G \quad (80)$$

$$v = -\frac{1}{E} [3Dy^2 + 2Cxy + 3Dx^2] + F \quad (81)$$

at  $y = 0$  these displacements turn to be

$$u = \frac{C}{E} x^2 + G \quad (82)$$

$$v = -\frac{3D}{E} x^2 + F \quad (83)$$

if we have displacement boundary conditions at  $y = 0$  as

$$u = ax^2 \quad (84)$$

$$v = bx^2 \quad (85)$$

we can determine coefficients  $C, D, E, G$  by solving eq. (82) to eq. (85). They are

$$C = Ea \quad (86)$$

$$G = 0 \quad (87)$$

$$D = -\frac{Eb}{3} \quad (88)$$

$$F = 0. \quad (89)$$

Thus solutions for our problem are

$$\sigma_{xx} = 2E(ax-by) \quad (90)$$

$$\sigma_{yy} = 0 \quad (91)$$

$$\sigma_{xy} = -2Eay \quad (92)$$

$$u = ax^2 - 2bxy - (v+2)ay^2 \quad (93)$$

$$v = bx^2 - 2axy + by^2. \quad (94)$$

If we superpose these solutions with solutions obtained in the preceding example, we obtain a complete solution for the inverse problem in which quadratic displacement functions are given as boundary conditions on the free surface.

By using higher order polynomials we can solve an inverse problem with more complicated boundary displacements condition although algebraic operations become increasingly laborious. More general approach can be made in terms of Fourier series expansion of Airy's stress function. It is noted, however, that as long as geodetic inverse problems are concerned the power series expansion gives sufficiently accurate solutions within measurement errors because numbers of measurements of data are usually not enough for using a Fourier analysis effectively.

### 3.3 Inverse Elastostatic Problem in Three Dimensions

A three-dimensional inverse elastostatic problem can be solved by the same procedure used in the two-dimensional inverse problem, i.e. the eigenfunction expansion-shooting method technique. The only difference is that we have to use so-called Galerkin vector instead of Airy's stress function and therefore have to solve three coupled biharmonic equations. Because this process leads to very lengthy calculations, we shall deal with each of the components of

the Galerkin vector separately as far as possible. It turns out that while a complete decoupling of each component is only possible for lower order eigenfunction expansions, a decoupling between vertical and horizontal components is always possible.

Denoting the Galerkin vector and its components by  $F$  and  $\phi_1, \phi_2, \phi_3$ , respectively, they satisfy equations

$$\nabla^4 \phi_i = 0 \quad i = 1, 2, 3 \quad (95)$$

$$F = i\phi_1 + j\phi_2 + k\phi_3 \quad (96)$$

where  $\nabla^4$  denotes a biharmonic operator and  $i, j, k$  denote unit vector components. Stress and displacement components associated with this Galerkin vector are represented in terms of  $\phi_1, \phi_2, \phi_3$  as

$$\sigma_{xx} = 2(1-\nu)\frac{\partial}{\partial x}\nabla^2\phi_1 + (\nu\nabla^2\frac{\partial^2}{\partial x^2})\theta \quad (97)$$

$$\sigma_{yy} = 2(1-\nu)\frac{\partial}{\partial y}\nabla^2\phi_2 + (\nu\nabla^2\frac{\partial^2}{\partial y^2})\theta \quad (98)$$

$$\sigma_{zz} = 2(1-\nu)\frac{\partial}{\partial z}\nabla^2\phi_3 + (\nu\nabla^2\frac{\partial^2}{\partial z^2})\theta \quad (99)$$

$$\sigma_{xy} = (1-\nu)\left(\frac{\partial}{\partial x}\nabla^2\phi_2 + \frac{\partial}{\partial y}\nabla^2\phi_1\right) - \frac{\partial^2}{\partial x\partial y}\theta \quad (100)$$

$$\sigma_{xz} = (1-\nu)\left(\frac{\partial}{\partial x}\nabla^2\phi_3 + \frac{\partial}{\partial z}\nabla^2\phi_1\right) - \frac{\partial^2}{\partial x\partial z}\theta \quad (101)$$

$$\sigma_{yz} = (1-\nu)\left(\frac{\partial}{\partial y}\nabla^2\phi_3 + \frac{\partial}{\partial z}\nabla^2\phi_2\right) - \frac{\partial^2}{\partial y\partial z}\theta \quad (102)$$

$$2\mu u = 2(1-\nu)\nabla^2\phi_1 - \frac{\partial}{\partial x}\theta \quad (103)$$

$$2\mu v = 2(1-\nu)\nabla^2\phi_2 - \frac{\partial}{\partial y}\theta \quad (104)$$

$$2\mu w = 2(1-\nu)\nabla^2\phi_3 - \frac{\partial}{\partial z}\theta \quad (105)$$

$$\theta = \frac{\partial}{\partial x}\phi_1 + \frac{\partial}{\partial y}\phi_2 + \frac{\partial}{\partial z}\phi_3 \quad (106)$$

where  $\sigma_{ij}$  are components of a stress tensor,  $u, v, w$  are  $x, y, z$  components of a displacement vector, and  $\nu, \mu$  are Poisson's ratio and the rigidity respectively. The coordinate system used is shown in Fig. 3.

We shall start our eigenfunction expansion with the lowest degree polynomial, i.e. a power polynomial of second order. Using this polynomial, we have  $\phi_3$  represented as

$$\phi_3 = ax^2 + by^2 + cz^2 + dxy + exz + fyz \quad (107)$$

which clearly satisfies eq. (95). Substituting this into eq. (97) to eq. (106), we have

$$\sigma_{xx} = \sigma_{yy} = \sigma_{xz} = \sigma_{xy} = \sigma_{xz} = \sigma_{yz} = 0 \quad (108)$$

$$2\mu u = -e \quad (109)$$

$$2\mu v = -f \quad (110)$$

$$2\mu w = 4(1-\nu)(a+b+c). \quad (111)$$

Therefore this eigenfunction represents a pure rigid body motion.

If we expand  $\phi_3$  by a third order polynomial, we have

$$\phi_3 = ax^3+by^3+cz^3+dx^2y+ex^2z+fy^2x \quad (112)$$

$$+ gy^2z+hz^2x+iz^2y+jxyz$$

which satisfies eq. (95). Substituting this into eq. (97) to eq. (106), we have

$$\sigma_{xx} = 2v(3c+g)-2(1-v)e \quad (113)$$

$$\sigma_{yy} = 2v(3c+e)-2(1-v)g \quad (114)$$

$$\sigma_{xy} = -j \quad (115)$$

$$\sigma_{zz} = 2(2-v)(g+e)+6(1-v)c \quad (116)$$

$$\sigma_{xz} = 2(1-v)(3a+f)-2vh \quad (117)$$

$$\sigma_{yz} = 2(1-v)(3b+d)-2vi \quad (118)$$

$$2\mu u = -2ex-jy-2hz \quad (119)$$

$$2\mu v = -jx-2gy-2iz \quad (120)$$

$$2\mu w = \{4(1-v)(3a+f)+2(1-2v)h\}x+\{4(1-v)(3b+d) \quad (121)$$

$$+ 2(1-2v)i\}y + \{4(1-v)(e+g)+6(1-2v)c\}z.$$

Coefficients of the polynomial, i.e.  $a, b, \dots, j$  can be determined by solving eq. (116) to eq. (121) together with boundary conditions for stresses and displacements at  $z = 0$ , i.e.

$$\sigma_{zz} = \sigma_{zx} = \sigma_{zy} = 0 \quad (122)$$

$$2\mu u = 2\mu v = 0 \quad (123)$$

$$2\mu w = A_3x + B_3y \quad (124)$$

Coefficients are therefore

$$c = e = g = j = 0 \quad (125)$$

$$h = \frac{A_3}{2} \quad (126)$$

$$i = \frac{B_3}{2} \quad (127)$$

$$3a + f = \frac{A_3}{2(1-\nu)} \quad (128)$$

$$3b + d = \frac{B_3}{2(1-\nu)}. \quad (129)$$

Substituting these coefficients into eq. (97) to eq. (106) we have a solution for stresses and displacements as

$$\sigma_{xx} = \sigma_{yy} = \sigma_{zz} = \sigma_{xy} = \sigma_{xz} = \sigma_{yz} = 0 \quad (130)$$

$$2\mu u = -A_3 z \quad (131)$$

$$2\mu v = -B_3 z \quad (132)$$

$$2\mu w = A_3 x + B_3 y. \quad (133)$$

These solutions represent a rigid body rotation.

Expanding  $\phi_1$  by the third order polynomial, we have

$$\phi_1 = ax^3 + by^3 + cz^3 + dx^2y + ex^2z + fy^2x \quad (134)$$

$$+ gy^2z + hz^2x + iz^2y + jxyz.$$

Substituting this into eq. (97) to eq. (106) we have

$$\sigma_{xx} = 2(2-\nu)(f+h) + 6(1-\nu)a \quad (135)$$

$$\sigma_{yy} = \nu(6a+2h) - 2(1-\nu)f \quad (136)$$

$$\sigma_{xy} = 2(1-\nu)(3b+i) - 2\nu d \quad (137)$$

$$\sigma_{zz} = 2\nu(3a+f) - 2(1-\nu)h \quad (138)$$

$$\sigma_{xz} = 2(1-\nu)(3c+g) - 2\nu e \quad (139)$$

$$\sigma_{yz} = j \quad (140)$$



$$2\mu u = \{4(1-\nu)(f+h)+6(1-2\nu)a\}x + \{4(1-\nu)(3b+i) \quad (141)$$

$$+ 2(1-2\nu)d\}y + \{4(1-\nu)(3c+g) + 2(1-2\nu)e\}z$$

$$2\mu V = -2dx-2fy-kz \quad (142)$$

$$2\mu W = -2ex-jy-2hz. \quad (143)$$

Using boundary conditions at  $z = 0$  as

$$\sigma_{xx} = \sigma_{xz} = \sigma_{yz} = 0 \quad (144)$$

$$2\mu u = A_1 x + B_1 y \quad (145)$$

$$2\mu v = 2\mu w = 0. \quad (146)$$

We solve eq. (138) to eq. (143) to obtain coefficients as

$$d = e = f = j = 3c + g = 0 \quad (147)$$

$$3b + i = \frac{B_1}{4(1-2\nu)} \quad (148)$$

$$a = \frac{A_1}{6} \quad (149)$$

$$h = \frac{\nu A_1}{2(1-\nu)} \quad (150)$$

Solutions for stresses and displacements are

$$\sigma_{xx} = \frac{A_1}{1-\nu} \quad (151)$$

$$\sigma_{yy} = \frac{\nu A_1}{1-\nu} \quad (152)$$

$$\sigma_{xy} = \frac{B_1}{2} \quad (153)$$

$$\sigma_{zz} = \sigma_{xz} = \sigma_{yz} = 0 \quad (154)$$

$$2\mu u = A_1 x + B_1 y \quad (155)$$

$$2\mu v = 0 \quad (156)$$

$$2\mu w = -\frac{\nu A_1}{(1-\nu)} z. \quad (157)$$

Stresses and displacements corresponding  $\phi_2$  with a polynomial expansion of the third order are obtained by merely interchanging  $x$  and  $y$ . Assuming boundary condition as

$$\sigma_{xz} = \sigma_{yz} = \sigma_{xz} = 0 \quad (158)$$

$$2\mu v = A_2 x + B_2 y \quad (159)$$

$$2\mu u = 2\mu w = 0, \quad (160)$$

solutions for stresses and displacements are obtained as

$$\sigma_{xx} = \frac{\nu}{1-\nu} B_2 \quad (161)$$

$$\sigma_{yy} = \frac{B_2}{1-\nu} \quad (162)$$

$$\sigma_{xy} = \frac{A_2}{2} \quad (163)$$

$$\sigma_{zz} = \sigma_{xz} = \sigma_{yz} = 0 \quad (164)$$

$$2\mu\nu = A_2x + B_2y \quad (165)$$

$$2\mu u = 2\mu w = 0. \quad (166)$$

These solutions associated with  $\phi_1$  and  $\phi_2$  represent a plane stress condition which is obtained by conventional triangulation geodetic measurements. To obtain a state of stress which is varying along  $z$  axis, we need higher order polynomials to expand the Galerkin vector.

A fourth order polynomial expansion of  $\phi_3$  is given as

$$\phi_3 = ax^4 + by^4 + cz^4 + dx^3y + ex^3z + fy^3x \quad (167)$$

$$+ gy^3z + hz^3x + iz^3y + jx^2y^2 + kx^2z^2 + ly^2z^2$$

$$+ mx^2yz + ny^2xz + oz^2xy.$$

Substituting this into eq. (97) to eq. (106), we have

$$\sigma_{xx} = \{2v(n+3h)-6(1-v)e\}x + \{6v(g+i)-2(1-v)m\}y \quad (168)$$

$$+ \{4v(\ell+6c) - 4(1-v)k\}z$$

$$\sigma_{yy} = \{6v(e+h)-2(1-v)n\}x + \{2v(m+3i)-6(1-v)g\}y \quad (169)$$

$$+ \{4v(k+6c)-4(1-v)\ell\}z$$

$$\sigma_{xy} = -2mx-2ny-20z \quad (170)$$

$$\sigma_{zz} = \{2(2-v)(3e+n)+6(1-v)h\}x + \{2(2-v)(3g+m) \quad (171)$$

$$+ 6(1-v)i\}y + \{4(2-v)(k+\ell) + 24(1-v)c\}z$$

$$\sigma_{xz} = \{4(1-v)(6a+j) - 4vk\}x + \{6(1-v)(d+f)-2vo\}y \quad (172)$$

$$+ \{2(1-v)(3e+n) - 6vh\}z$$

$$\sigma_{yz} = \{6(1-v)(d+f)-2vo\}x + \{4(1-v)(6b+j)-4v\ell\}y \quad (173)$$

$$+ \{2(1-v)(3g+m) - 6vi\}z$$

$$2\mu u = - \{3ex^2 + ny^2 + 3hz^2 + 2mxy + 4kxz + 20yz\} \quad (174)$$

$$2\mu v = - \{mx^2 + 3gy^2 + 3iz^2 + 2nxy + 20xz + 4\ell yz\} \quad (175)$$

$$\begin{aligned}
2\mu w = & \{4(1-\nu)(6a+j) + 2(1-2\nu)k\}x^2 + \{4(1-\nu)(6b+j) \\
& + 2(1-2\nu)\ell\}y^2 + \{4(1-\nu)(k+\ell)+12(1-2\nu)c\}z^2 \\
& + \{12(1-\nu)(d+f) + 2(1-2\nu)o\}xy + \{4(1-\nu)(3e+n) \\
& + 6(1-2\nu)h\}xz + \{4(1-\nu)(3g+m) + 6(1-2\nu)i\}yz.
\end{aligned} \tag{176}$$

Since  $\phi_3$  should satisfy a biharmonic equation, i.e. eq. (95), we have an auxiliary condition as

$$3(a+b+c) + (j+k+\ell) = 0. \tag{177}$$

Assuming boundary conditions at  $z = 0$  as

$$\sigma_{zz} = \sigma_{xz} = \sigma_{yz} = 0 \tag{178}$$

$$2\mu u = A_1 x^2 + B_1 y^2 + C_1 xy \tag{179}$$

$$2\mu v = 2\mu w = 0 \tag{180}$$

we can solve eq. (171) to eq. (177) for coefficients  $a, b, \dots, o$ . They are,

$$e = g = h = i = m = n = 0 \quad (181)$$

$$6a + j = \frac{vA_3}{2(1-\nu)} \quad (182)$$

$$6b + j = \frac{vB_3}{2(1-\nu)} \quad (183)$$

$$f + d = \frac{vC_3}{6(1-\nu)} \quad (184)$$

$$c = -\frac{(2-\nu)(A_3+B_3)}{12(1-\nu)} \quad (185)$$

$$k = \frac{A_3}{2} \quad (186)$$

$$l = \frac{B_3}{2} \quad (187)$$

$$o = \frac{C_3}{2} \quad (188)$$

Solutions for stresses and displacements are, therefore,

$$\sigma_{xx} = -\frac{2}{1-\nu} (A_3 + vB_3)z \quad (189)$$

$$\sigma_{yy} = -\frac{2}{1-\nu} (vA_3 + B_3)z \quad (190)$$

$$\sigma_{xy} = -C_3z \quad (191)$$

$$\sigma_{zz} = \sigma_{zx} = \sigma_{zy} = 0 \quad (192)$$

$$2\mu u = -2A_3xz - C_3yz \quad (193)$$

$$2\mu v = -C_3xz - 2B_3yz \quad (194)$$

$$2\mu w = A_3x^2 + B_3y^2 + C_3xy + \frac{\nu}{1-\nu}(A_3+B_3)z^2. \quad (195)$$

Other components of the Galerkin vector are obtained in the same way. Expanding  $\phi_1$  by the fourth order polynomial, we have

$$\begin{aligned} \phi_1 = & ax^4 + by^4 + cz^4 + dx^3y + ex^3z + fy^3x + gy^3z \quad (196) \\ & + hz^3x + iz^3y + jx^2y^2 + kx^2z^2 + ly^2z^2 + mx^2yz \\ & + ny^2xz + oz^2xy. \end{aligned}$$

Stresses and displacements are, using eq. (97) to eq. (106),

$$\sigma_{xx} = \{4(2-\nu)Cj+k\} + 24(1-\nu)a\}x + \{2(2-\nu)(3f + o) \quad (197)$$

$$+ 6(1-\nu)d\}y + \{2(2-\nu)(3h+n) + 6(1-\nu)e\}z$$

$$\sigma_{yy} = \{4\nu(6a+k) - 4(1-\nu)j\}x + \{2\nu(3d+o) \quad (198)$$

$$- 6(1-\nu)f\}y + \{6\nu(e+h) - 2(1-\nu)n\}z$$

$$\sigma_{xy} = \{2(1-\nu)(3f+o) - 6vd\}x + \{4(1-\nu)(6b+l) \quad (199)$$

$$- 4vj\}u + \{6(1-\nu)(g+i) - 2vm\}z$$

$$\sigma_{zz} = \{4\nu(6a+j) - 4(1-\nu)k\}x + \{6\nu(d+f)-2(1-\nu)o\}y \quad (200)$$

$$+ \{2\nu(3e+n) - 6(1-\nu)h\}z$$

$$\sigma_{xz} = \{2(1-\nu)(3h+n)-6ve\}x + \{6(1-\nu)(g+i)-2vm\}y \quad (201)$$

$$+ \{4(1-\nu)(6c+l) - 4vk\}z$$

$$\sigma_{yz} = -2mx-2ny-2oz \quad (202)$$

$$2\mu u = \{4(1-\nu)(j+k) + 12a(1-\nu)\}x^2 + \{4(1-\nu)(6b+l) \quad (203)$$

$$+ 2(1-2\nu)j y^2 + \{4(1-\nu)(3f+o) + 6(1-2\nu)d\} xy$$

$$+ \{4(1-\nu)(6c+l) + 2(1-2\nu)k\}z^2 + \{4(1-\nu)(3h+n)$$

$$+ 6(1-2\nu)e\}xz + \{12(1-\nu)(i+g) + 2(1-2\nu)m\}yz$$

$$2\mu v = -(3dx^2 + 3fy^2 + 4jxy + 2mxz + 2nyz + oz^2) \quad (204)$$

$$2\mu w = -(3ex^2 + 2ny^2 + 2mxy + 4kxz + 2oyz + 3hz^2). \quad (205)$$



Assuming boundary conditions at  $z = 0$  as

$$\sigma_{zz} = \sigma_{xz} = \sigma_{yz} = 0 \quad (206)$$

$$2\mu u = A_1 x^2 + B_1 y^2 \quad (207)$$

$$2\mu v = C_2 xy \quad (208)$$

$$2\mu w = 0 \quad (209)$$

we can solve a set of linear equations, i.e. eq. (200) to eq. (205) together with the auxiliary equation, i.e. eq. (177) to obtain coefficients as

$$d = e = f = h = m = n = o = g + i = 0 \quad (210)$$

$$a = \frac{A_1 + C_2}{12} \quad (211)$$

$$j = -\frac{C_2}{4} \quad (212)$$

$$k = \frac{\nu}{4(1-\nu)} (2A_1 + C_2) \quad (213)$$

$$6b + \ell = \frac{1}{8(1-\nu)} \{2B_1 + (1-2\nu)C_2\} \quad (214)$$

$$6c + \ell = -\frac{1}{2(1-\nu)} \{4(1+\nu)A_1 + 2B_1 + (1+2\nu)C_2\} \quad (215)$$

Solutions for stresses and displacements are

$$\sigma_{xx} = \frac{1}{1-\nu} (2A_1 + \nu C_2)x \quad (216)$$

$$\sigma_{yy} = \frac{1}{1-\nu} (2\nu A_1 + C_2)x \quad (217)$$

$$\sigma_{xy} = \frac{1}{2} (2B_1 + C_2)y \quad (218)$$

$$\sigma_{xz} = -\frac{-1}{2(1-\nu)} \{4A_1 + 2(1-\nu)B_1 + (1+\nu)C_2\}z \quad (219)$$

$$\sigma_{zz} = \sigma_{yz} = 0 \quad (220)$$

$$2\mu u = A_1 x^2 + B_1 y^2 - \frac{1}{2(1-\nu)} \{2(2-\nu)A_1 + 2(1-\nu)B_1 + C_2\}z^2 \quad (221)$$

$$2\mu v = C_2 xy \quad (222)$$

$$2\mu w = \frac{-1}{1-\nu} (2A_1 + C_2)xz \quad (223)$$

Solutions for stresses and displacements based on  $\phi_2$  can be obtained by interchanging  $x$  and  $y$ . Assuming boundary conditions as

$$\sigma_{zz} = \sigma_{xz} = \sigma_{yz} = 0 \quad (224)$$

$$2\mu u = C_1 xy \quad (225)$$

$$2\mu v = A_2 x^2 + B_2 y^2 \quad (226)$$

$$2\mu w = 0, \quad (227)$$

Solutions are

$$\sigma_{xx} = \frac{1}{1-\nu} (2\nu B_2 + C_1) y \quad (228)$$

$$\sigma_{yy} = \frac{1}{1-\nu} (2B_2 + \nu C_1) y \quad (229)$$

$$\sigma_{xy} = -\frac{1}{2} (2A_2 + C_1) x \quad (230)$$

$$\sigma_{yz} = -\frac{1}{2(1-\nu)} \{4B_2 + 2(1-\nu)A_2 + (1+\nu)C_1\} z \quad (231)$$

$$\sigma_{zz} = \sigma_{xz} = 0 \quad (232)$$

$$2\mu u = C_1 xy \quad (233)$$

$$2\mu v = A_2 x^2 + B_2 y^2 - \frac{1}{2(1-\nu)} \{2(2-\nu)B_2 + 2(1-\nu)A_2 + C_1\} z \quad (234)$$

$$2\mu w = -\frac{\nu}{1-\nu} (2B_2 + C_1) yz. \quad (235)$$

By superposing these solutions based on the Galerkin vector expanded by the fourth order polynomial to solutions obtained by lower order polynomials, we can obtain stresses and displacements inside the elastic body when

displacements up to a quadratic variation are specified on the free surface boundary. Boundary conditions and solutions are as follows.

Boundary conditions at  $z = 0$ :

$$u|_{z=0} = A_1x^2 + B_1y^2 + C_1xy + D_1x + E_1y + F_1 \quad (236)$$

$$v|_{z=0} = A_2x^2 + B_2y^2 + C_2xy + D_2x + E_2y + F_2 \quad (237)$$

$$w|_{z=0} = A_3x^2 + B_3y^2 + C_3xy + D_3x + E_3y + F_3 \quad (238)$$

solutions:

$$\sigma_{xx} = \frac{2\mu}{1-\nu} \{ (2A_1 + \nu C_2)x + (2\nu B_2 + C_1)y - 2(A_3 + \nu B_3)z + D_1 + \nu E_2 \} \quad (239)$$

$$\sigma_{yy} = \frac{2\mu}{1-\nu} \{ (2\nu A_1 + C_2)x + (2B_2 + \nu C_1)y - 2(\nu A_3 + B_3)z + \nu D_1 + E_2 \} \quad (240)$$

$$\sigma_{zz} = 0 \quad (241)$$

$$\sigma_{xy} = \mu \{ (2A_2 + C_1)x + (2B_1 + C_2)y - 2C_3z + E_1 + D_2 \} \quad (242)$$

$$\sigma_{xz} = -\frac{\mu}{1-\nu} \{ 4A_1 + 2(1-\nu)B_1 + (1+\nu)C_2 \} z \quad (243)$$

$$\sigma_{yz} = -\frac{\mu}{1-\nu} \{ 4B_2 + 2(1-\nu)A_1 + (1+\nu)C_1 \} z \quad (244)$$

$$u = A_1x^2 + B_1y^2 + C_1xy + D_1x + E_1y + F_1 \quad (245)$$

$$- \frac{1}{2(1-\nu)} \{2(2-\nu)A_1 + 2(1-\nu)B_1 + C_2\}z^2 - 2A_3xz$$

$$- C_3yz - D_3z$$

$$v = A_2x^2 + B_2y^2 + C_2xy + D_2x + E_2y + F_2 - \frac{1}{2(1-\nu)} \quad (246)$$

$$\{2(1-\nu)A_2 + 2(2-\nu)B_2 + C_1\}z^2 - C_3xz - 2B_3yz - E_3z$$

$$w = A_3x^2 + B_3y^2 + C_3xy + D_3x + E_3y + F_3 + \frac{\nu}{1-\nu} (A_3 + B_3)z^2 \quad (247)$$

$$- \frac{\nu}{1-\nu} (2A_1 + C_2)xz - \frac{\nu}{1-\nu} (2B_2 + C_1)yz - \frac{\nu}{1-\nu} (D_1 + E_2)z$$

Since there are six parameters to specify the displacements on the boundary, we must have at least six data points on the boundary.

Although solutions for the inverse problem given by eq. (239) to eq. (247) are exact and thus describe a complete state of stress in certain situations i.e. when displacements vary quadratically on the boundary, they have a limitation that they present only linearly varying stress components. Thus a higher order eigenfunction expansion might be necessary for some situations. It is given by a fifth order polynomial expansion of the Galerkin vector. For  $\phi_3$  we have

$$\phi_3 = ax^5 + by^5 + cz^5 + dx^4y + ex^4z + fy^4x \quad (248)$$

$$+ gy^4z + hz^4x + iz^4y + jx^3y^2 + kx^3z^2 + ly^3x^2$$

$$+ my^3z^2 + nz^3x^2 + oz^3y^2 + px^3yz + qy^3xz$$

$$+ rz^3xy + sx^2y^2z + tx^2z^2y + \bar{u}y^2z^2x$$

where  $\bar{u}$  denotes a coefficient. Substituting this into eq. (97) to eq. (106), we have

$$\sigma_{xx} = \{v(2s+6n)-(1-v)12e\}x^2 + \{v(12g+6o)-(1-v)2s\}y^2 \quad (249)$$

$$+ \{v(6g+6r)-(1-v)6p\}xy + 2\{v(2\bar{u}+12h)-(1-v)6k\}xz$$

$$+ 2\{v(6m+12i)-(1-v)2t\}yz + 3\{v(2o+20c)-(1-v)2n\}z^2$$

$$\sigma_{yy} = \{v(12e+6n)-(1-v)2s\}x^2 + \{v(2s+6o)-(1-v)12g\}y^2 \quad (250)$$

$$+ \{v(6p+6r)-(1-v)6q\}xy + 2\{v(6k+12h)-(1-v)2u\}xz$$

$$+ 2\{v(2t+12i)-(1-v)6m\}yz + 3\{v(2n+20c)-(1-v)2o\}z^2$$

$$\sigma_{xy} = -(3px^2 + 3qy^2 + 3rz^2 + 4sxy + 4txz + 4\bar{u}yz) \quad (251)$$

$$\begin{aligned}
\sigma_{zz} = & 3\{(2-\nu)(2n+2o)+(1-\nu)20c\}z^2 + 2\{(2-\nu)(6k+2\bar{u}) \\
& + (1-\nu)12h\}zx + 2\{(2-\nu)(6m+2t)+(1-\nu)12i\}zy \\
& + \{(2-\nu)(12e+2s)+(1-\nu)6n\}x^2 + \{(2-\nu)(12g+2s) \\
& + (1-\nu)6o\}y^2 + \{(2-\nu)(6p+6q) + (1-\nu)6r\}xy
\end{aligned} \quad (252)$$

$$\begin{aligned}
\sigma_{xz} = & 3\{(1-\nu)(20a+2j)-2vk\}xz + 2\{(1-\nu)(12d+6\ell)-2vt\}xy \quad (253) \\
& + \{(1-\nu)(12f+6j)-2vu\}yz + \{(1-\nu)(6k+2\bar{u})-12vh\}z^2 \\
& + 2\{(1-\nu)(12e+2s)-6vn\}xz + \{(1-\nu)(6p+6q)-6vr\}yz
\end{aligned}$$

$$\begin{aligned}
\sigma_{yz} = & 3\{(1-\nu)(20b+2\ell)-2vm\}y^2 + \{(1-\nu)(12d+6\ell) \\
& - 2vt\}x^2 + 2\{(1-\nu)(12f+6j)-2v\bar{u}\}xy + \{(1-\nu)(6m+2t) \\
& - 12vi\}z^2 + 2\{(1-\nu)(12g+2s)-6vo\}yz + \{(1-\nu)(6p+6q) \\
& - 6vr\}xz
\end{aligned} \quad (254)$$

$$\begin{aligned}
2\mu u = & - (4ex^3+4hz^3+6kx^2z+6nz^2x+3px^2y+qy^3) \\
& + 3rz^2y+2sxy^2+rtxzy+2\bar{u}y^2z) \quad (255)
\end{aligned}$$

$$\begin{aligned}
2\mu v = & - (4gy^3+4iz^3+6my^2z+6oz^2y+px^3+3qy^2x \\
& + 3rz^2x+2sx^2y+2tx^2z+4\bar{u}xyz) \quad (256)
\end{aligned}$$

$$\begin{aligned}
2\mu w = & \{2(1-\nu)(20a+2j)+(1-2\nu)2k\}x^3 + \{2(1-\nu)(2\ell+20b) \quad (257) \\
& + (1-2\nu)2m\}y^3 + \{2(1-\nu)(12d+6\ell)+(1-2\nu)2t\}x^2y \\
& + \{2(1-\nu)(6j+12f)+(1-2\nu)2t\}y^2x + \{2(1-\nu)(2n+2o) \\
& + (1-2\nu)20c\}z^3 + \{2(1-\nu)(6k+2\bar{u}) + (1-2\nu)12h\}z^2x \\
& + \{2(1-\nu)(2t+6m) + (1-2\nu)12i\}z^2y + \{2(1-\nu)(12e+2s) \\
& + (1-2\nu)6n\}x^2z + \{2(1-\nu)(2s+12g) + (1-2\nu)6o\}y^2z \\
& + \{2(1-\nu)(6p+6q) + (1-2\nu)6r\}xyz.
\end{aligned}$$

Since  $\phi_3$  should satisfy the biharmonic equation as before, we have the auxiliary equation as

$$\begin{aligned}
& \{15a+3(f+h+j+k)+\bar{u}\}x + \{(15b+3(d+i+\ell+m) \quad (258) \\
& + t\}y + \{15c+3(e+g+h+o) + s\}z = 0
\end{aligned}$$



This set of linear equations, i.e. eq. (252) to eq. (258) can be solved for coefficients  $a$  to  $\bar{u}$ , assuming boundary conditions as

$$\sigma_{zz} = \sigma_{xz} = \sigma_{yz} = 0 \quad (259)$$

$$2\mu u = 2\mu v = 0 \quad (260)$$

$$2\mu w = A_3 x^3 + B_3 y^3 + C_3 x^2 y + D_3 x y^2. \quad (261)$$

Coefficients are,

$$c = e = g = n = o = p = q = r = s = 0 \quad (262)$$

$$h = - \frac{2-\nu}{12(1-\nu)} (3A_3 + D_3) \quad (263)$$

$$i = - \frac{2-\nu}{12(1-\nu)} (3B_3 + C_3) \quad (264)$$

$$k = \frac{A_3}{2} \quad (265)$$

$$m = \frac{B_3}{2} \quad (266)$$

$$t = \frac{C_3}{2} \quad (267)$$

$$\bar{u} = \frac{D_3}{2} \quad (268)$$

$$20a + 2j = \frac{\nu A_3}{1-\nu} \quad (269)$$

$$20b + 2k = \frac{\nu B_3}{1-\nu} \quad (270)$$

$$12d + 6l = \frac{\nu C_3}{1-\nu} \quad (271)$$

$$12f + 6j = \frac{\nu D_3}{1-\nu} \quad (272)$$

Substituting these coefficients into eq. (249) to eq. (257) we obtain solutions for stresses and displacements as

$$\sigma_{xx} = -\frac{2}{1-\nu} (\nu D_3 + 3A_3)xz - \frac{2}{1-\nu} (3\nu B_3 + C_3)yz \quad (273)$$

$$\sigma_{yy} = -\frac{2}{1-\nu} (3\nu A_3 + D_3)xz - \frac{2}{1-\nu} (3B_3 + \nu C_3)yz \quad (274)$$

$$\sigma_{zz} = 0 \quad (275)$$

$$\sigma_{xy} = -2C_3xz - 2D_3yz \quad (276)$$

$$\sigma_{xz} = \frac{1}{1-\nu} (3A_3 + D_3)z^2 \quad (277)$$

$$\sigma_{yz} = \frac{1}{1-\nu} (3B_3 + C_3)z^2 \quad (278)$$

$$2\mu u = \frac{2-\nu}{3(1-\nu)} (3A_3+D_3)z^3 - 3A_3x^2z \quad (279)$$

$$- D_3y^2z - 2C_3xyz \}$$

$$2\mu v = \frac{2-\nu}{3(1-\nu)} (3B_3 + C_3)z^3 - C_3x^2z - 3B_3y^2z \quad (280)$$

$$- 2D_3xyz$$

$$2\mu w = A_3x^3 + B_3y^3 + C_3x^2y + D_3xy^2 \quad (281)$$

$$+ \frac{\nu}{1-\nu} (3A_3+D_3)z^2x + \frac{\nu}{1-\nu} (3B_3+C_3)z^2y .$$

The other components of the Galerkin vector, i.e.  $\phi_1$  and  $\phi_2$  are obtained in the same manner but we have to deal them simultaneously because no decoupling of horizontal displacements occurs. Thus fifth order polynomial expansions for  $\phi_1$  and  $\phi_2$  are represented as

$$\phi_1 = ax^5 + by^5 + cz^5 + dx^4y + ex^4z + fy^4x \quad (282)$$

$$+ gy^4z + hz^4x + iz^4y + jx^3y^2 + kx^3z^2 + ly^3x^2$$

$$+ my^3z^2 + nz^3x^2 + oz^3y^2 + px^3yz + qy^3xz + rz^3xy$$

$$+ sx^2y^2z + tx^2z^2y + \bar{u}y^2z^2x$$

$$\phi_2 = a*x^5 + b*y^5 + c*z^5 + \bar{d}*x^4*y + e*x^4*z + f*y^4*x \quad (283)$$

$$+ g*y^4*z + h*z^4*x + i*z^4*y + j*x^3*y^2 + k*x^3*z^2 + \bar{l}*y^3*x^2$$

$$+ m*y^3*z^2 + n*z^3*x^2 + o*z^3*y^2 + p*x^3*y*z + q*y^3*x*z + r*z^3*x*y$$

$$+ s*x^2*y^2*z + t*x^2*z^2*y + \bar{u}*y^2*z^2*x.$$

where stars denote another set of coefficients. Substituting them into eq. (97) to eq. (106) as before, we have

$$\sigma_{xx} = [3\{(2-\nu)(2j+2k)+(1-\nu)20a\} + \{\nu(6\bar{l}+2t^*) \quad (284)$$

$$- (1-\nu)12\bar{d}^*\}]x^2 + [\{(2-\nu)(12f+2\bar{u})+(1-\nu)6j\}$$

$$+ 3\{\nu(20b^*+2m^*)-(1-\nu)2\bar{l}^*\}]y^2 + 2[\{(2-\nu)(6\bar{l}+2t)$$

$$+ (1-\nu)12\bar{d}\} + \{\nu(12f^*+2\bar{u}^*) - (1-\nu)6j^*\}]xy$$

$$+ [\{(2-\nu)(2\bar{u}+12h) + (1-\nu)6k\} + \{\nu(6m^*+12i^*)-(1-\nu)2t^*\}]z^2$$

$$+ [2\{(2-\nu)(2s+6n) + (1-\nu)12e\} + \{\nu(6q^*+6r^*)$$

$$- (1-\nu)6p^*\}]xz + [\{(2-\nu)(6q+6r) + (1-\nu)6p\}$$

$$+ 2\{\nu(12g^*+6o^*) - (1-\nu)2s^*\}]yz$$

$$\begin{aligned}
\sigma_{yy} = & [3\{v(20a+2k) - (1-v)2j\} + \{(2-v)(12d^*+2t^* \\
& + (1-v)6\ell^*)\}x^2 + [\{v(6j+2\bar{u}) - (1-v)12f\} \\
& + 3\{(2-v)(2\ell^*+2m^*) + (1-v)20b^*\}y^2 + 2[\{v(12d+2t) \\
& - (1-v)6\ell\} + \{(2-v)(6j^*+2\bar{u}^*) + (1-v)12f^*\}]xy \\
& + [\{v(6k+12h) - (1-v)2\bar{u}\} + \{(2-v)(2t^*+12i^*) + \\
& (1-v)6m^*\}]z^2 + [2\{v(12e+6n) - (1-v)2s\} + \\
& \{(2-v)(6p^*+6r^*) + (1-v)6q^*\}]xz + [\{v(6p+6r) \\
& - (1-v)6q\} + 2\{(2-v)(2s^*+6o^*) + (1-v)12g^*\}]yz
\end{aligned}
\tag{285}$$

$$\begin{aligned}
\sigma_{xy} = & [\{(1-n)(6P+2t)-v12d\} + 3\{(1-v)(20a^*+2k^*) \\
& - v2j^*\}]x^2 + [3\{(1-v)(20b+2m) - v2\ell\} \\
& + \{(1-v)(6j^*+2u^*)-v12f^*\}]y^2 + 2[\{(1-v)(12f+2\bar{u}) \\
& - v6j\}+\{(1-v)(12d^*+2t^*)-v6\ell^*\}]xy + [\{(1-v)(6m+12i) \\
& - v2t\}+\{(1-v)(6k^*+12h^*)-v2u^*\}]z^2 \\
& + [\{(1-v)(6q+6r)-v6p\}+2\{(1-v)(12e^*+6n^*)-v2s^*\}]xz \\
& + [2\{(1-v)(12g+6o)-v2s\} + \{(1-v)(6p^*+6r^*)-v6q^*\}]yz
\end{aligned}
\tag{286}$$

$$\begin{aligned}
\sigma_{zz} = & [3\{v(20a+2j)-(1-v)2k\} + \{v(12d^*+6\ell^*)-(1-v)2t^*\}]x^2 \quad (287) \\
& + [\{v(6j+12f)-(1-v)2\bar{u}\} + 3\{v(2\ell^*+20b^*)-(1-v)2m^*\}]y^2 \\
& + 2[\{v(12d+6\ell)-(1-v)2t\} + \{v(6j^*+12f^*)-(1-v)2\bar{u}^*\}]xy \\
& + [\{v(6k+2u)-(1-v)12h\} + \{v(6m^*+2t^*)-(1-v)12i^*\}]z^2 \\
& + [2\{v(12e+2s)-(1-v)6n\} + \{v(6p^*+6q^*)-(1-v)6r^*\}]xz \\
& + [\{v(6p+6q)-(1-v)6r\} + 2\{v(2s^*+12g^*)-(1-v)6o^*\}]yz
\end{aligned}$$

$$\begin{aligned}
\sigma_{xz} = & [\{(1-v)(2s+6n)-v12e\} - 3p^*]x^2 + [\{(1-v)(12g+6o) \quad (288) \\
& - v2s\}-3q^*]y^2 + [\{(1-v)(6q+6r)-v6p\}-4s^*]xy \\
& + [3\{(1-v)(20+2oc)-v2n\}-3r^*]z^2 + [2\{(1-v)(2\bar{u}+12h) \\
& - 4t^*\}]xz + [2\{(1-v)(6m+12i)-v2t\}-4\bar{u}^*]yz
\end{aligned}$$

$$\begin{aligned}
6yz = & [ \{ (1-v)(12e^*+6n^*)-v2s^* \} - 3p ] x^2 + [ \{ (1-v)(2s^*+6o^*) \\
& - v12g^* \} - 3q ] y^2 + [ \{ (1-v)(6p^*+6r^*)-v6q^* \} \\
& - 4s ] xy + [ 3 \{ (1-v)(2n^*+20c^*)-v2j^* \} - 3r ] z^2 \\
& + [ 2 \{ (1-v)(6k^*+12h^*)-v2\bar{u}^* \} - 4t ] xz + [ 2 \{ (1-v)(2t^*+12i^*) \\
& - v6m^* \} - 4\bar{u} ] yz
\end{aligned}$$

$$\begin{aligned}
2\mu u = & [ \{ 2(1-v)(2j+2k)+(1-2v)20a \} - 4d^* ] x^3 + [ \{ 2(1-v)(20b+2m) \\
& + (1-2v)2\ell \} - 4f^* ] y^3 + [ \{ 2(1-v)(6\ell+2t)+(1-2v)12d \} \\
& - 6j^* ] x^2 y + [ \{ 2(1-v)(12f+2u)+(1-2v)6j \} \\
& - 6\ell^* ] y^2 x + [ \{ 2(1-v)(2o+20c)+(1-2v)2n \} - r^* ] z^3 \\
& + [ \{ 2(1-v)(2\bar{u}+12h)+(1-2v)6k \} - 2t^* ] z^2 x + [ \{ 2(1-v)(6m+12i) \\
& + (1-2v)2t \} - 2\bar{u}^* ] z^2 y + [ \{ 2(1-v)(2s+6n)+(1-2v)12e \} \\
& - 3p^* ] x^2 z + [ \{ 2(1-v)(12g+6o)+(1-2v)2s \} - 3q^* ] y^2 z \\
& + [ \{ 2(1-v)(6q+6r)+(1-2v)6p \} - 4s^* ] xyz
\end{aligned}$$

$$\begin{aligned}
2\mu\nu = & [ 2(1-\nu)(20a^*+2k^*)+(1-2\nu)2j^*]-4d]x^3 + [ \{2(1-\nu) \\
& (2\ell^*+2m^*)+(1-2\nu)2ob^*}-4f]y + [ \{2(1-\nu)(12d^*+2t^*) \\
& + (1-2\nu)6\ell^*}-6j]x^2y + [ \{2(1-\nu)(6j^*+2\bar{u}^*)+(1-2\nu)12f^* \\
& - 6\ell]y^2x + [ \{2(1-\nu)(2n^*+20c^*)+(1-2\nu)2o^*]-r]z^3 \\
& + [ \{2(1-\nu)(6k^*+12h^*)+(1-2\nu)2u^*}-2t]z^2x + [ \{2(1-\nu) \\
& (2t^*+12i^*)+(1-2\nu)6m^*}-2\bar{u}]z^2y + [ \{2(1-\nu)(12e^*+6n^*) \\
& + (1-2\nu)2s^*}-3p]x^2z + [ \{2(1-\nu)(2s^*+6o^*) \\
& + (1-2\nu)12g^*}-3q]y^2z + [ \{2(1-\nu)(6p^*+6r^*)+(1-2\nu)6q^* \\
& - 4s]xyz
\end{aligned}
\tag{291}$$

$$\begin{aligned}
2\mu w = & -\{(4e+p^*)x^3+(q+4g^*)y^3+(3p+2s^*)x^2y \\
& + (2s+3q^*)y^2x + (4h+4i^*)z^3 + (6n+3r^*)z^2x \\
& + (3r+6o^*)z^2y + (6k + 2t^*)x^2z + (2\bar{u}+6m^*)y^2z \\
& + (4t + 4\bar{u}^*)xyz
\end{aligned}
\tag{292}$$

$$\begin{aligned}
& \{15a+3(f+h+j+k)+\bar{u}\}x + \{15b+3(d+i+\ell+m) \\
& + t\}y + \{15c + 3(e+g+h+o)+s\}z = 0.
\end{aligned}
\tag{293}$$

$$\begin{aligned}
& \{15a^*+3(f^*+h^*+j^*+k^*)+\bar{u}^*\}x + \{15b^*+3(d^*+i^*+\ell^*+m^*) \\
& + t^*\}y + \{15c^*+3(e^*+g^*+h^*+o^*)+s^*\}z = 0.
\end{aligned}
\tag{294}$$



This set of linear equations, i.e. eq. (287) to eq. (294) can be solved together with boundary conditions at  $z = 0$  as

$$\sigma_{zz} = \sigma_{zx} = \sigma_{zy} = 0 \quad (295)$$

$$2\mu u = A_1 x^3 + B_1 y^3 + C_1 x^2 y + D_1 x y^2 \quad (296)$$

$$2\mu w = A_2 x^3 + B_2 y^3 + C_2 x^2 y + D_2 x y^2 \quad (297)$$

to obtain coefficients  $a$  to  $\bar{u}$  and  $a^*$  to  $\bar{u}^*$ . Solutions are,

$$e = j = l = n = p = q = r = s = 0 \quad (298)$$

$$12g + 6o = 0 \quad (299)$$

$$20c + 2o = 0 \quad (300)$$

$$a = \frac{1}{20} \left( A_1 + \frac{C_2}{6} \right) \quad (301)$$

$$d = \frac{C_1}{12} \quad (302)$$

$$f = \frac{D_1}{24} \quad (303)$$

$$k = \frac{\nu}{2(1-\nu)} \left( A_1 + \frac{C_2}{6} \right) \quad (304)$$

$$t = \frac{v}{2(1-v)} C_1 \quad (305)$$

$$u = \frac{v}{4(1-v)} D_1 \quad (306)$$

$$20b + 2m = \frac{1}{2(1-v)} \left( B_1 + \frac{D_2}{3} \right) \quad (307)$$

$$2u + 12h = - \frac{1}{2(1-v)} \{ (1+v)6A_1 + (1+v)C_2 + D_1 \} \quad (308)$$

$$6m + 12i = - \frac{1}{2(1-v)} \{ 3B_1 + 2(1+v)C_1 + D_2 \} \quad (309)$$

$$g^* = j^* = l^* = o^* = p^* = q^* = r^* = s^* = 0 \quad (310)$$

$$12e^* + 6n^* = 0 \quad (311)$$

$$20c^* + 2n^* = 0 \quad (312)$$

$$b^* = \frac{1}{20} \left( B_2 + \frac{D_1}{6} \right) \quad (313)$$

$$d^* = \frac{C_2}{24} \quad (314)$$

$$f^* = \frac{D_2}{12} \quad (315)$$

$$m^* = \frac{v}{2(1-v)} \left( B_2 + \frac{D_1}{6} \right) \quad (316)$$

$$t^* = \frac{\nu}{4(1-\nu)} C_2 \quad (317)$$

$$u^* = \frac{\nu}{2(1-\nu)} D_2 \quad (318)$$

$$20a^* + 2k^* = \frac{1}{2(1-\nu)} \left( A_2 + \frac{C_1}{3} \right) \quad (319)$$

$$6k^* + 12h^* = - \frac{1}{2(1-\nu)} \{ 3A_2 + C_1 + 2(1+\nu)D_2 \} \quad (320)$$

$$2t^* + 12i^* = - \frac{1}{2(1-\nu)} \{ 6(1+\nu)B_2 + C_2 + (1+\nu)D_1 \}. \quad (323)$$

Substituting these coefficients into eq. (284) to eq. (322), we obtain solutions for stresses and displacements as

$$\sigma_{xx} = \frac{1}{2(1-\nu)} (6A_1 + 2\nu C_2)x^2 + \frac{1}{2(1-\nu)} (6\nu B_2 + 2D_1)y^2 \quad (322)$$

$$+ \frac{2}{1-\nu} (C_1 + \nu D_2)xy - \frac{1}{2(1-\nu)} \{ 12A_1 + 6\nu B_2 + 2(1+\nu)C_2 + 2D_1 \} z^2$$

$$\sigma_{yy} = \frac{1}{2(1-\nu)} (6\nu A_1 + 2C_2)x^2 + \frac{1}{2(1-\nu)} (6B_2 + 2\nu D_1)y^2 \quad (323)$$

$$+ \frac{2}{1-\nu} (\nu C_1 + D_2)xy - \frac{1}{2(1-\nu)} \{ 6\nu A_1 + 12B_2 + 2C_2$$

$$+ 2(1+\nu)D_1 \} z^2$$

$$\sigma_{zz} = \frac{1}{2(1-\nu)} (6A_1 + 6B_2 + 2C_2 + 2D_1)z^2 \quad (324)$$

$$\sigma_{xy} = \frac{1}{2} (3A_2 + C_1)x^2 + \frac{1}{2} (3B_1 + D_2)y^2 + (C_2 + D_1)xy \quad (325)$$

$$- \frac{1}{2(1-\nu)} \{3(1-\nu)(A_2 + B_1) + (1+\nu)(C_1 + D_2)\}z^2$$

$$\sigma_{xz} = - \frac{1}{1-\nu} \{6A_1 + (1+\nu)C_2 + (1-\nu)D_1\}xz \quad (326)$$

$$+ \{(1-\nu)3B_1 + (1+\nu)D_2 + 2C_1\}yz]$$

$$\sigma_{yz} = - \frac{1}{1-\nu} \{3(1-\nu)A_2 + (1+\nu)C_1 + 2D_2\}xz \quad (327)$$

$$+ \{6B_2 + (1-\nu)C_2 + (1+\nu)D_1\}yz]$$

$$2\mu u = A_1x^3 + B_1y^3 + C_1x^2y + D_1xy^2 - \frac{1}{1-\nu} \{3(2-\nu)A_1 \quad (328)$$

$$+ C_2 + (1-\nu)D_1\}z^2x - \frac{1}{1-\nu} \{3(1-\nu)B_1 + (2-\nu)C_1 + D_2\}z^2y$$

$$2\mu v = A_2x^3 + B_2y^3 + C_2x^2y + D_2xy^2 - \frac{1}{1-\nu} \{3(1-\nu)A_2 \quad (329)$$

$$+ C_1 + (2-\nu)D_2\}z^2x - \frac{1}{1-\nu} \{3(2-\nu)B_2 + (1-\nu)C_2 + D_1\}z^2y$$

$$2\mu w = \frac{1+\nu}{3(1-\nu)}(3A_1+3B_2 + C_2 + D_1)z^3 - \frac{\nu}{1-\nu} (3A_1+C_2)x^2z \quad (330)$$

$$- \frac{\nu}{1-\nu} (3B_2+D_1)y^2z - \frac{2\nu}{1-\nu} (C_1+D_2)xyz.$$

By superposing these solutions based on the fifth order polynomial expansion of the Galerkin vector to solutions already obtained by lower order expansion, i.e. eq. (239) to eq. (247), we obtain a complete solution for stresses and displacements in the elastic body when displacements of cubic polynomials are specified on the free surface boundary. They are represented in the following equations.

Boundary conditions at  $z = 0$ :

$$u|_{z=0} = A_1x^3+B_1y^3+C_1x^2y+D_1xy^2+E_1x^2+F_1y^2 \quad (331)$$

$$+ G_1xy+H_1x+I_1y+J_1$$

$$v|_{z=0} = A_2x^3+B_2y^3+C_2x^2y+D_2xy^2+E_2x^2+F_2y^2 \quad (332)$$

$$+ G_2xy+H_2x+I_2y+J_2$$

$$w|_{z=0} = A_3x^3+B_3y^3+C_3x^2y+D_3xy^2+E_3x^2+F_3y^2 \quad (333)$$

$$+ G_3xy+H_3x+I_3y+J_3$$

Solutions:

$$\sigma_{xx} = \frac{2\mu}{1-\nu} [(3A_1 + \nu C_2)x^2 + (3\nu B_2 + D_1)y^2] \quad (334)$$

$$- \{6A_1 + 3\nu B_2 + (1+\nu)C_2 + D_1\}z^2]$$

$$+ \frac{4\mu}{1-\nu} \{(C_1 + \nu D_2)xy - (\nu D_3 + 3A_3)xz$$

$$- (3\nu B_3 + C_3)yz\} + \frac{2\mu}{1-\nu} \{(2E_1 + \nu G_2)x$$

$$+ (2\nu F_2 + G_1)y - 2(E_3 + \nu F_3)z + H_1 + \nu I_2\}$$

$$\sigma_{yy} = \frac{2\mu}{1-\nu} [(3\nu A_1 + C_2)x^2 + (3B_2 + \nu D_1)y^2 - \{3\nu A_1 + 6B_2 \quad (335)$$

$$+ C_2 + (1+\nu)D_1\}z^2] + \frac{4\mu}{1-\nu} \{(\nu C_1 + D_2)xy - (3\nu A_3 + D_3)xz$$

$$- (3B_3 + \nu C_3)yz\} + \frac{2\mu}{1-\nu} \{(2\nu E_1 + G_2)x + (2F_2 + \nu G_1)y$$

$$- 2(\nu E_3 + F_3)z + \nu H_1 + I_2\}$$

$$\sigma_{zz} = \frac{2\mu}{1-\nu} (3A_1 + 3B_2 + C_2 + D_1)z^2 \quad (336)$$

$$\sigma_{xy} = \mu \{(3A_2 + C_1)x^2 + (3B_1 + D_2)y^2\} - \frac{\mu}{1-\nu} \quad (337)$$

$$\{3(1-\nu)(A_2 + B_1) + (3-\nu)(C_1 + D_2)\}z^2 + 2\mu \{(C_2 + D_1)xy$$

$$- 2C_3xz - 2D_3yz\} + \mu \{2E_2 + G_1\}x + (2F_1 + G_2)y$$

$$- 2G_3z + H_2 + I_1\}$$

$$\sigma_{xz} = \frac{2\mu}{1-\nu} [(3A_3+D_3)z^2 - \{6A_1+(1+\nu)C_2+(1-\nu)D_1\}xz] \quad (338)$$

$$- \{3(1-\nu)B_1+2C_1+(1+\nu)D_2\}yz] - \frac{\mu}{1-\nu} \{4E_1+2(1-\nu)F_1$$

$$+ (1+\nu)G_2\}z$$

$$\sigma_{yz} = \frac{2\mu}{1-\nu} [(3B_3+C_3)z^2 - \{3(1-\nu)A_2+(1+\nu)C_1+2D_2\}xz] \quad (339)$$

$$- \{6B_2+(1-\nu)C_2+(1+\nu)D_1\}yz] - \frac{\mu}{1-\nu} \{4F_2+2(1-\nu)E_2$$

$$+ (1+\nu)G_1\}z$$

$$u = A_1x^3 + B_1y^3 + C_1x^2y + D_1xy^2 + E_1x^2 + F_1y^2 \quad (340)$$

$$+ G_1xy + H_1x + I_1y + J_1 + \frac{2-\nu}{3(1-\nu)} (3A_3+D_3)z^3$$

$$- 3A_3x^2z - 2C_3xyz - D_3y^2z - \frac{1}{1-\nu} [\{3(2-\nu)A_1+C_2$$

$$+ (1-\nu)D_1\}z^2x + \{3(1-\nu)B_1+(2-\nu)C_1+D_2\}z^2y]$$

$$- \frac{1}{2(1-\nu)} \{2(2-\nu)E_1+2(1-\nu)F_1+G_2\}z^2 - 2E_3xz$$

$$- G_3yz - H_3z$$

$$v = A_2x^3 + B_2y^3 + C_2x^2y + D_2xy^2 + E^2x^2 + F_2y^2 + G_2xy \quad (341)$$

$$+ H_2x + I_2y + J_2 + \frac{2-\nu}{3(1-\nu)} (3B_3 + C_3)z^3$$

$$- C_3x^2z - 2D_3xyz - 3B_3y^2z - \frac{1}{1-\nu} [\{3(1-\nu)A_2 + C_1$$

$$+ (2-\nu)D_2\}z^2x + \{3(2-\nu)B_2 + (1-\nu)C_2 + D_1\}z^2y]$$

$$- \frac{1}{2(1-\nu)} \{2(1-\nu)E_2 + 2(2-\nu)F_2 + G_1\}z^2 - G_3xz$$

$$- 2F_3yz - I_3z$$

$$w = A_3x^3 + B_3y^3 + C_3x^2y + D_3xy^2 + E_3x^2 + F_3y^2 + G_3xy \quad (342)$$

$$+ H_3x + I_3y + J_3 + \frac{1+\nu}{3(1-\nu)} (3A_1 + 3B_2 + C_2 + D_1)z^3$$

$$- \frac{\nu}{1-\nu} \{(3A_1 + C_2)x^2z + (3B_2 + D_1)y^2z + 2(C_1 + D_2)xyz$$

$$- (3A_3 + D_3)z^2x - (3B_3 + C_3)z^2y - (E_3 + F_3)z^2$$

$$+ (2E_1 + G_2)xz + (2F_2 + G_1)yz + (H_1 + I_2)z\}.$$

Since these displacements on the boundary are presented by ten parameters, we need at least ten data points on the boundary to obtain solutions. Possible networks are shown in Fig. 6.



### 3.4 Inversion by Finite Element Method

The finite element method has been used in inverse problem, especially in parameter estimation and optimization problems, in many fields of science and engineering during the last decade (Lions, 1977) because this method provides very general and flexible approach to the problems in spite of sometimes prohibitively high computer cost.

An application of the finite element method to the elastostatic inverse problem in three dimension was first made by Ikeda (1980). He studied basic numerical procedure for obtaining a finite element inversion scheme and analyzed errors involved in the method. Because of its generality and wide applicability to the inverse problems not only in the elastostatics but also in electromagnetics or fluid mechanics, we shall briefly summarize the inversion method based on the finite element method. Detailed derivation of general finite element families and special purpose programs as well as error analysis of the method are described elsewhere (Ikeda, 1980).

Using a standard finite element method based on a displacement formulation such as given in Zienkiewicz (1972), we have a discretized form of the operator equation as

$$[K][U] = [R] \quad (343)$$

where  $[K]$  is the so-called stiffness matrix,  $[U]$  and  $[R]$  are matrices that consist of displacement and load at each node. Written explicitly, this equation is in a partitioned form,

$$\begin{array}{cccc}
 & k & l & m & n & & (344) \\
 k & \left[ \begin{array}{cccc} K_{11} & K_{12} & K_{13} & K_{14} \end{array} \right] & \left[ \begin{array}{c} U_1^* \\ U_2^* \\ U_3 \\ U_4 \end{array} \right] & = & \left[ \begin{array}{c} R_1^* \\ R_2 \\ R_3 \\ R_4 \end{array} \right] \\
 l & \left[ \begin{array}{c} K_{21} \\ K_{31} \\ K_{41} \end{array} \right] & \left[ \begin{array}{cccc} K_{22} & K_{23} & K_{24} \\ K_{32} & K_{33} & K_{34} \\ K_{42} & K_{43} & K_{44} \end{array} \right] & & & & \\
 m & & & & & & \\
 n & & & & & & 
 \end{array}$$

where  $k, l, m, n$  denote numbers of rows and columns of each block, and thus  $K_{11}$  is a  $(k \times k)$  matrix,  $K_{12}$  is a  $(k \times l)$  matrix,  $K_{13}$  is a  $k \times m$  matrix,  $K_{14}$  is a  $(k \times n)$  matrix,  $K_{22}$  is a  $(l \times l)$  matrix,  $K_{23}$  is a  $(l \times m)$  matrix,  $K_{24}$  is a  $(l \times n)$  matrix,  $K_{33}$  is a  $(m \times m)$  matrix,  $K_{34}$  is a  $(m \times n)$  matrix,  $K_{44}$  is a  $(n \times n)$  matrix, and  $K_{21}, K_{31}, K_{32}, K_{41}, K_{42}, K_{43}$  are transpose of  $K_{12}, K_{13}, K_{23}, K_{14}, K_{24}, K_{34}$ , respectively.  $U_1^*$  is a  $(k \times 1)$  matrix,  $U_2^*$  is a  $(l \times 1)$  matrix,  $U_3$  is a  $(m \times 1)$  matrix.  $U_4$  is a  $(n \times 1)$  matrix.  $R_1^*$  is a  $(k \times 1)$  matrix,  $R_2$  is a  $(l \times 1)$  matrix,  $R_3^*$  is a  $(m \times 1)$  matrix, and  $R_4$  is a  $(n \times 1)$  matrix, and a star represents that elements of matrix that are known quantities. These known quantities are observed three components of displacement vectors on the surface, stress free conditions on the surface and force balance conditions inside the boundaries. The latter two conditions give zero values to the load matrix  $[R]$ . It is noted that free surface conditions are not satisfied exactly in this formulation because only the continuity of displacements

is assured between elements in the displacement based formulation.

The above matrix equation can be modified to give a more convenient form to analyze, that is: (345)

$$\begin{array}{cccc}
 & m & n & \\
 k & \left[ \begin{array}{cc} K_{13} & K_{14} \\ K_{23} & K_{24} \\ K_{33} & K_{34} \\ K_{43} & K_{44} \end{array} \right. & & \\
 \ell & & & \\
 m & & & \\
 n & & & 
 \end{array}
 \begin{array}{cc}
 \ell & n \\
 \left[ \begin{array}{cc} 0 & 0 \\ -I & 0 \\ 0 & 0 \\ 0 & -I \end{array} \right] & \left[ \begin{array}{c} U_3 \\ U_4 \\ R_2 \\ R_4 \end{array} \right]
 \end{array}
 =
 \begin{array}{cccc}
 & k & \ell & k & m \\
 \left[ \begin{array}{cccc} -K_{11} & -K_{12} & I & 0 \\ -K_{21} & -K_{22} & 0 & 0 \\ -K_{31} & -K_{32} & 0 & I \\ -K_{41} & -K_{42} & 0 & 0 \end{array} \right] & & & 
 \end{array}
 \begin{array}{c}
 \left[ \begin{array}{c} U_1^* \\ U_2^* \\ R_1^* \\ R_3^* \end{array} \right]
 \end{array}$$

where [I] denotes a unit matrix of appropriate order. As can be seen from the above equation, our problem is overdetermined if  $\ell+m+2n < k+\ell+m+n$ , underdetermined if  $k+\ell+m+n < \ell+m+2n$ , and ill-posed if  $\text{rank of } L_n < k+\ell+m+n$  and  $\text{rank of } L_n < \ell+m+2n$ , and well-posed if  $\text{rank of } L_n = k+\ell+m+n = \ell+m+2n$ , where  $L_n$  represents the matrix on L.H.S. of eq. (345).

We need, therefore, to have the rank of  $L_n = k+\ell+m+n = \ell+m+2n$  which reduces to  $k=n$ . Since  $k$  is the number of components of which we know both displacements and forces and  $n$  is the number of components for which we know neither of them, the last equation shows that the number of surface nodes where we have both stress free conditions and observed displacements (this excludes the boundary nodes on the surface) need to be the same as the number of boundary nodes inside the earth where we know neither tractions nor displacements. To attain this condition, we need to choose a special family of finite element mesh configuration. This is mathematically equivalent to specify a base of a solution

space and thus gives a discrete analogue of the eigenfunction expansion method studied in previous sections. Because stress free conditions are not satisfied exactly, we use no discrete analogue for the shooting method.

The simplest mesh configuration which satisfies the above condition is shown in Fig. 7. This mesh configuration has a certain advantage that it allows us to increase the order of interpolation function without changing the whole configuration. This is shown in Fig. 8. The value of  $k$ ,  $\ell$ ,  $m$ ,  $n$  in cases of 8 nodes interpolation and 20-nodes interpolation are presented in Table 1.

Since in the parabolic interpolation using 20 nodes in an element the highest term is square, we expect that a strain change in the element is at most linear. Thus if we have to approximate a rapidly changing stress field inside a block, the block must be further subdivided. We can improve the accuracy of solution by subdividing the inner block in Fig. 8 into 7 small blocks as shown in Fig. 9. The values of  $k$ ,  $\ell$ ,  $m$ ,  $n$  are also shown in Table 1. It is clear that the condition  $k=n$  still holds after this subdivision.

Even though the above method enables us to solve the discretized three dimensional inverse problem without using any stabilizing or regularizing techniques such as a generalized inverse or a singular value decomposition, computational cost is still very large because the resultant matrix  $L_n$  is fully populated and therefore we need to use a large in-core memory. Therefore while the above method of

inversion based on the finite element discretization of the problem gives quite general and flexible approach to our inverse problem, the analytic solutions obtained in the previous sections has computational advantage as long as three dimensional elastostatic inverse problem is concerned. For other inverse problems such as the inverse potential problem studied by Garabedian and Lieberstein (1958) the above method of inversion based on the finite element method may provide a very effective numerical technique.

Table 1. Values of  $k$ ,  $\ell$ ,  $m$ ,  $n$ 

Case	$k$	$\ell$	$m$	$n$	Total
1	12	12	12	12	48
2	36	36	36	36	144
3	36	36	120	36	228

Case 1. Five 8 nodes element are used (Fig. 5)

Case 2. Five 20 nodes element are used (Fig. 6)

Case 3. Twelve 20 nodes element are used (Fig. 7)

Figure Captions for Chapter 3

Fig. 2. Coordinate system and boundary conditions used for the two dimensional elastostatic inverse problem.

Fig. 3. Coordinate system used for the three dimensional elastostatic inverse problem.

Fig. 4. Example of 10 points network for data input for the inversion.

Fig. 5. Mesh configuration by 8 nodes element used in the finite element inversion.

Fig. 6. Mesh configuration by 20 nodes element used in the finite element inversion.

Fig. 7. Mesh configuration by 20 nodes element used in the finite element inversion.

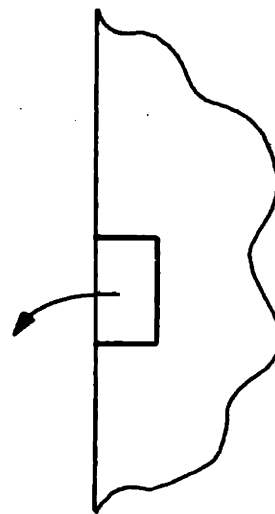
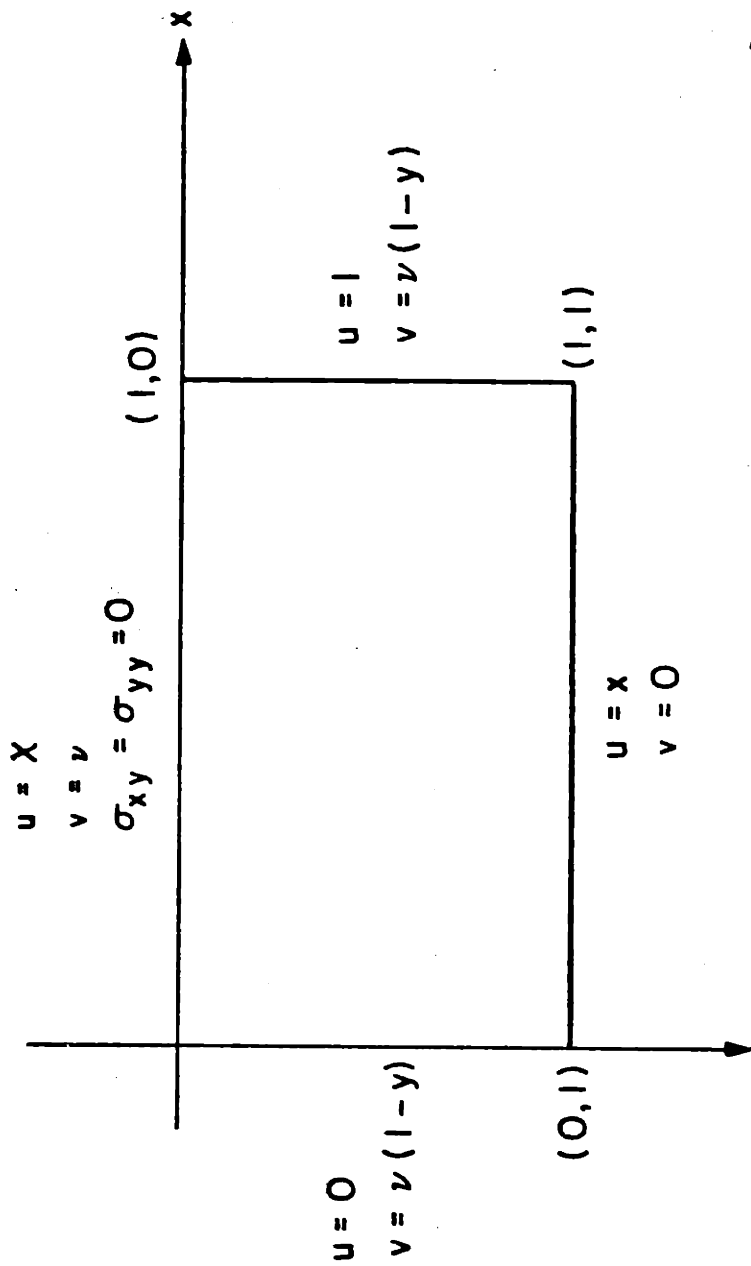


FIG. 2



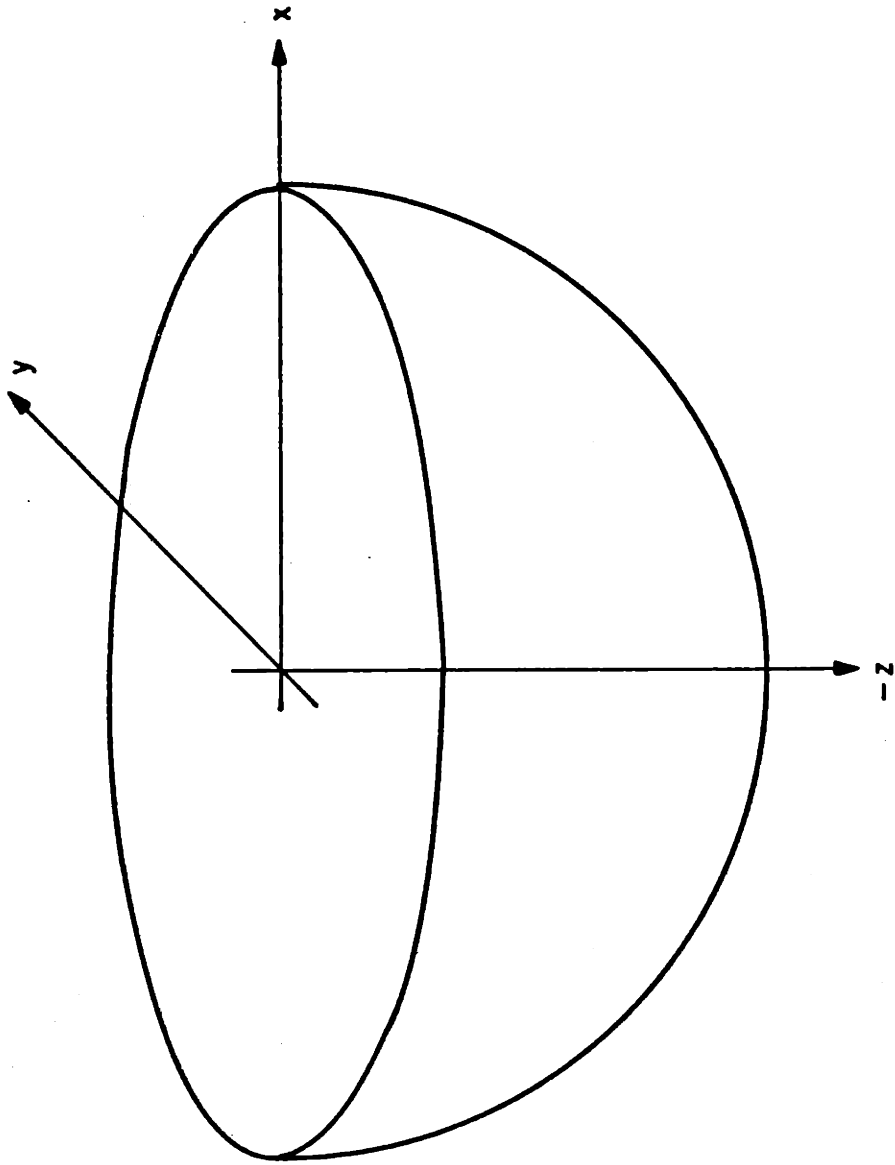


FIG. 3

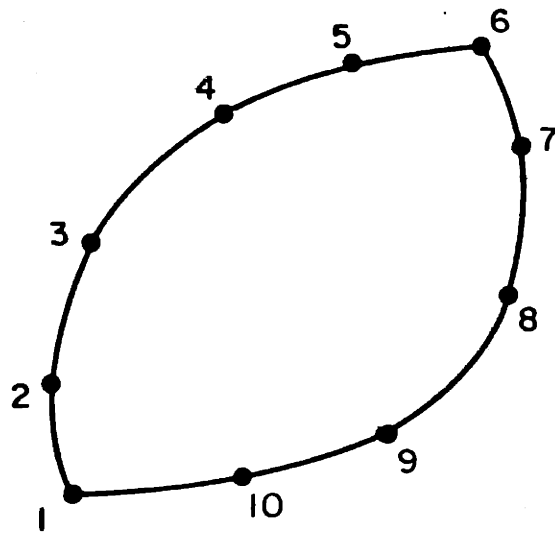
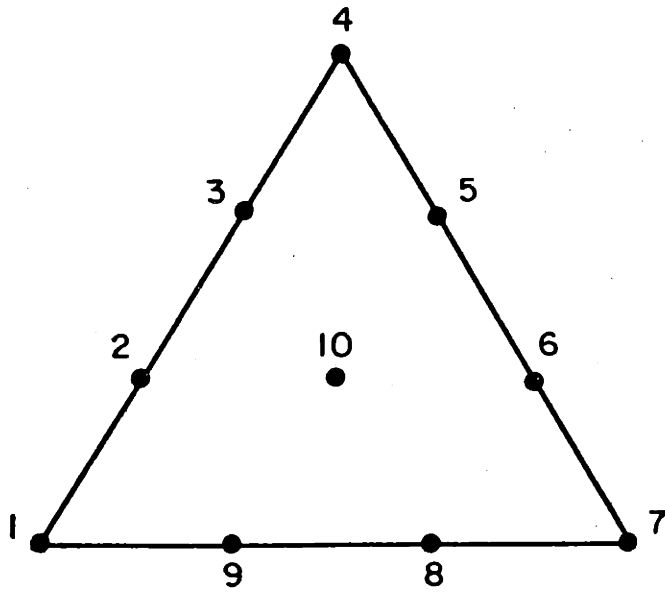


FIG. 4

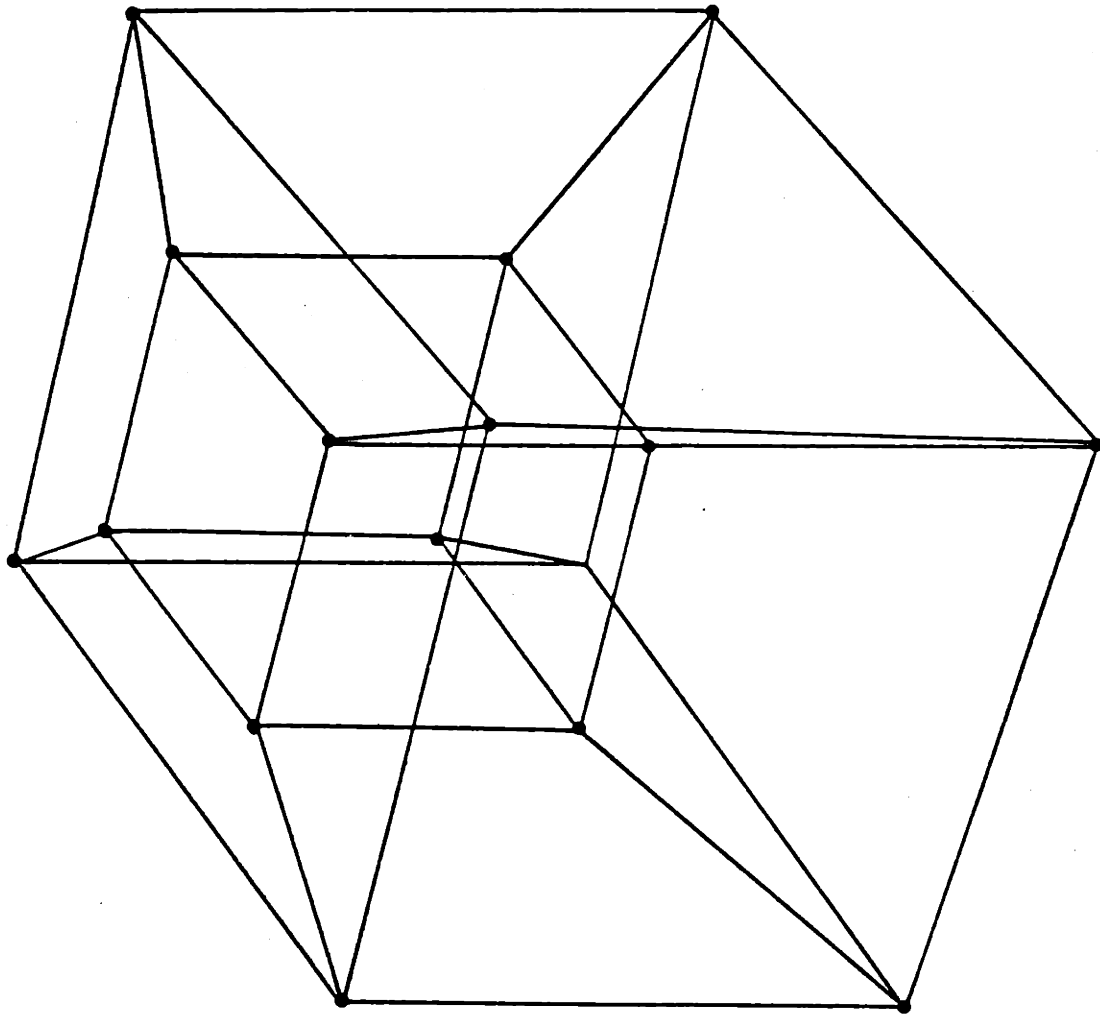


FIG. 5

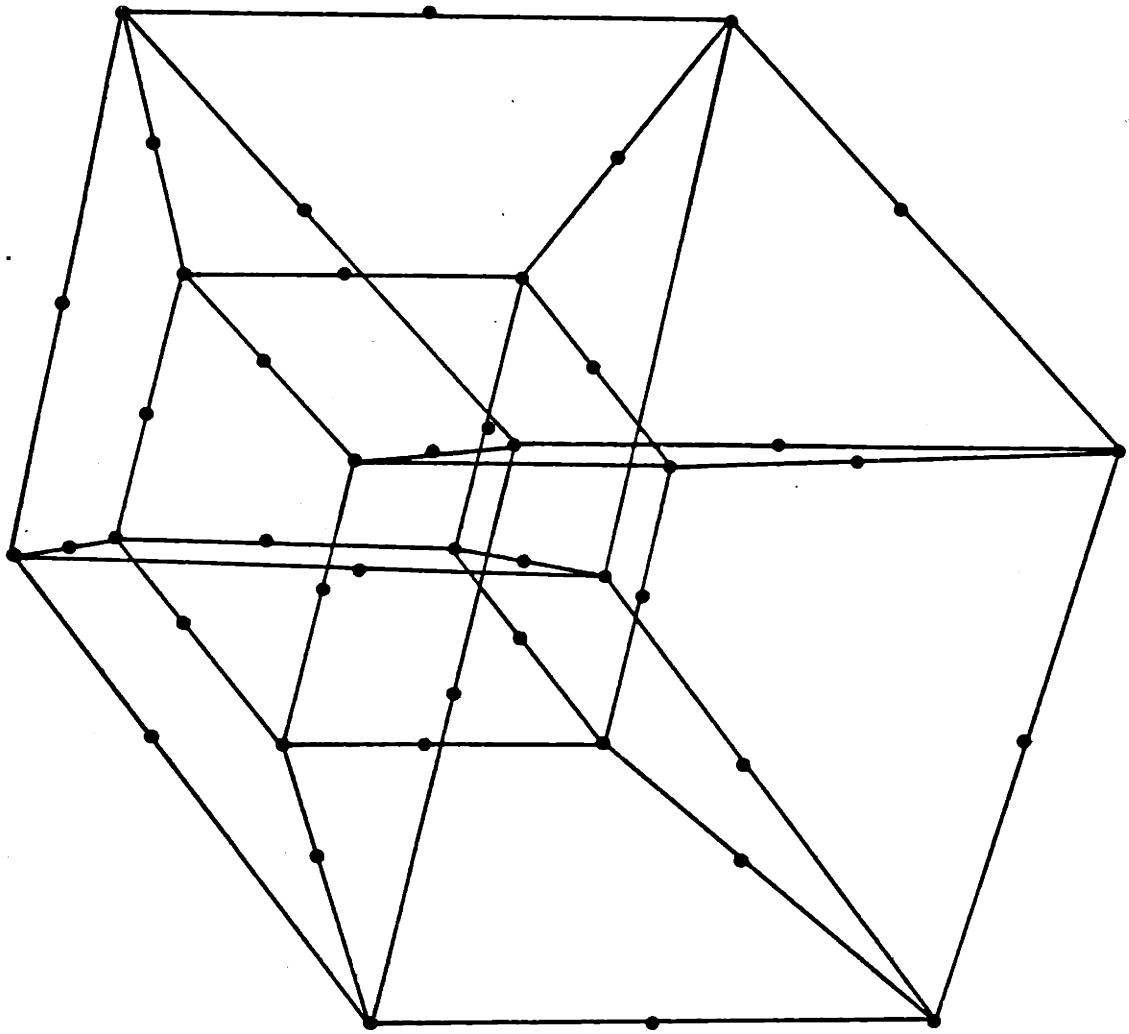


FIG. 6

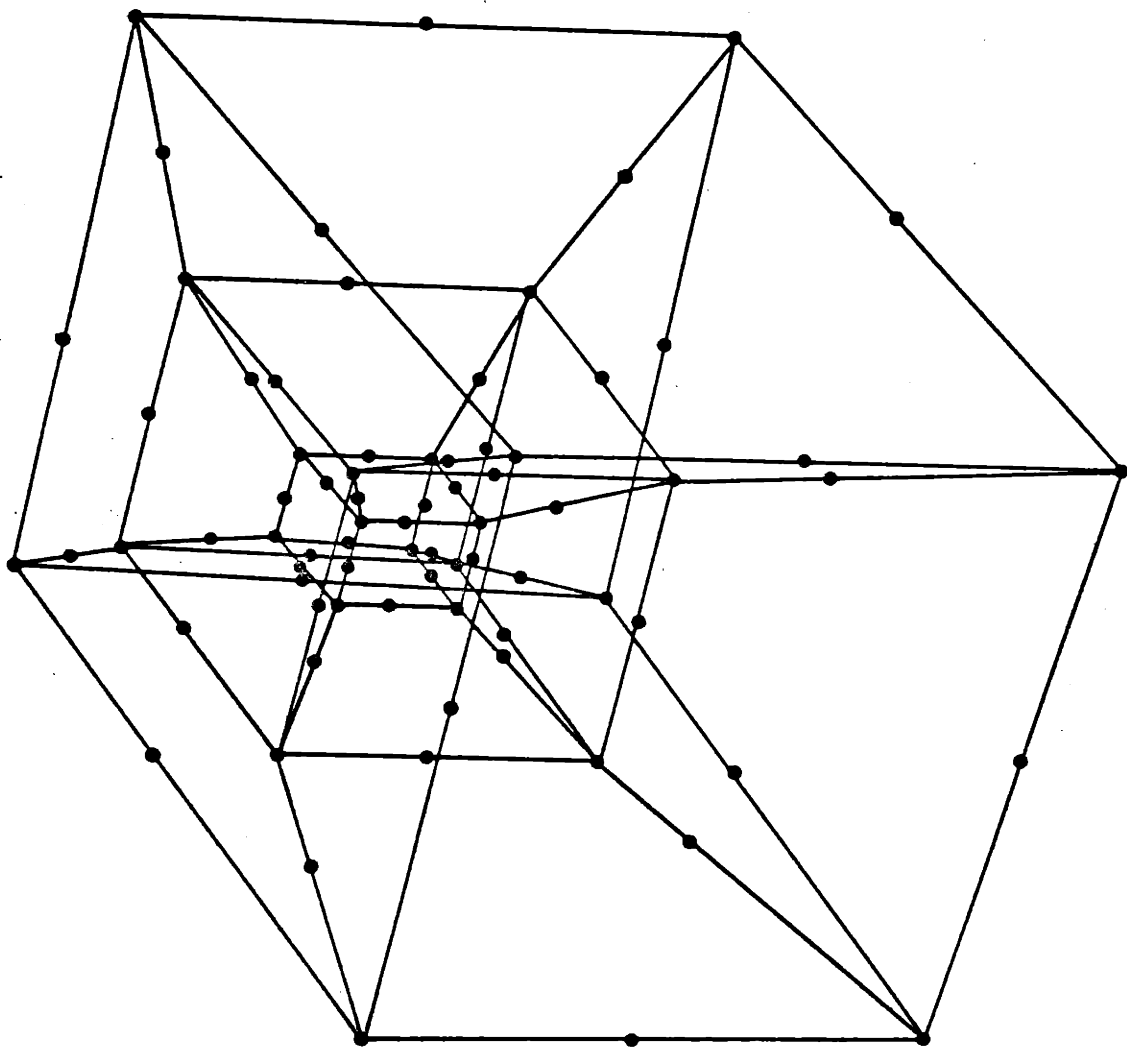


FIG. 7

## CHAPTER 4. ERROR ANALYSIS

4.1. Exactness and uniqueness of solutions

Solutions obtained for the three dimensional elastostatic inverse problem using the eigenfunction expansion-shooting method technique applied to the Galerkin vector in the preceding chapter are exact solutions. Their validity can be proved by substituting these solutions into equations of balance and equations of compatibility in elasticity. Those equations are,

$$\frac{\partial \sigma_{xx}}{\partial x} + \frac{\partial \sigma_{xy}}{\partial y} + \frac{\partial \sigma_{xz}}{\partial z} = 0 \quad (346)$$

$$\frac{\partial \sigma_{xy}}{\partial x} + \frac{\partial \sigma_{yy}}{\partial y} + \frac{\partial \sigma_{yz}}{\partial z} = 0 \quad (347)$$

$$\frac{\partial \sigma_{xz}}{\partial x} + \frac{\partial \sigma_{yz}}{\partial y} + \frac{\partial \sigma_{zz}}{\partial z} = 0 \quad (348)$$

$$\sigma_{xx} = (\lambda + 2\mu) \frac{\partial u}{\partial x} + \lambda \left( \frac{\partial v}{\partial y} + \frac{\partial w}{\partial z} \right) \quad (349)$$

$$\sigma_{yy} = (\lambda + 2\mu) \frac{\partial v}{\partial y} + \lambda \left( \frac{\partial u}{\partial x} + \frac{\partial w}{\partial z} \right) \quad (350)$$

$$\sigma_{zz} = (\lambda + 2\mu) \frac{\partial w}{\partial z} + \lambda \left( \frac{\partial u}{\partial x} + \frac{\partial v}{\partial y} \right) \quad (351)$$

$$\sigma_{xy} = \mu \left( \frac{\partial v}{\partial x} + \frac{\partial u}{\partial y} \right) \quad (352)$$

$$\sigma_{xz} = \mu \left( \frac{\partial w}{\partial x} + \frac{\partial u}{\partial z} \right) \quad (353)$$

$$\sigma_{yz} = \mu \left( \frac{\partial w}{\partial y} + \frac{\partial v}{\partial z} \right) \quad (354)$$

where  $\lambda$ ,  $\mu$  are Lamé's constants.

Applying the Cauchy-Kowalewsky theorem to the set of equations, from eq. (346) to eq. (354) with zero boundary conditions as we have done in Chapter 2 for the Cauchy problem for the Laplace equation, we can easily prove that these solutions are also unique.

Although those solutions are proved to be valid and unique, we have to know errors involved in the solutions if we are going to apply those solutions to actual problems. An error is possible because our solutions are based on the eigenfunction expansion up to a certain order and therefore they cease to be exact if actual boundary conditions require eigenfunction expansions of the order higher than the one used in obtaining the solutions.

#### 4.2. Geodetic network

As shown in the preceding chapter, the solutions based on the eigenfunction expansion of the Galerkin vector by the polynomial of fifth order, we need 10 parameters for each component of displacement vector to be specified on the boundary where displacement components are approximated by cubic polynomials. Since we are dealing with the geodetic inverse problem, these parameters on the surface must be chosen so that error introduced by the cubic approximation of displacements is kept minimum while geodetic measurement procedure on the surface to obtain displacements is kept as simple as possible, i.e. these parameters should be obtained from geodetic measurements directly without any interpolation and extrapolation that usually introduce another error.

Since current measurement techniques to obtain horizontal components of displacement vectors are based on triangulation measurements or trilateration measurements with geodimeters, geodetic networks used have always a shape of polygon with straight side lines which is constructed by adding many triangular networks (Bomford, 1971, Ewing and Mitchell, 1970). The leveling measurement to obtain the vertical component of displacement vectors on the surface is conducted on a closed loop which consists of curved line segments whose shapes depend on the topography. Most of the data obtainable to us, such as Fig. 16 which present the shape of the Palmdale uplift between 1959 to 1974 are the consequence of heavy use of interpolations and extrapolations of original data to obtain meaningful contour lines (Castle, personal communication).

Considering the above factors in current geodetic measurements, the shape of geodetic network on which we obtain necessary components of displacement vectors becomes very suitable for this purpose if we choose it as a polygon. A triangle with equal side lengths as shown in Fig. 4 is one of the best choices because of its simplicity to obtain geodetic data on the side lines. It also minimizes the interpolations of data requiring only one internal data point at the center. This shape also has an advantage of reducing unnecessary bias due to orientations of the network which can be introduced if an arbitrary polygonal shape is used. (A circular net has no orientation problem, but it leads to unstable results). The use of a least squares method to obtain polynomial coefficients may not be advisable because we



need further interpolations to obtain necessary data. If we increase the number of data points along each side line of the geodetic network to use for the least square fitting the result may give better approximations for displacement vectors provided that we are dealing with data obtained on the network directly. If we are dealing with published data such as the case of the Palmdale uplift, the increase of data points may not necessarily bring better accuracy.

The size of the geodetic network is also an important factor for our inversion scheme because it is related to the accuracy of approximation of components of displacement vector on the surface by the polynomial expansion. It also determines how deep an error on the surface is propagated and amplified. If we use a smaller network we can match the data of higher frequency component, but the continuation of the data downward become more unstable unless data is error free as in the example of Chapter 2. In order to analyze errors involved in our inversion scheme, we shall use artificial data such as those generated by a buried point source or by a buried dislocation source.

#### 4.3. Testing with Artificial Data

In order to analyze the error involved in the inversion especially its dependence on the size of geodetic network, two sets of artificial data will be used. One is the displacement on the surface generated by a buried point force in a homogeneous half space (Mindlin, 1936) and the other is the displacement generated by a buried strip of dislocation in a homogeneous half space (Chinnery, 1958). The calculated stresses at depth by the inversion scheme are then compared with true stresses generated by these sources.

We used a configuration shown in Fig. 8 for the testing by the buried point force. A point force directed upward is placed along the vertical axis at various depths while a triangular geodetic network with various side lengths is set up at the center of coordinates on the surface. The configuration used for the testing by the buried dislocation source is shown in Fig. 9. An infinite vertical strip of dislocation with the horizontal Burger's vector with width of 60 km are placed along the x axis with its top at 20 km depth. The triangular geodetic network with various side lengths is set up at 15km off the center of coordinates on the surface. It is noted that the configuration used for the testing by the dislocation source is essentially similar to those used by Brown (1975) and Prescott and Savage (1976) to model the slip along the San Andreas fault in the big bend section. The rigidity and Poisson's ratio are assumed to be  $3.0 \times 10^{11}$  dyne/cm<sup>2</sup> and 0.25 respectively.

Fig. 10 shows the absolute error between the exact solution and inverted solution at  $(0, 0, -5\text{km})$  for a point force placed at various depths. The inverted solution was obtained by the use of a triangular network with 10km side. Fig. 11 shows the absolute error at  $(0, 0, -5\text{km})$  again as a function of the depth of the point force. In this case the side of the triangular network was chosen to be 30km. These figures show that the absolute errors are in general one order of magnitude smaller than the magnitude of the maximum principal stresses, when the artificial data generated by a point force is used.

In order to compare errors between our new analytic method the finite element method used previously (Ikeda, 1980), we inverted the artificial data due to the point force by both methods to obtain stress at  $(15, 15, -3.75\text{km})$ . The depth of the point force is varied from 30km to 80km. The difference between the exact solution and inverted one computed by the analytic method is shown in Fig. 12 as a function of the depth of the point force. A similar plot for the finite element is shown in Fig. 13.

It is shown that when the point source is located at a depth shallower than 30km, errors in both methods would be of the same order of magnitude, 10% or more of the maximum principal stress. When the location of the point force is deeper than 30km, however the analytic method gives errors of one order of magnitude smaller than the finite element method. For depth of the source greater than 50km, the error in the analytic method is less than 1% of the maximum principal

stress. The dependence of error on the depth of the point force, that is, the little difference between the two methods at shallow depths can be attributed to the fact that the finite element method with twelve 20 nodes isoparametric elements as shown in Fig. 7 has greater number of data sampling points on the surface than the analytic method. Thus even though the stress free conditions are not satisfied exactly in the finite element method solutions, it can accomodate small scale lateral variations in displacement somewhat more faithfully than the analytic method.

When the depth of the point force increases the lateral variation in displacement becomes smoother at the surface and the fit by polynomials in the analytic method become effective and the exactness of its solution gives better results than the finite element method.

The above examples show that these two methods of inversion, i.e. the analytic method and the finite element method may complement each other. Since it is easier in principle to improve the accuracy in the finite element method comparing to the formidable task of obtaining solutions with higher order of polynomials in the analytic method, we recommend the use of the analytic method to obtain a large-scale picture of the distribution of stress in the earth while the local, small-scale variation of stress may be better treated by the finite element method by introducing higher order interpolant such as 32 nodes isoparametric elements. Since the latter method requires a huge amount of memory space and computational time, it is recommended for application only

to important local spots requiring a special attention.

The efficiency of the analytic method when long wavelength components are dominant in data is demonstrated in Fig. 14 and Fig. 15 where the displacement due to a strip of dislocation is used as the artificial data and errors are presented as a function of the depth of the upper edge of the strip of dislocation. Fig. 14 shows that in the case of a triangular network with 10km side length, the absolute error between exact solution and inverted one is less than 1% of the absolute value of the maximum principal stress. The choice of 30km side length would increase the error, but still gives the errors smaller than a few % of the maximum principal stress.

Since most of the sources expected in nature are not as concentrated as the point source, we expect that when we apply our inverse scheme to real data errors are closer to those obtained for the strip of dislocation. This implies that if we use a triangular network of 30km side length, we can obtain solutions up to 10km depth with a reasonable accuracy provided that sources are located deeper than 20km. This situation may be applicable to the San Andreas fault region to which we apply our analytic method to find stresses at depths in the next chapter.

#### 4.4 Theoretical error estimate

Even though the numerical experiment using artificial sources such as the point force and the dislocation source in the previous section gives certain feelings about an error associated with the solution obtained by our analytic inverse method, there arises a question whether the accuracy of the inversion scheme holds for other types of source or not, and if not, what are contributing factors to affect the accuracy of the analytic inversion scheme. To resolve this question we must analyze the error theoretically and derive a theoretical bound of the error associated with the scheme.

Since the analytic scheme is essentially based on the application of the Cauchy-Kowalewsky theorem to Navier's equation in the elastostatics, i.e. eq. (346) to eq. (354), and the method is based on a generalized Taylor expansion of the solution in the neighborhood of a surface where Cauchy data are given and a determination of derivatives in this generalized Taylor expansion using Navier's equation and Cauchy data, we can analyze the error associated with the solution by analyzing errors associated with these Cauchy data and its derivatives.

We shall analyze the error associated with Cauchy data at first. Since Cauchy data for the inversion scheme are obtained using the triangular network and the stress free condition, the problem turns out to be an estimation of errors in an interpolation of a function in a triangular region when values are given at points on side lines of the triangle.

In the theoretical error estimate it is usually necessary to assume a differentiability of the exact solution up to a certain order. Since we are using the cubic polynomial as an interpolation function on the surface, we assume that the exact solution belongs  $C^4$ , i.e. a class of functions that have fourth order derivatives. Then we shall use a theorem for the interpolation of a function in the triangular region. That is:

Theorem: Given a function  $f(x,y) \in C^4$  and a cubic Lagrange polynomial  $P_3(x,y)$  which has values coincide with those of  $f$  at 9 nodes on sides of the triangle and a center node of the triangle, there exist a constant  $C_k$  which is independent of  $f$ ,  $h$ ,  $\theta$  such as

$$\left| \frac{\partial^k}{\partial x^i \partial y^j} f - \frac{\partial^k}{\partial x^i \partial y^j} P_3 \right| < C_k \frac{h^{4-k}}{\sin \theta} \max \left| \frac{\partial^4}{\partial x^m \partial y^n} f \right| \quad (355)$$

where  $\theta < i + j = k < 3$ ,  $m + n = 4$ ,  $\theta$  is a minimum angle of the triangle, and  $h$  is a maximum distance between nodes. A proof of this theorem is given in Prenter (1975) or Zlamal (1968).

Using this theorem we have error bounds for the displacement component  $u$  and its derivatives on the free surface. They are, explicitly (Zlamal, 1968)

$$|u - u_n| < \frac{3h^4}{\sin \theta} \max \left| \frac{\partial^4 u}{\partial x^m \partial y^n} \right| \quad (356)$$

$$\left| \frac{\partial u}{\partial x} - \frac{\partial u_n}{\partial x} \right| < \frac{5h^3}{\sin \theta} \max \left| \frac{\partial^4 u}{\partial x^m \partial y^n} \right| \quad (357)$$

$$\left| \frac{\partial u}{\partial y} - \frac{\partial u_n}{\partial y} \right| < \frac{5h^3}{\sin \theta} \max \left| \frac{\partial^4 u}{\partial x^m \partial y^n} \right| \quad (358)$$

$$\left| \frac{\partial^2 u}{\partial x^2} - \frac{\partial^2 u_n}{\partial x^2} \right| < \frac{9h^2}{\sin \theta} \max \left| \frac{\partial^4 u}{\partial x^m \partial y^n} \right| \quad (359)$$

$$\left| \frac{\partial^2 u}{\partial x \partial y} - \frac{\partial^2 u_n}{\partial x \partial y} \right| < \frac{9h^2}{\sin \theta} \max \left| \frac{\partial^4 u}{\partial x^m \partial y^n} \right| \quad (360)$$

$$\left| \frac{\partial^2 u}{\partial y^2} - \frac{\partial^2 u_n}{\partial y^2} \right| < \frac{9h^2}{\sin \theta} \max \left| \frac{\partial^4 u}{\partial x^m \partial y^n} \right| \quad (361)$$

$$\left| \frac{\partial^3 u}{\partial x^3} - \frac{\partial^3 u_n}{\partial x^3} \right| < \frac{12h}{\sin \theta} \max \left| \frac{\partial^4 u}{\partial x^m \partial y^n} \right| \quad (362)$$

$$\left| \frac{\partial^2 u}{\partial x^2 \partial y} - \frac{\partial^2 u_n}{\partial x^2 \partial y} \right| < \frac{12h}{\sin \theta} \max \left| \frac{\partial^4 u}{\partial x^m \partial y^n} \right| \quad (363)$$

$$\left| \frac{\partial^3 u}{\partial x \partial y^2} - \frac{\partial^3 u_n}{\partial x \partial y^2} \right| < \frac{12h}{\sin \theta} \max \left| \frac{\partial^4 u}{\partial x^m \partial y^n} \right| \quad (364)$$

$$\left| \frac{\partial^3 u}{\partial y^3} - \frac{\partial^3 u_n}{\partial y^3} \right| < \frac{12h}{\sin \theta} \max \left| \frac{\partial^4 u}{\partial x^m \partial y^n} \right| \quad (365)$$



where  $u_n$  is an approximated value and  $m, n = 1, 2, 3, 4$  with  $m + n = 4$ . Similar error bounds for other displacement components are obtained by replacing  $u$  and  $u_n$  in eq. (356) to eq. (365) with  $V, W, V_n$  and  $W_n$ . These equations represent the error associated with Cauchy data and their derivatives on the surface. It is apparent from these equations that the truncation error on the surface is governed by fourth order derivatives of data functions and parameters  $h$  and  $\theta$ . Thus an equal length triangle with equal distances between nodes is an optimal choice to interpolate surface data with minimum truncation error.

The error associated with the stress components below the free surface is obtained by using these error estimates for Cauchy data and their derivatives in applying Cauchy-Kowalewsky theorem to Navier's equation.

To obtain the error estimate associated with stress components, we shall assume that the solution belongs to a class of function  $\epsilon R^3$ , i.e. differentiable up to third order. Expanding the solution near origin  $(0, 0, \Delta z)$  into the generalized Taylor series we have for  $\sigma_{xx}$  as

$$\begin{aligned} \sigma_{xx}(0, 0, \Delta z) = & \sigma_{xx} \Big|_{z=0} + \frac{\partial \sigma_{xx}}{\partial z} \Big|_{z=0} \Delta z + \frac{\partial^2 \sigma_{xx}}{2 \partial z^2} \Big|_{z=0} \Delta z^2 \\ & + \frac{\partial^3 \sigma_{xx}}{6 \partial z^3} \Big|_{z=0} \Delta z^3. \end{aligned} \quad (366)$$

Eq. (366) shows that the error associated with  $\sigma_{xx}$  is equivalent to a sum of errors associated with these Cauchy data and their derivatives.

Using Navier's equation, i.e. eq. (346) to eq. (354) the first term in R.H.S. of eq. (366) is represented as

$$\sigma_{xx} = (\lambda + 2\mu) \frac{\partial u}{\partial x} + \mu \frac{\partial v}{\partial y} + \mu \frac{\partial w}{\partial z}. \quad (367)$$

Since we have, by stress free condition on the surface

$$\frac{\partial w}{\partial z} = - \frac{\mu}{\lambda + 2\mu} \left( \frac{\partial u}{\partial x} + \frac{\partial v}{\partial y} \right) \quad (368)$$

$$\frac{\partial u}{\partial z} = - \frac{\partial w}{\partial x} \quad (369)$$

$$\frac{\partial v}{\partial z} = - \frac{\partial w}{\partial y}, \quad (370)$$

eq. (367) is further modified as

$$\sigma_{xx} = \frac{(\lambda + 2\mu)^2 - \mu^2}{\lambda + 2\mu} \frac{\partial u}{\partial x} + \frac{(\lambda + 2\mu)\mu - \mu^2}{\lambda + 2\mu} \frac{\partial v}{\partial y} \quad (371)$$

The second, third and the fourth terms of R.H.S. of eq. (366) are represented as

$$\frac{\partial \sigma_{xx}}{\partial z} = \frac{\mu^2 - (\lambda + 2\mu)^2}{\lambda + 2\mu} \frac{\partial^2 w}{\partial x^2} + \frac{\mu^2 - (\lambda + 2\mu)\mu}{\lambda + 2\mu} \frac{\partial^2 w}{\partial y^2}. \quad (372)$$

$$\begin{aligned} \frac{\partial^2 \sigma_{xx}}{\partial z^2} &= \frac{\mu^2 - (\lambda + 2\mu)^2}{\lambda + 2\mu} \frac{\partial}{\partial z} \left( \frac{\partial^2 w}{\partial x^2} \right) + \frac{\mu^2 - (\lambda + 2\mu)\mu}{\lambda + 2\mu} \frac{\partial}{\partial z} \frac{\partial^2 w}{\partial y^2} \\ &= \frac{\mu^2 - (\lambda + 2\mu)^2}{\lambda + 2\mu} \frac{\partial^2}{\partial x^2} \left\{ \frac{-\mu}{\lambda + 2\mu} \left( \frac{\partial u}{\partial x} + \frac{\partial v}{\partial y} \right) \right\} + \end{aligned} \quad (373)$$

$$\frac{\mu^2 - (\lambda + 2\mu)\mu}{\lambda + 2\mu} \frac{\partial^2}{\partial y^2} \left\{ \frac{-\mu}{\lambda + 2\mu} \left( \frac{\partial u}{\partial x} + \frac{\partial v}{\partial y} \right) \right\}$$

$$\begin{aligned} &= \frac{-\mu^3 + (\lambda + 2\mu)^2 \mu}{(\lambda + 2\mu)^2} \left( \frac{\partial^3 u}{\partial x^3} + \frac{\partial^3 v}{\partial x^2 \partial y} \right) + \frac{-\mu^3 + (\lambda + 2\mu)\mu^2}{(\lambda + 2\mu)^2} \left( \frac{\partial^2 u}{\partial x \partial y^2} + \frac{\partial^3 v}{\partial y^3} \right) \end{aligned} \quad (374)$$

$$\frac{\partial^3 \sigma_{xx}}{\partial z^3} = \frac{\mu^3 - (\lambda + 2\mu)^2 \mu}{(\lambda + 2\mu)^2} \left( \frac{\partial^4 w}{\partial x^4} + \frac{\partial^4 w}{\partial x^2 \partial y^2} \right) + \frac{\mu^3 - (\lambda + 2\mu)\mu^2}{(\lambda + 2\mu)^2} \left( \frac{\partial^4 w}{\partial x^2 \partial y^2} + \frac{\partial^4 w}{\partial y^4} \right)$$

Since error bounds for derivatives in eq. (367) to eq. (374) are given by eq. (356) to eq. (365), we obtain the error bound by summing them up. This summation of these error bounds can be simplified further if we assume a Poisson solid, i.e.  $\lambda = \mu$ . The error bounds for each term in R.H.S. of eq. (366) are therefore

$$\begin{aligned} \sigma_{xx} \Big|_{z=0} - \sigma_{xx_n} \Big|_{z=0} &< \frac{8 \mu 5h^3}{3 \sin \theta} \max |D^4 u| + \frac{2 \mu 5h^3}{3 \sin \theta} \max |D^4 v| \\ &< \frac{17 \mu h^3}{\sin \theta} \max \{|D^4 u|, |D^4 v|\} \end{aligned} \quad (375)$$

$$\frac{\partial \sigma_{xx}}{\partial z} \Big|_{z=0} - \frac{\partial \sigma_{xx_n}}{\partial z} \Big|_{z=0} < \frac{30 \mu h^2}{\sin \theta} \max |D^4 w| \quad (376)$$

$$\begin{aligned} \frac{\partial^2 \sigma_{xx}}{\partial z^2} \Big|_{z=0} - \frac{\partial^2 \sigma_{xx_n}}{\partial z^2} \Big|_{z=0} &< \frac{10}{9} \frac{12h}{\sin \theta} \max |D^4 u| + \frac{10}{9} \frac{12h}{\sin \theta} \max |D^4 v| \\ &< \frac{14 \mu h}{\sin \theta} \max \{|D^4 u|, |D^4 v|\} \end{aligned} \quad (377)$$

$$\frac{\partial^3 \sigma_{xx}}{\partial z^3} \Big|_{z=0} - \frac{\partial^3 \sigma_{xx_n}}{\partial z^3} \Big|_{z=0} < \frac{20 \mu}{9} \max |D^4 w| \quad (378)$$

where  $\sigma_{xx_n}$  denotes an approximation of the solution and

$$D^4 u = \frac{\partial^4 u}{\partial x^m \partial y^n} \quad 0 \leq m, n \leq 4 \quad m + n = 4. \quad (379)$$

Plugging these error bounds for Cauchy data and their derivatives into the generalized Taylor expansion i.e. eq. (366), we have total error bound for  $\sigma_{xx}$  at the depth of  $\Delta z$  as

$$|\sigma_{xx} - \sigma_{xx_n}| < \frac{17 \mu h^3}{\sin \theta} \max \{|D^4 u|, |D^4 v|\} + \frac{30 \mu h^2}{\sin \theta} \max |D^4 w| \Delta z$$

$$\frac{7 \mu h}{\sin \theta} \max \{|D^4 u|, |D^4 v|\} \Delta z^2$$

(380)

$$+ \frac{20 \mu}{54} \max |D^4 w| \Delta z^3$$

$$< \frac{(17h^3 + 30h^2 \Delta z + 7h \Delta z^2 + 0.4 \Delta z^3) \mu}{\sin \theta} \max \{|D^4 u|, |D^4 v|, |D^4 w|\}.$$

Error bounds for other stress components can be obtained in a similar manner and thus we have a general expression for the theoretical error bounds for stresses at depth as

$$|\sigma_{ij} - \sigma_{ij_n}| < \frac{K h_0^3 \mu}{\sin \theta} \max \{|D^4 u|, |D^4 v|, |D^4 w|\} \quad (381)$$

where  $h_0 = \max \{|h|, |\Delta z|\}$  and  $K$  is a constant which is independent with the triangle and  $u, v, w$ .

The above general expression for the error bound shows that contributing factors for the error involved in our analytic inversion scheme based on the cubic polynomial expansion are the minimum angle of the triangle, the maximum distance between nodes along the side of the triangle, the depth at which solution should be obtained, and the fourth order derivative

of the solution. If the displacement on the surface are represented by the second order polynomial i.e.  $f \in R^3$ , then the analytic inversion scheme gives an exact solution throughout the half space as expected.

It should be stated that actual errors involved in the analytic scheme are usually smaller than those indicated by previous analysis because these estimates are giving only upper bounds of possible errors. It is also well known that errors are considerably less on each node when one is approximating a function by polynomials (Douglas and Dupont, 1974). Therefore constants in the error estimate can be taken to be smaller ones if we calculate solutions along an axis which passes the center node.

It is also clear from this analysis that we should use the equal angle triangle geodetic network as small as possible to obtain necessary Cauchy data because the error bound decreases when the maximum distance between nodes on the triangle decreases. Therefore a limitation of the analytic inversion scheme is imposed by an availability of necessarily dense coverage of geodetic networks. Since current geodimeter measurements are performed along the line which has commonly 30 km of length, it is useless to use geodetic triangles with side lengths less than 30 km as long as the error contribution from geodimeter measurement is concerned. On the other hand the error contribution from levelling measurement can be improved if we use smaller triangular networks provided that we can use initially obtained data along such a small closure for the levelling route.

## Figure Captions for Chapter 4

- Fig. 8. Model of the point force used for generating artificial data.
- Fig. 9. Model of the dislocation source used for generating artificial data.
- Fig. 10. Absolute error by the analytic method at (0.0, -5km) as a function of depth of the point force in the case of the triangle network of 10km side length. The top curve shows a maximum signal level.
- Fig. 11. Absolute error by the analytic method at (0.0, -10km) as a function of depth of the point force in the case of the triangle network of 30km side length. The top curve shows a maximum signal level.
- Fig. 12. Absolute error by the analytic method at (15km, 15km, -3.75km) as a function of depth of the point force in the case of the triangle network of 10km side length. The top curve shows a maximum signal level.
- Fig. 13. Absolute error by the finite element method at (15km, 15km, -3.75km) as a function of depth of the point force in the case of depth of the rectangular cube of 10km side length. The top curve shows a maximum signal level.
- Fig. 14. Absolute error by the analytic method at (15km, 15km, -5km) as a function of depth of the dislocation source in the case of the triangle network of 10km side length. The top curve shows a maximum signal level.

Fig. 15. Absolute error by the analytic method at (15km, 15km, -10km) as a function of depth of the dislocation source in the case of the triangle network of 30km side length. The top curve shows a maximum signal level.



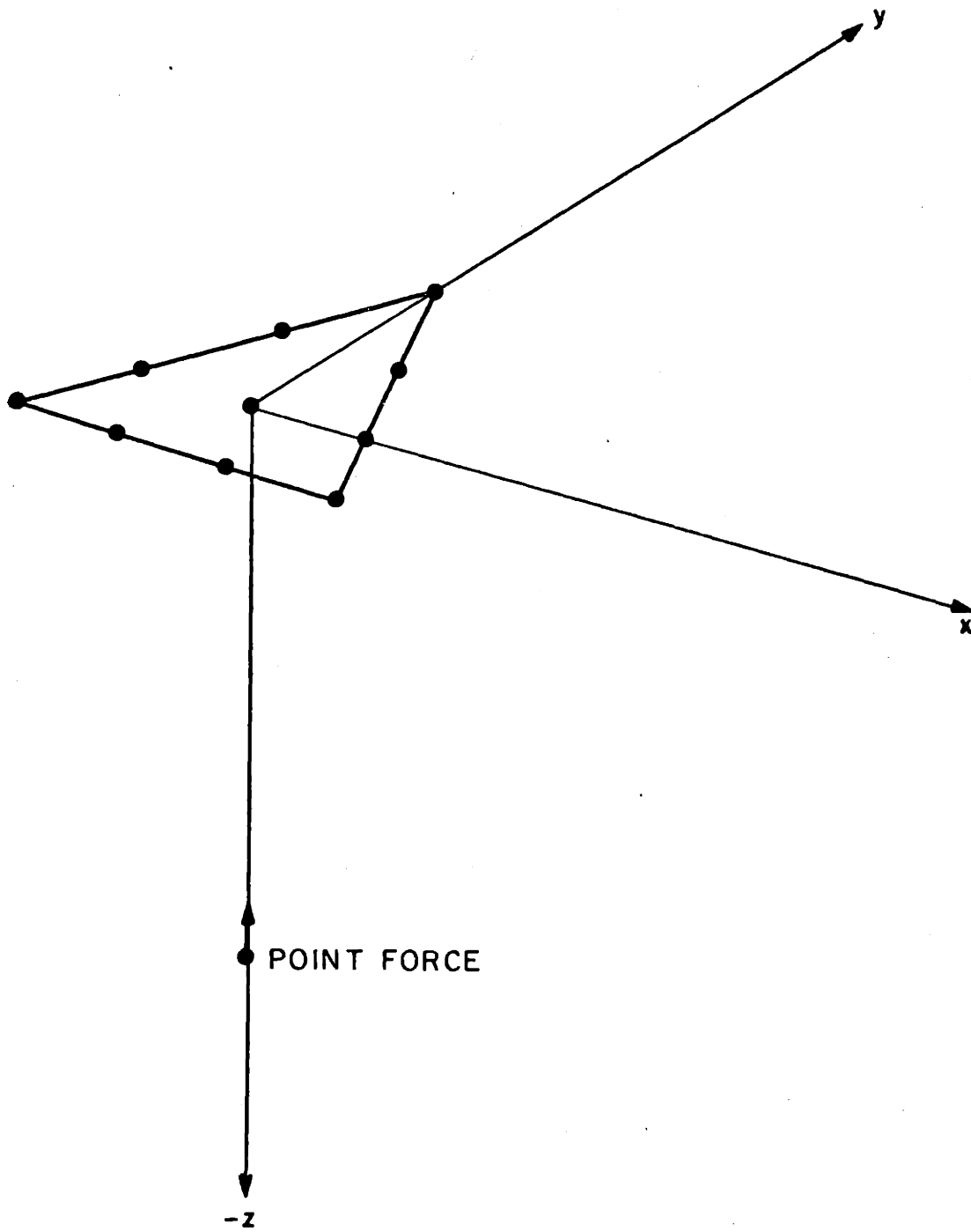


FIG. 8

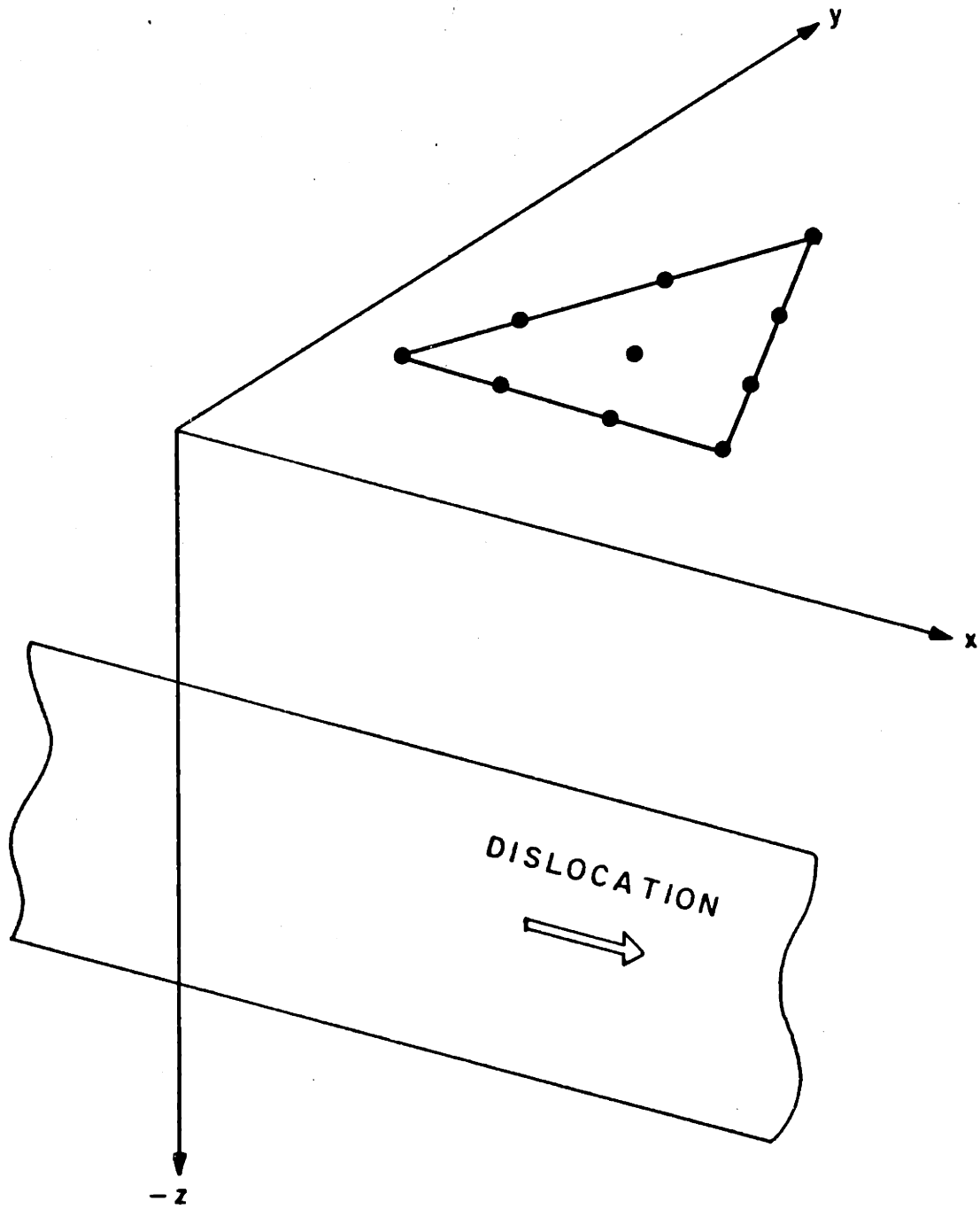


FIG. 9

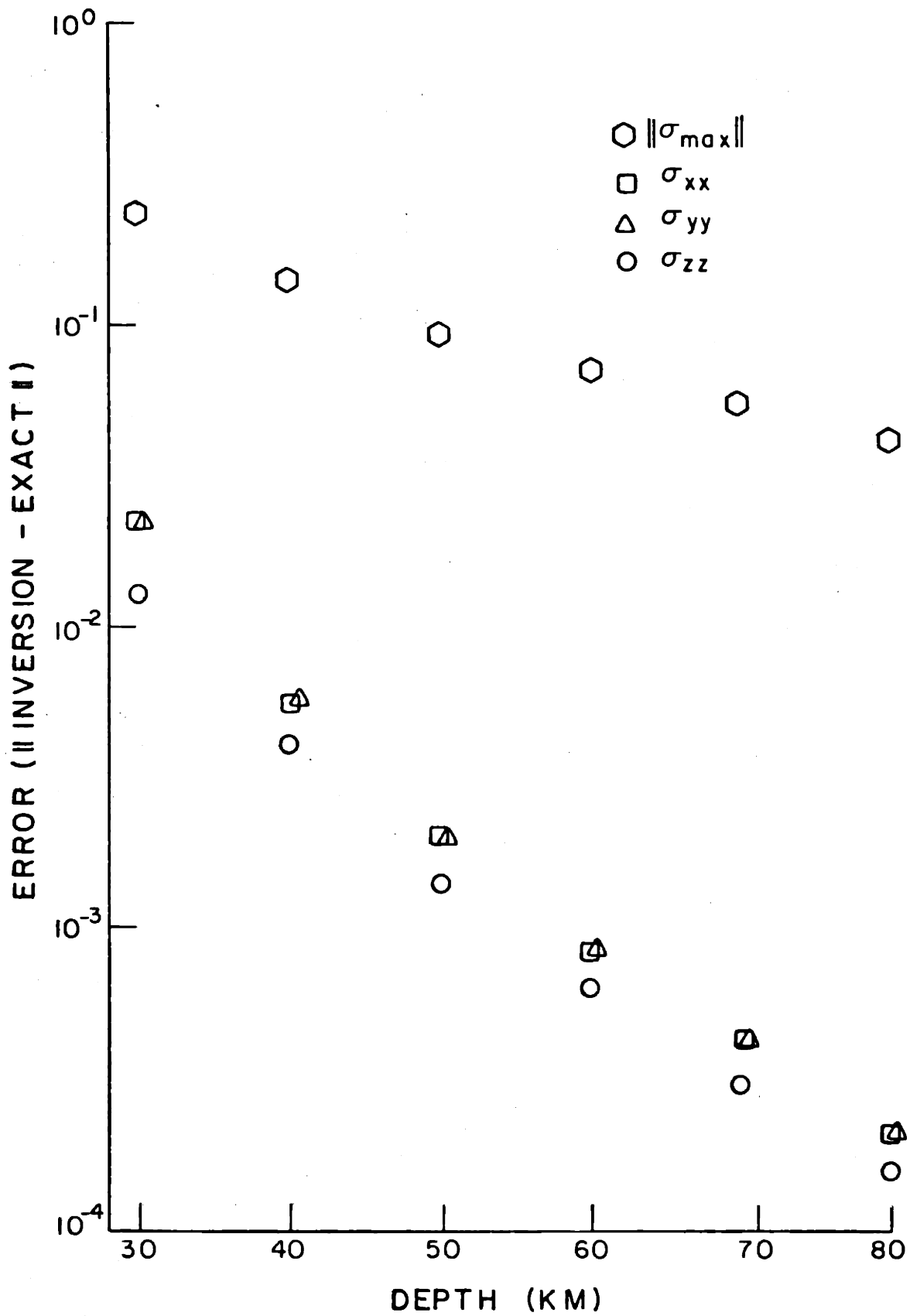


FIG. 10

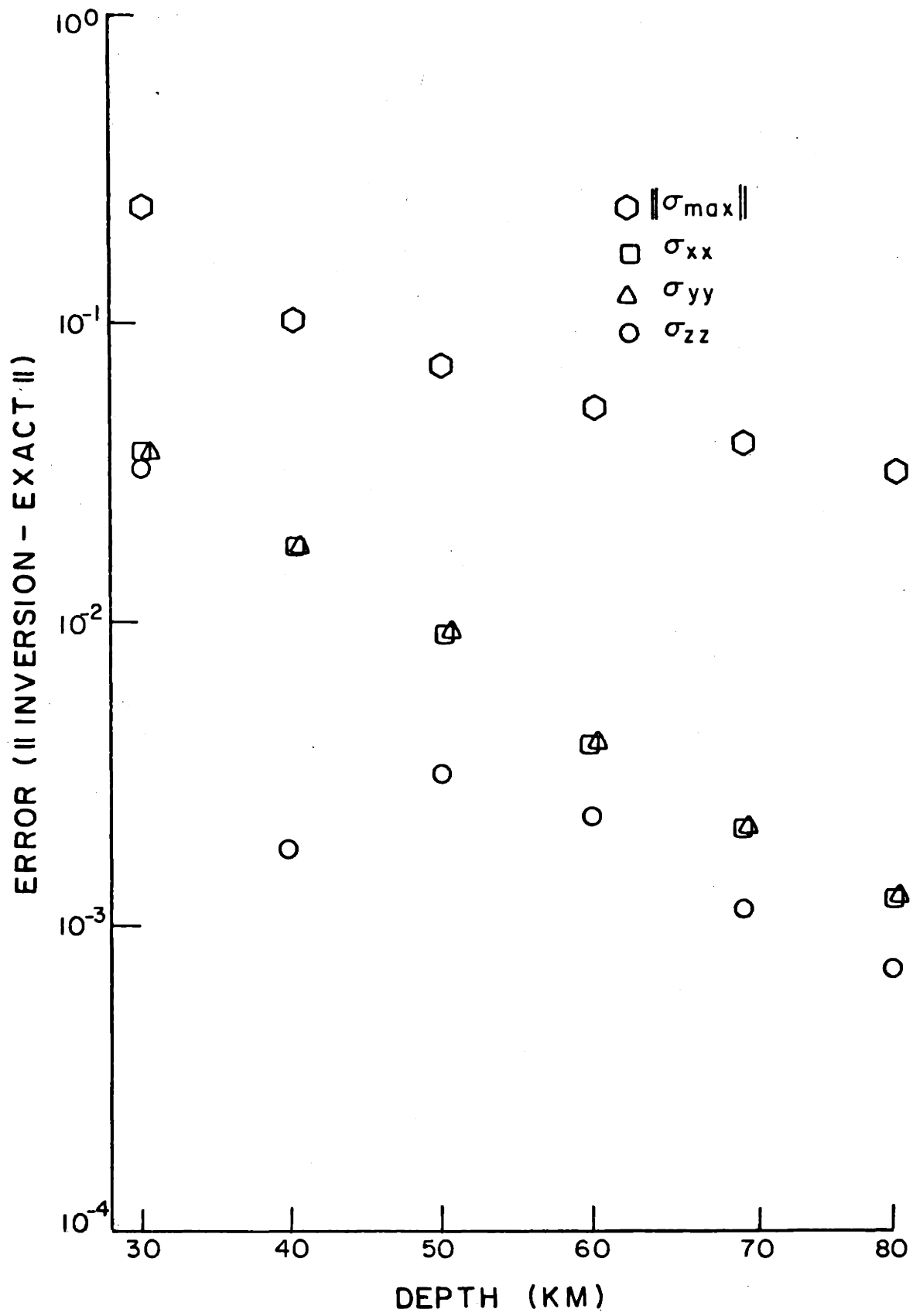


FIG. II

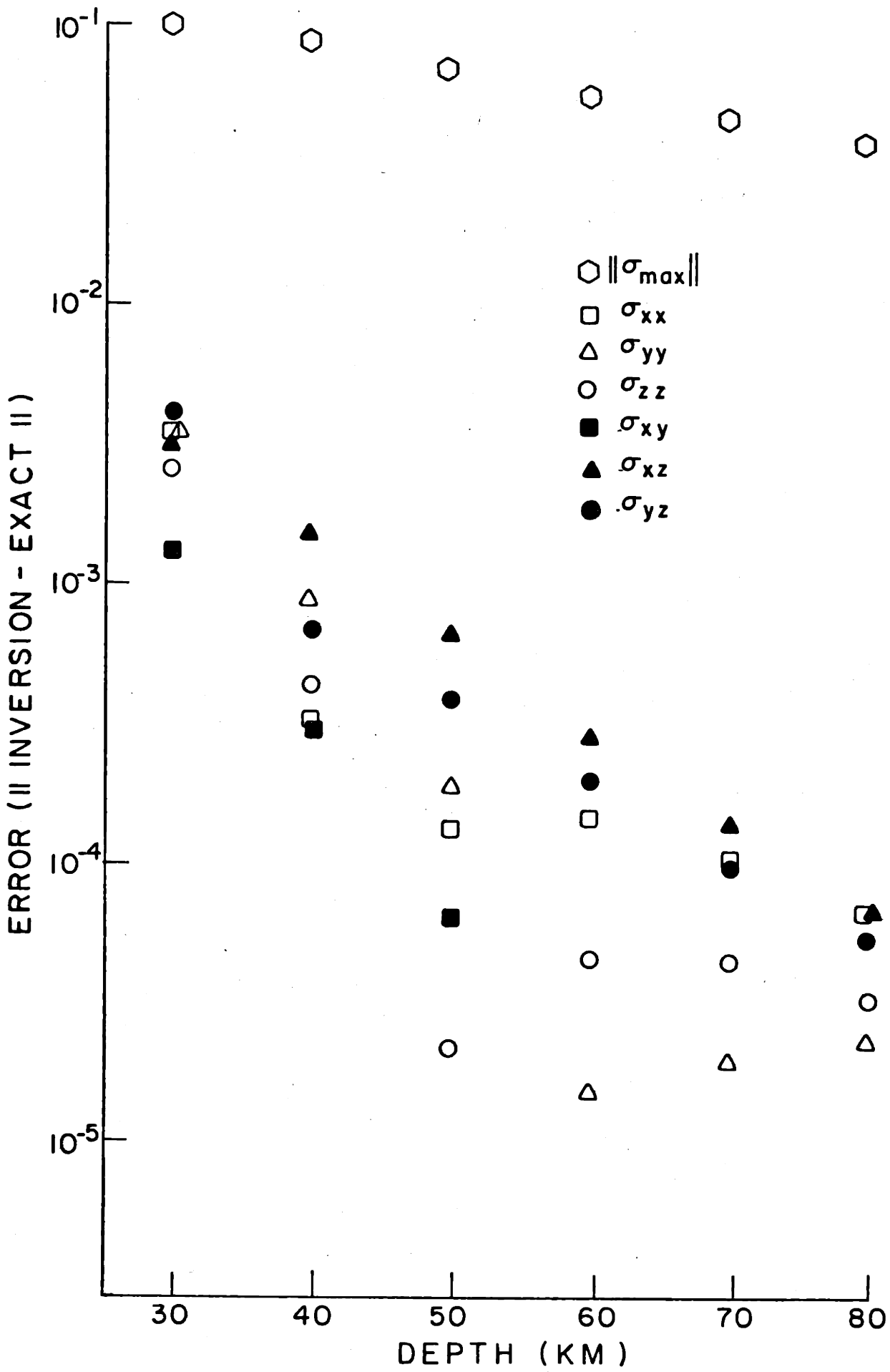


FIG. 12

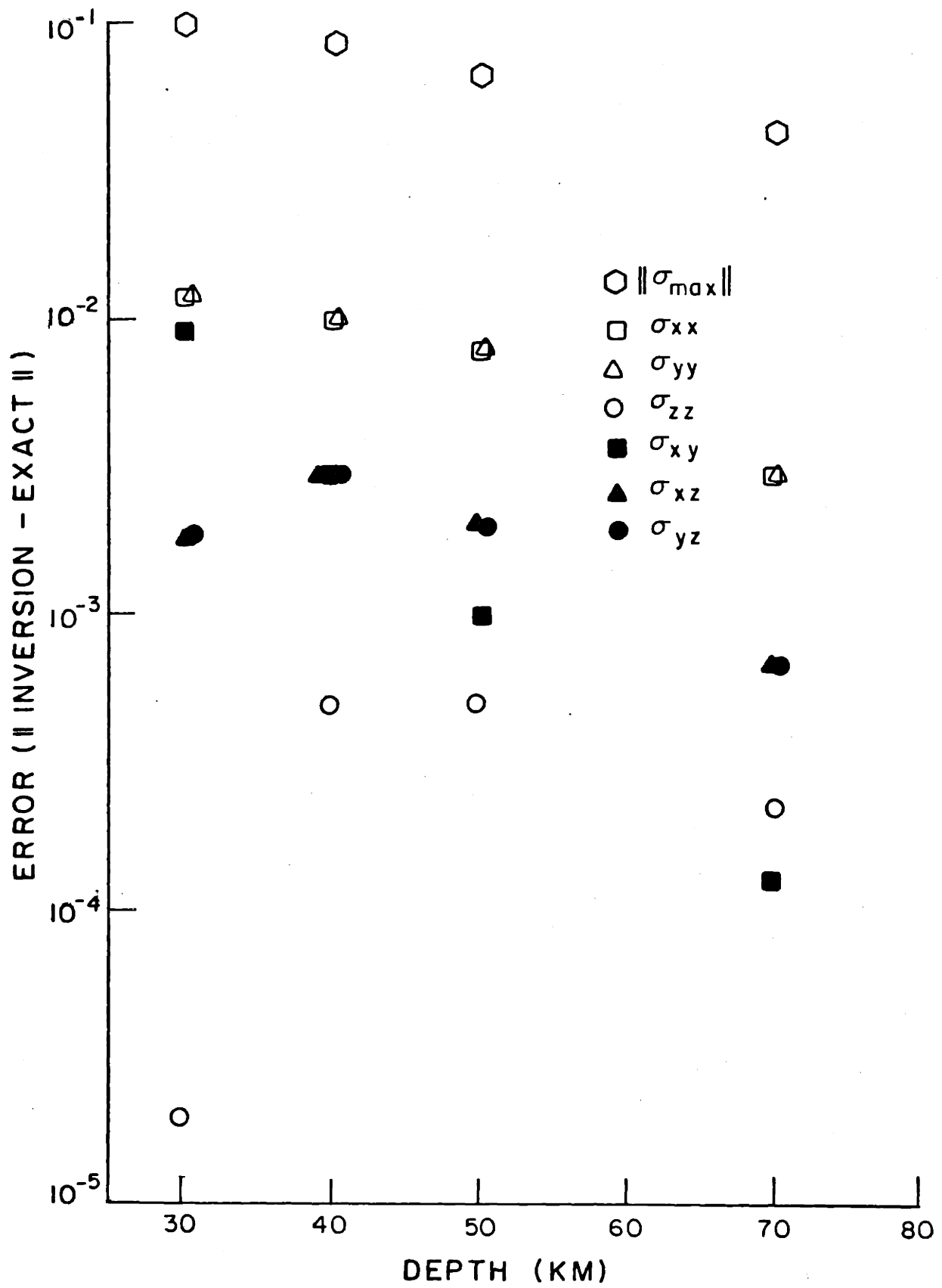


FIG. 13

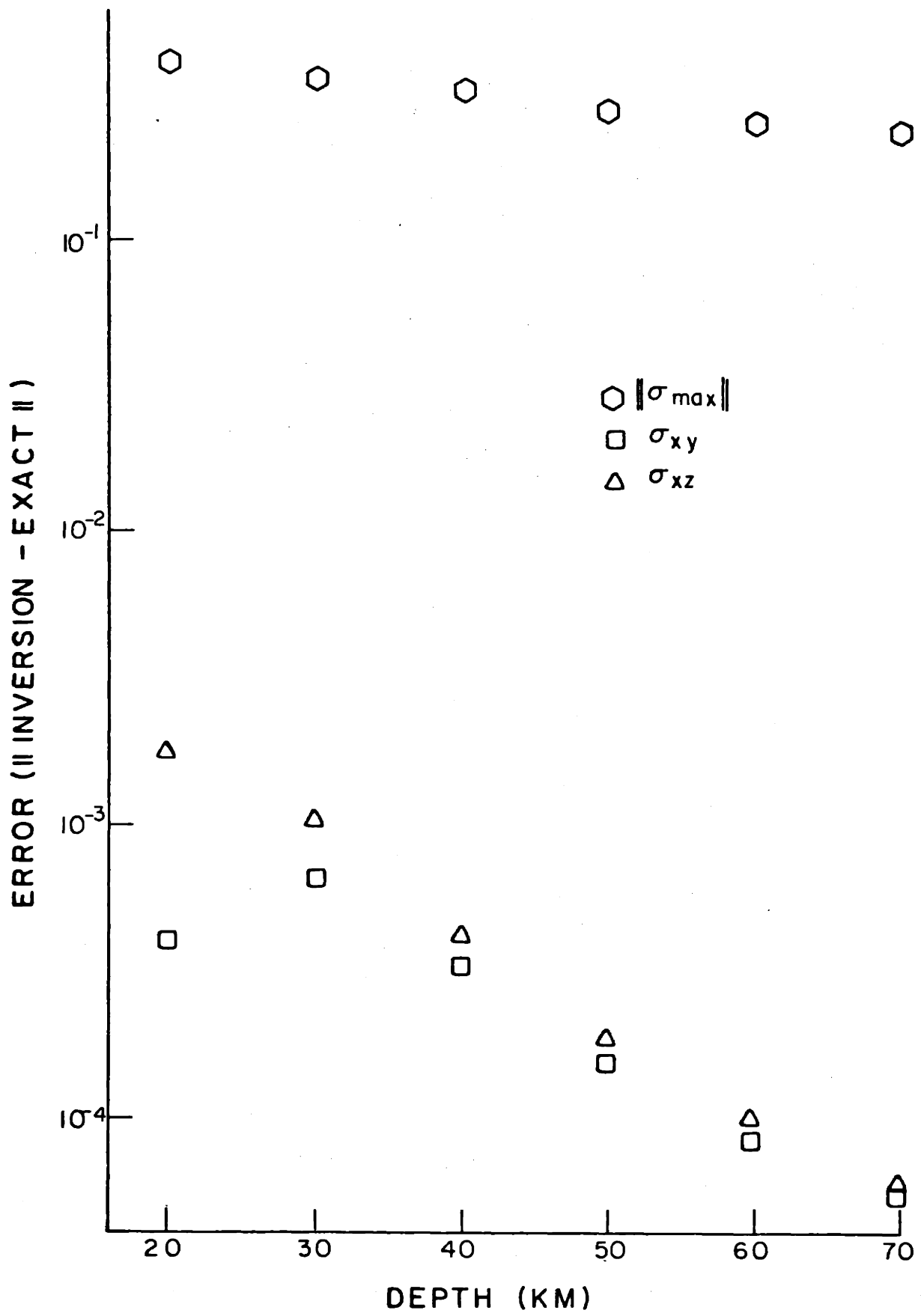


FIG. 14

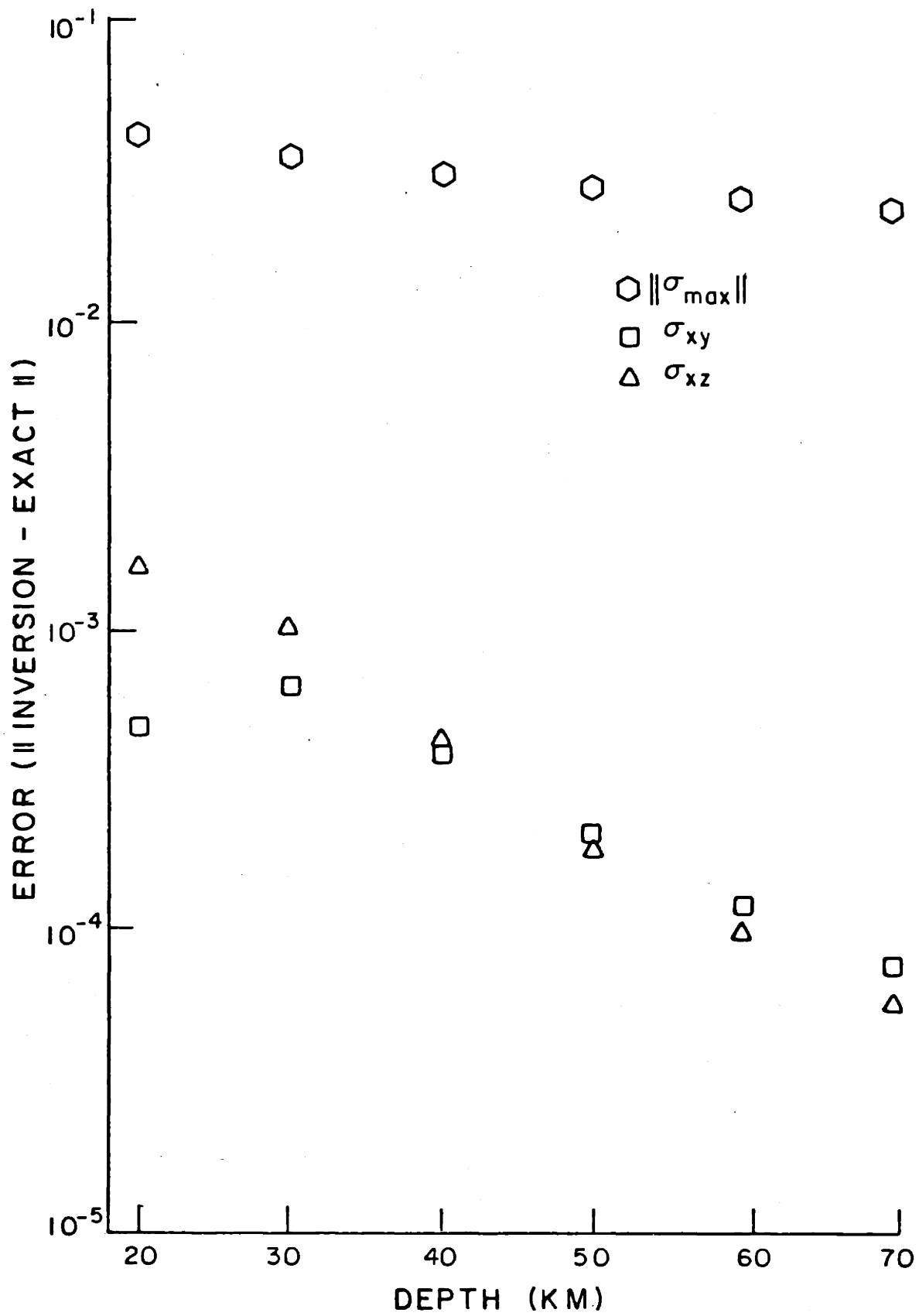


FIG. 15



## CHAPTER 5. PALMDALE UPLIFT

5.1 Geodetic data

In Southern California an uplift called Palmdale bulge, over an area of 300km x 150 km along the San Andreas fault, was first discovered in 1975 from the levelling work relative to a bench mark called "tidal 8" at San Pedro and reported by Castle et al. (1976). The pattern of uplift is shown in Fig. 16. This observation was mainly based on the levelling survey conducted between 1959 and 1968, and large scale high precision levelling survey was conducted since then. The result of these continued measurements revealed that the bulge was wider than estimated at first and also greater in displacement (Castle, 1978). It was also found that part of initial uplift subsided since 1974 although the space-time history of this subsidence or "downwarp" is quite uncertain. These results are shown in Fig. 17.

According to Castle (1978), the whole episode of uplift consists of three stages.

Stage 1: The uplift began near the intersection of the Garlock fault and the San Andreas fault in late 1959 and spread eastward which is confirmed by the continuous levelling near Palmdale showing that this area uplifted by 20 cm during 1959-1962 period. This is shown in Fig. 18. The uplift gradually increased by another 15 cm in the next 10 years.

Stage 2: Between late 1972 and early 1974, the area of uplift expanded to the southeast, where a maximum uplift of 45 cm occurred near Yucca Valley.

Stage 3: Between late 1974 and late 1976, much of the uplift subsided. This downwarp reached 18 cm near Palmdale, 16 cm near Cajon, and 24 cm in Mojave.

Although there have been some arguments that attribute some parts of the uplift to measurement errors associated with calibrations of rod (Lee and Jackson, 1978), in the present paper, we shall accept that the uplift shown in Fig. 18 was real.

Since Reid's suggestion on monitoring a strain accumulation as an earthquake precursor (Reid, 1910), extensive triangulation survey has been conducted in California by several agencies (Savage et al., 1973, Thatcher, 1976). These data show that the general trend of horizontal strain accumulation near Big Bend is 0.3~0.4 microstrain per year of contraction in NS direction and 0.0~0.1 microstrain per year of extension in EW direction. This pattern of strain accumulation is consistent with the regional stress expected here from plate tectonics (Atwater and Molnar, 1973).

After the discovery of the Palmdale Bulge, interest in the relationship between horizontal strain accumulation and uplift during the uplift period is increased and many data were reanalyzed.

Using triangulation network near Big Bend shown in Fig. 19 Thatcher (1976) discussed that the direction of strain axes were significantly different from the long term regional trend

during the uplift period 1959-1963. He suggested that the compressional axes are perpendicular to the contour of uplift almost everywhere. But his conclusion was based on Frank's method that uses only the change of angle in a triangulation network and therefore we can superpose an arbitrary amount of dilatation on his result. As Savage and Prescott stated, this fact makes his result model dependent.

Savage et al. (1973) analyzed geodimeter data along the San Andreas fault as shown in Fig. 19 and revealed no special change during the period 1950-1972. The obtained data shows 0.4 microstrain per year of contraction in N13°E direction and 0.1 microstrain per year of extension in the direction of N77°W near the intersection of Garlock fault and San Andreas fault. Near Palmdale, they observed 0.31 microstrain per year of contraction in the direction of N7°E and 0.07 microstrain per year of extension in the direction of N83°W. These results are based on the change of the length of line and are therefore not model dependent.

## 5.2 Inversion

In order to apply our inversion scheme to Palmdale Bulge, we used the triangular network as shown in Fig. 4 with the length of each side to be 30 km. The horizontal displacements at points of each triangular network are obtained using Savage's data for accumulated strains between 1959 to 1974, assuming a constant strain rate uniform within each triangle.

Vertical displacements are read from the contour map given by Castle et al., (1976). Rigidity of  $3 \times 10^{11}$  dyne/cm<sup>2</sup> and Poisson's ratio of 0.25 are assumed. Since the space-time distribution of downwarp is not well-defined, we analyze only the data obtained during 1959-1974 which is based on the map of the bulge shown in Fig. 16.

With these data on three-components of the displacement vector as input to our inversion scheme, we obtained incremental stresses inside each triangular network that are distributed along the San Andreas fault as shown in Fig. 20. Denoting centers of each triangle as point 1, ...8, 1N...8N, 1S...8S, points 1 to 8 are set up along the San Andreas fault with 25 km intervals between each other. Points 1N to 8N are set up 25 km north of points 1 to 8 and points 1S to 8S are set up 25 km south of points 1 to 8. Data for each triangular network are listed in Table 2.

Principal axes of incremental stresses accumulated during the period 1959 to 1974 are calculated below the center of each triangle at 5 km and 10 km depth as listed in Table 3.

At the surface, the principal stresses are composed of a horizontal compressional stress directed nearly in the north-south, a horizontal vanishingly small stress directed nearly in the east-west, and a vertical stress with zero magnitude. We shall call these three principal stresses as the E-W principal stress, the N-S principal stress and the near vertical principal stress.

It is easy to identify these three principal stresses at depths although their direction rotates with depth. The near vertical stress is identified as the one with the greatest dip angle. The E-W stress is identified, then, as one of the two remaining stresses having the azimuth closer to the east-west. Once the identification is made, the magnitude and orientation are shown separately for each stress on the map in Fig. 21 to Fig. 30.

The N-S principal stress at 10km depth is everywhere compressional. Its azimuth and dip are nearly the same as at the surface, with rotation up to  $28^\circ$ . The magnitude, however, increases up to 12 bars from the surface value of 3.5-4.5 bar. The maximum increase occurs along the fault near Palmdale where the vertical displacement has also the maximum value.

The E-W principal stress, on the other hand, changes the orientation considerably with depth especially with respect to the dip angle (up to  $44^\circ$ ). This stress is compressional almost everywhere, and again shows the maximum of 6 bars in the same area where the N-S principal stress reaches the peak value. This result shows that the incremental shear stress along the fault at 10km depth near Palmdale is only slightly greater than at the surface, but the incremental normal compressional stress increases with depth considerably, suggesting a locking mechanism on the San Andreas fault during the period of Palmdale uplift.

It is interesting to note that a swarm of microearthquakes occurred in this area during 1977 to 1978

(McNally et al., 1979) which may be attributed to a sudden release of this high compressional stress due to the downwarp of the bulge.

Finally, the near vertical principal stress at 10km depth shows quite a variable orientation from place to place. It is, however, significant that this stress is tensional almost everywhere with the magnitude up to 1.7 bars. Thus, the state of incremental stress at 10km depth under the Palmdale bulge is characterized by an increased horizontal compression and an increased vertical tension while the shear stress on the fault was only slightly greater than at the surface.

### 5.3 Error estimate for the result from Palmdale data

In the preceding chapter we observed that the error associated with the triangle of 30 km side length at the point (0, 0, -10 km) was an order of magnitude smaller than the magnitude of the maximum principal stress when artificial data from the point source was used. Although this error bound is very attractive it is based on an assumption that data obtained at nodes are original data, i.e. without any processing of data such as linear interpolations and also they are not contaminated by measurement errors. This assumption is obviously not applicable when we use real geodetic data to apply our inverse scheme to real problems such as Palmdale uplift.

The first part of the assumption, i.e. no processing or manipulation on original data is most severely violated in triangulation or geodimeter measurements for horizontal displacements because these measurements are performed along

single lines with two nodes at the end of line and therefore we can obtain only a linear variation of horizontal displacements along each measurement line. If these measurements along lines are connected together we can obtain higher order variations of horizontal displacements by using piecewise linear interpolations but usually this is not the case. At Palmdale network, geodimeter measurements are performed along lines that have typically 30 km length and therefore we can obtain only linearly interpolated data of actual horizontal displacements if we use a triangle of 30 km side length for our inversion.

On the other hand, levelling data are in a better position than geodimeter data even though they are processed heavily to draw meaningful contours for vertical displacements. This is because measurements are made usually at short intervals along a levelling route, and, therefore, the use of many sampling points is worthwhile even after original data are processed by some countering schemes. This higher spatial resolution is the advantage of levelling data as compared to the geodimeter data. Thus, the truncation error would be less serious for levelling data than for geodimeter data.

To analyze the effect of the truncation error in horizontal displacement data due to linear interpolations, we again use the numerical experiment with the point source

because this extreme case gives us certain upper bounds for errors involved in the inversion with actual geodetic data. We use the same configuration as Fig. 8 but use linearly interpolated horizontal displacements and original vertical displacements. The linear interpolation of horizontal components is done by taking data at three peaks of the triangle and then interpolating the data linearly along each side of the triangle. Vertical components are used without any processing. The absolute errors between solutions of our inversion scheme and theoretical ones at a point (0, 0, -10 km) are plotted as a function of depth of the point source in Fig. 31.

This figure shows that it is very dangerous to use interpolations of different orders for different components of displacements because the error reaches the same order of magnitude as the magnitude of maximum principal stress if point source is placed very shallow. Since a configuration of vertical contours of Palmdale uplift near Palmdale is more or less comparable with displacements generated by the point source located at depths 30 km to 40 km, we can estimate an upper bound of absolute errors involved in our inversion at Palmdale using real geodetic data with linearly interpolated horizontal components to be 90% of maximum principal stresses from Fig. 31.

This rough estimate for the upper bound of errors is considerably large and may cause a question about a practicality of our inversion scheme as long as currently



available geodetic data are being used. Fortunately, we can lower this upper bound of errors for the inversion near Palmdale because we have horizontal displacement data from another geodimeter network which consists of lines of short length less than 10 km (Prescott and Savage, 1976). Since data from this smaller network are showing the same linear horizontal displacements as those obtained by the larger geodimeter network with 30 km line lengths that provides basic data used in the inversion in the previous section, we can assume that near Palmdale. The linearity of horizontal displacement is not a result of a small number of sampling points but is reflecting real linearly varying displacements. In that case we can assume that the error bound in our inversion solutions are those obtained in the numerical experiment with the point force and cubic interpolations of displacements as shown in Fig. 11. Therefore we conclude that our solution near Palmdale, i.e. solutions at point 5 in the previous section is not contaminated by the error due to insufficiency of horizontal data and has maximum error less than 10%. For other parts of Southern California the situation is not so good as near Palmdale because we do not have separate measurements for horizontal displacements along the San Andreas fault. Therefore it is possible that solutions obtained at points along the San Andreas have considerably large error up to 90% although the linear consistent variation of horizontal displacements seems to be typical in Southern California and is consistent with an implication from plate tectonic theory.

Assuming we have enough number of observations to allow us to use cubic polynomial interpolations in all displacement components, we still have to consider errors originated from the geodetic measurement itself at each node. This error can be studied by calculating the sensitivity of solution to small perturbations of data at each node.

In Fig. 32 the maximum perturbations in inversion solutions at the point (0, 0, -10 km) are plotted as a function of perturbations in horizontal displacement components and as a function of perturbations in vertical displacement components. Data at each node of the triangle with 30 km side length are perturbed separately and the maximum perturbation in the solution associated with these data perturbations is plotted. It is shown that a sensitivity of solutions to the perturbation of horizontal components is one third of the sensitivity of solutions to the perturbation of vertical components. This is a very nice character of our inversion scheme because we usually have greater accuracy in vertical components than horizontal components as mentioned before. At Palmdale, we have the error in geodimeter measurements estimated as  $\pm 30\%$  and the error in levelling measurements estimated as  $\pm 5\%$  within the triangle of 30 km side length. Therefore we can estimate the error involved in the inversion near Palmdale due to geodetic measurements is close to  $20\%$  as a whole. Combining this error to the error generated by the finiteness of the order of interpolations, we conclude that our inversion solution near Palmdale has a possible error within  $30\%$ .

The above analysis shows that the combined use of smaller geodimeter networks are crucial to bound errors in our inversion scheme. In order to apply the cubic interpolation, we need data at least 10 points. One simple way to achieve this is to divide the triangle into pieces of smaller triangles and perform geodimeter measurements along each side of small triangles as shown in Fig. 33. This procedure may improve the accuracy of our inversion scheme by one order of magnitude as can be seen from the comparison of Fig. 31 with Fig. 11.

If, on the other hand, we use the data at only 6 points as shown in Fig. 34, we can not apply the cubic interpolation but the quadratic, which would give about 50% increase in accuracy, because from the numerical experiment using the finite element method (Ikeda, 1980). The error in inverse solution generally decreased linearly with the number of nodes.

If we cut down to 4 points as shown in Fig. 34, we cannot use a full quadratic interpolation, the improvement in accuracy would even be less.

Table 2. Geodetic Data (unit cm)

Network at point 1<sup>N</sup>

Node	u	v	w
1	-.2570641	7.333315	11.00000
2	-1.120489	1.643909	10.00000
3	-1.983891	-4.045531	7.50000
4	-2.847305	-9.734953	4.80000
5	-.8634135	-5.689423	9.00000
6	1.120489	-1.643909	11.70000
7	3.104369	2.401639	14.00000
8	1.983891	4.045531	13.60000
9	.8634135	5.689423	12.20000
10	.0	.0	10.50000

Network at point 2<sup>N</sup>

Node	u	v	w
1	-.2570641	7.333315	15.00000
2	-1.120489	1.643909	13.10000
3	-1.983891	-4.045531	11.00000
4	-2.847305	-9.734953	8.80000
5	-.8634135	-5.689423	11.70000
6	1.120489	-1.643909	14.50000
7	3.104369	2.401639	17.50000
8	1.983891	4.045531	17.00000
9	.8634135	5.689423	15.50000
10	.0	.0	13.60000

Network at point 3<sup>N</sup>

Node	u	v	w
1	-.2570641	7.333315	18.89999
2	-1.120489	1.643909	17.10001
3	-1.983891	-4.045531	14.50000
4	-2.847305	-9.734953	11.80000
5	-.8634135	-5.689423	15.00000
6	1.120489	-1.643909	17.60001
7	3.104369	2.401639	19.80000
8	1.983891	4.045531	19.50000
9	.8634135	5.689423	19.39999
10	.0	.0	17.50000

Network at point 4<sup>N</sup>

Node	u	v	w
1	-.2570641	7.333315	22.50000
2	-1.120489	1.643909	20.00000
3	-1.983891	-4.045531	18.30000
4	-2.847305	-9.734953	16.20000
5	-.8634135	-5.689423	18.30000
6	1.120489	-1.643909	20.00000
7	3.104369	2.401639	22.20000
8	1.983891	4.045531	22.50000
9	.8634135	5.689423	22.50000
10	.0	.0	19.80000

Network at point 5<sup>N</sup>

Node	u	v	w
1	-2.045119	2.919487	24.50000
2	-.9653528	-.6894846	22.80000
3	.1144336	-4.298442	21.39999
4	1.194210	-7.907406	19.30000
5	1.079776	-3.608964	20.50000
6	.9653528	.6894846	22.39999
7	.8509092	4.987919	23.00000
8	-.1144336	4.298442	23.70000
9	-1.079776	3.608964	24.00000
10	.0	.0	22.50000

Network at point 6<sup>N</sup>

Node	u	v	w
1	-2.045119	2.919487	24.50000
2	-.9653528	-.6894846	23.60001
3	.1144336	-4.298442	22.20000
4	1.194210	-7.907406	20.20000
5	1.079776	-3.608964	22.00000
6	.9653528	.6894846	22.70000
7	.8509092	4.987919	23.30000
8	-.1144336	4.298442	23.80000
9	-1.079776	3.608964	24.10001
10	.0	.0	23.00000

Network at point 7<sup>N</sup>

Node	u	v	w
1	-2.045119	2.919487	24.20000
2	-.9653528	-.6894846	23.50000
3	.1144336	-4.298442	22.50000
4	1.194210	-7.907406	21.20000
5	1.079776	-3.608964	21.89999
6	.9653528	.6894346	21.70000
7	.8509092	4.987919	20.00000
8	-.1144336	4.298442	21.00000
9	-1.079776	3.608964	22.50000
10	.0	.0	22.80000

Network at point 8<sup>N</sup>

Node	u	v	w
1	-2.045119	2.919487	15.60000
2	-.9653528	-.6894846	18.89999
3	.1144336	-4.298442	20.50000
4	1.194210	-7.907406	20.80000
5	1.079776	-3.608964	18.20000
6	.9653528	.6894846	16.30000
7	.8509092	4.987919	12.00000
8	-.1144336	4.298442	14.10000
9	-1.079776	3.608964	15.00000
10	.0	.0	17.60001

## Network at point 1

Node	u	v	w
1	-.2570641	7.333315	15.50000
2	-1.120489	1.643909	15.50000
3	-1.983891	-4.045531	14.20000
4	-2.847305	-9.734953	12.10000
5	-.8634135	-5.689423	15.00000
6	1.120489	-1.643909	18.80000
7	3.104369	2.401639	20.00000
8	1.983891	4.045531	19.50000
9	.8634135	5.689423	17.00000
10	.0	.0	17.00000

## Network at point 2

Node	u	v	w
1	-.2570641	7.333315	17.50000
2	-1.120489	1.643909	20.30000
3	-1.983891	-4.045531	18.00000
4	-2.847305	-9.734953	15.00000
5	-.8634135	-5.689423	18.80000
6	1.120489	-1.643909	21.50000
7	3.104369	2.401639	18.00000
8	1.983891	4.045531	17.50000
9	.8634135	5.689423	17.50000
10	.0	.0	21.00000

## Network at point 3

Node	u	v	w
1	-.2570641	7.333315	14.00000
2	-1.120489	1.643909	18.00000
3	-1.983891	-4.045531	21.80000
4	-2.847305	-9.734953	19.00000
5	-.8634135	-5.689423	21.80000
6	1.120489	-1.643909	22.50000
7	3.104369	2.401639	20.00000
8	1.983891	4.045531	17.50000
9	.8634135	5.689423	15.00000
10	.0	.0	20.00000

## Network at point 4

Node	u	v	w
1	-.2570641	7.333315	13.70000
2	-1.120489	1.643909	19.00000
3	-1.983891	-4.045531	23.80000
4	-2.847305	-9.734953	22.00000
5	-.8634135	-5.689423	23.80000
6	1.120489	-1.643909	25.00000
7	3.104369	2.401639	27.00000
8	1.983891	4.045531	22.50000
9	.8634135	5.689423	17.50000
10	.0	.0	25.00000

## Network at point 5

Node	u	v	w
1	-2.045119	2.919487	17.50000
2	-.9653528	-.6894846	25.00000
3	.1144336	-4.298442	24.80000
4	1.194210	-7.907406	23.50000
5	1.079776	-3.608964	24.30000
6	.9653528	.6894846	25.00000
7	.8509092	4.987919	25.50000
8	-.1144336	4.298442	25.00000
9	-1.079776	3.608964	20.00000
10	.0	.0	27.50000

## Network at point 6

Node	u	v	w
1	-2.045119	2.919487	16.30000
2	-.9653528	-.6894846	24.89999
3	.1144336	-4.298442	24.89999
4	1.194210	-7.907406	23.700000
5	1.079776	-3.608964	24.39999
6	.9653528	.6894846	22.50000
7	.8509092	4.987919	16.70000
8	-1.079776	4.298442	17.50000
9	.0	3.608964	17.50000
10	.0	.0	24.89999



## Network at point 7

Node	u	v	w
1	-2.045119	2.919487	10.80000
2	-.9653528	-.6894846	15.00000
3	.1144336	-4.298442	20.00000
4	1.194210	-7.907406	22.50000
5	1.079776	-3.608964	19.00000
6	.9653528	.6894846	14.50000
7	.8509092	4.987919	10.20000
8	-.1144336	4.298442	10.50000
9	-1.079776	3.608964	10.70000
10	.0	.0	15.00000

## Network at point 8

Node	u	v	w
1	-2.045119	2.919487	4.00000
2	-.9653528	-.6894846	7.50000
3	.1144336	-4.298442	12.00000
4	1.194210	-7.907406	15.10000
5	1.079776	-3.608964	10.60000
6	.9653528	.6894846	5.00000
7	.8509092	4.987919	1.300000
8	-.1144336	4.298442	2.500000
9	-1.079776	3.608964	3.600000
10	.0	.0	7.500000

Network at point 1<sup>S</sup>

Node	u	v	w
1	-.2570641	7.333315	9.00000
2	-1.120489	1.643909	11.70000
3	-1.983891	-4.045531	15.00000
4	-2.847305	-9.734953	18.50000
5	-.8634135	-5.689423	15.60000
6	1.120489	-1.643909	12.50000
7	3.104369	2.401639	9.20000
8	1.983891	4.045531	9.80000
9	.8634135	5.689423	9.80000
10	.0	.0	12.50000

Network at point 2<sup>S</sup>

Node	u	v	w
1	-.2570641	7.333315	8.50000
2	-1.120489	1.643909	10.60000
3	-1.983891	-4.045531	14.50000
4	-2.847305	-9.734953	19.10001
5	-.8634135	-5.689423	14.50000
6	1.120489	-1.643909	9.50000
7	3.104369	2.401639	7.50000
8	1.983891	4.045531	7.50000
9	.8634135	5.689423	8.20000
10	.0	.0	10.00000

Network at point 3<sup>S</sup>

Node	u	v	w
1	-.2570641	7.333315	5.20000
2	-1.120489	1.643909	7.00000
3	-1.983891	-4.045531	9.50000
4	-2.847305	-9.734953	16.70000
5	-.8634135	-5.689423	13.00000
6	1.120489	-1.643909	10.00000
7	3.104369	2.401639	8.80000
8	1.983891	4.045531	6.70000
9	.8634135	5.689423	5.50000
10	.0	.0	8.40000

Network at point 4<sup>S</sup>

Node	u	v	w
1	-.2570641	7.333315	4.00000
2	-1.120489	1.643909	8.00000
3	-1.983891	-4.045531	13.60000
4	-2.847305	-9.734953	20.20000
5	-.8634135	-5.689423	18.00000
6	1.120489	-1.643909	15.00000
7	3.104369	2.401639	11.70000
8	1.983891	4.045531	8.80000
9	.8634135	5.689423	5.00000
10	.0	.0	11.50000

Network at point 5<sup>S</sup>

Node	u	v	w
1	-2.045119	2.919487	2.50000
2	-.9653528	-.6894846	9.20000
3	.1144336	-4.298442	15.10000
4	1.194210	-7.907406	24.80000
5	1.079776	-3.608964	17.80000
6	.9653528	.6894846	12.50000
7	.8509092	4.987919	8.00000
8	-.1144336	4.298442	6.00000
9	-1.079776	3.608964	4.80000
10	.0	.0	11.30000

Network at point 6<sup>S</sup>

Node	u	v	w
1	-2.045119	2.919487	.60000
2	-.9653528	-.6894846	5.80000
3	.1144336	-4.298442	12.00000
4	1.194210	-7.907406	18.70000
5	1.079776	-3.608964	12.50000
6	.9653528	.6894846	8.00000
7	.8509092	4.987919	3.70000
8	-.1144336	4.298442	3.00000
9	-1.079776	3.608964	2.20000
10	.0	.0	8.00000

Network at point 7<sup>S</sup>

Node	u	v	w
1	-2.045119	2.919487	.0
2	-.9653528	-.6894846	2.00000
3	.1144336	-4.298442	6.80000
4	1.194210	-7.907406	11.50000
5	1.079776	-3.608964	6.30000
6	.9653528	.6894846	2.00000
7	.8509092	4.987919	.0
8	-.1144336	4.298442	.0
9	-1.079776	3.608964	.0
10	.0	.0	2.50000

Network at point 8<sup>S</sup>

Node	u	v	w
1	-2.045119	2.919487	.0
2	-.9653528	-.6894846	.0
3	.1144336	-4.298442	.0
4	1.194210	-7.907406	4.000000
5	1.079776	-3.608964	.0
6	.9653528	.6894846	.0
7	.8509092	4.987919	.0
8	-.1144336	4.298442	.0
9	.0	3.608964	.0
10	.0	.0	.0

Table 3. Principal Incremental Stresses at Depth

Point	Depth (km)	Magnitude (bar)	Azimuth (deg.)	Dip (deg.)
1 <sup>N</sup>	0.0	0.0	N103E	0
		0.0	0	90
		-4.5	N13E	0
	5.0	0.3	N102E	1
		0.0	N93W	90
		-4.4	N12E	0
	10.0	0.5	N102E	1
		0.0	N109W	89
		-4.4	N11E	1
1	0.0	0.0	N103E	0
		0.0	0	90
		-4.5	N13E	0
	5.0	0.5	N106E	43
		-0.4	N78W	47
		-5.2	N14E	2
	10.0	2.0	N111E	44
		-1.7	N85W	44
		-6.1	N13E	8
1 <sup>S</sup>	0.0	0.0	N103E	0
		0.0	0	90
		-4.5	N13E	0
	5.0	0.0	N60W	89
		-0.3	N103E	1
		-4.4	N167W	10
	10.0	0.0	N45W	87
		-0.6	N102E	2
		-4.3	N168W	2
2 <sup>N</sup>	0.0	0.0	N103E	0
		0.0	0	90
		-4.5	N13E	0
	5.0	0.3	N104E	24
		-0.1	N74W	65
		-4.4	N165W	1
	10.0	0.9	N104E	33
		-0.4	N79W	56
		-4.2	N164W	4

Point	Depth (km)	Magnitude (bar)	Azimuth (deg.)	Dip (deg.)
2	0.0	0.0	N103E	0
		0.0	0	90
		-4.5	N13E	0
	5.0	0.1	N149E	83
		-1.0	N83W	4
		-7.7	N7E	5
	10.0	0.7	N170E	75
		-2.0	N87W	4
		-11.6	N4E	14
2 <sup>S</sup>	0.	0.0	N103E	0
		0.0	0	90
		-4.5	N13E	0
	5.0	0.5	N73W	30
		-0.1	N95E	60
		-3.0	N166W	5
	10.0	1.7	N59W	40
		-0.4	N73E	39
		-2.6	N174W	27
3 <sup>N</sup>	0.	0.0	N103E	0
		0.0	0	90
		-4.5	N13E	0
	5.0	0.3	N81W	73
		-0.3	N102E	17
		-4.9	N12E	1
	10.0	0.2	N84W	73
		-0.7	N101E	17
		-5.2	N11E	1
3	0.0	0.0	N103E	0
		0.0	0	90
		-4.5	N13E	0
	5.0	0.4	N100E	44
		-0.3	N70W	45
		-5.7	N165W	5
	10.0	1.7	N90E	48
		-0.9	N58W	38
		-7.5	N161W	16

Point	Depth (km)	Magnitude (bar)	Azimuth (deg.)	Dip (deg.)
3 <sup>S</sup>	0.0	0.0	N103E	0
		0.0	0	90
		-4.5	N13E	0
	5.0	0.2	N85W	46
		-0.2	N102E	44
		-4.1	N9E	4
	10.0	1.0	N100W	46
		-0.7	N108E	40
		-3.9	N6E	14
4 <sup>N</sup>	0.0	0.0	N103E	0
		0.0	0	90
		-4.5	N13E	0
	5.0	0.3	N76W	0
		0.0	N14E	88
		-3.9	N166W	2
	10.0	0.7	N75W	1
		0.1	N23E	79
		-3.4	N165W	11
4	0.0	0.0	N103E	0
		0.0	0	90
		-4.5	N13E	0
	5.0	0.1	N52E	85
		-2.0	N69W	3
		-7.4	N159W	5
	10.0	0.6	N39E	77
		-5.0	N63W	3
		-12.4	N153W	12
4 <sup>S</sup>	0.0	0.0	N103E	0
		0.0	0	90
		-4.5	N13E	0
	5.0	0.3	N99E	49
		-0.4	N87W	41
		-4.6	N168W	2
	10.0	1.2	N94E	47
		-1.3	N72W	41
		-4.8	N168W	7

Point	Depth (km)	Magnitude (bar)	Azimuth (deg.)	Dip (deg.)
5 <sup>N</sup>	0.0	0.0	0	90
		-0.1	N83E	0
		-3.5	N7W	0
	5.0	0.2	N87E	50
		-0.2	N94W	40
		-3.6	N5W	1
	10.0	0.7	N91E	46
		-0.7	N100W	44
		-3.7	N4W	6
5	0.0	0.0	0	90
		-0.1	N83E	10
		-3.5	N7W	0
	5.0	0.1	N122E	82
		-3.0	N84W	7
		-7.6	N6E	4
	10.0	0.7	N129E	73
		-6.0	N81W	15
		-12.2	N12E	8
5 <sup>S</sup>	0.0	0.0	0	90
		-0.1	N83E	0
		-3.5	N7W	0
	5.0	0.3	N109W	60
		-0.7	N82E	30
		-4.0	N11W	5
	10.0	0.5	N121W	52
		-1.9	N94E	33
		-4.9	N8W	17
6 <sup>N</sup>	0.0	0.0	0	90
		-0.1	N83E	0
		-3.5	N7W	0
	5.0	0.3	N97W	6
		0.0	N69E	84
		-3.5	N173E	1
	10.0	0.1	N97W	5
		0.0	N36E	82
		-3.5	N173E	6



Point	Depth (km)	Magnitude (bar)	Azimuth (deg.)	Dip (deg.)
6	0.0	0.0	0	90
		-0.1	N83E	0
		-3.5	N7W	0
	5.0	0.1	N121W	80
		-2.1	N88E	9
		-7.5	N3W	5
	10.0	0.9	N140W	71
		-4.3	N93E	14
		-12.1	N0E	13
6 <sup>S</sup>	0.0	0.0	0	90
		-0.1	N83E	0
		-3.5	N7W	0
	5.0	0.0	N134E	89
		-1.1	N97W	1
		-4.0	N7W	1
	10.0	0.0	N147E	86
		-2.0	N97W	2
		-4.6	N7W	4
7 <sup>N</sup>	0.0	0.0	0	90
		-0.1	N83E	0
		-3.5	N7W	0
	5.0	0.0	N132W	89
		-0.4	N82E	1
		-4.4	N8W	1
	10.0	0.0	N141W	87
		-0.8	N81E	2
		-5.3	N9W	2
7	0.0	0.0	0	90
		-0.1	N83E	0
		-3.5	N7W	0
	5.0	0.1	N69E	70
		-0.3	N103W	19
		-3.4	N175E	6
	10.0	0.6	N46E	62
		-0.6	N83W	18
		-3.8	N180E	20

Point	Depth (km)	Magnitude (bar)	Azimuth (deg.)	Dip (deg.)
7 <sup>S</sup>	0.0	0.0	0	90
		-0.1	N83E	0
		-3.5	N7W	0
	5.0	0.1	N63E	70
		-0.3	N95W	18
		-2.7	N172E	7
	10.0	0.8	N30E	58
		-0.6	N85W	14
		-2.5	N177E	28
8 <sup>N</sup>	0.0	0.0	0	90
		-0.1	N83E	0
		-3.5	N7W	0
	0.5	0.1	N96E	65
		-0.4	N94W	24
		-4.2	N3W	4
	10.0	0.7	N107E	55
		-1.0	N99W	32
		-5.1	N1W	12
8	0.0	0.0	0	90
		-0.1	N83E	0
		-3.5	N7W	0
	5.0	0.0	N18W	84
		-1.1	N82E	1
		-3.8	N172E	6
	10.0	0.6	N12W	70
		-2.1	N80E	1
		-4.7	N170E	20
8 <sup>S</sup>	0.0	0.0	0	90
		-0.1	N83E	0
		-3.5	N7W	0
	5.0	0.1	N123W	69
		-0.1	N86E	18
		-3.6	N7W	10
	10.0	1.3	N164W	61
		-0.1	N90E	9
		-4.8	N5W	27

## Figure Captions for Chapter 5

- Fig. 16. Palmdale uplift 1959-1974 (from Castle et al., 1976).
- Fig. 17. Palmdale uplift between 1959 to 1974 and subsidence between 1974 to 1978. Numerals with minus signs show the amount of the subsidence.
- Fig. 18. Elevation of bench mark 3219 located just south of Palmdale as a function of time from 1926 to 1977.
- Fig. 19. Geodimeter and triangulation network used for the analysis of strain accumulations in Southern California.
- Fig. 20. Location of points at which stress is calculated at depths, 5 and 10km.
- Fig. 21. Orientation of the axis of the N-S principal stress on the surface. Upper number corresponds to the azimuth measured from north clockwise. Lower number shows the dip angle of the axis measured downward from the direction of azimuth.
- Fig. 22. Magnitude of the N-S principal stress on the surface.
- Fig. 23. Orientation of the axis of the E-W principal stress on the surface. (See Fig. 21 for detail).
- Fig. 24. Magnitude of the E-W principal stress on the surface.
- Fig. 25. Orientation of the axis of the N-S principal stress at the depth of 10km. (See Fig. 21 for detail).
- Fig. 26. Magnitude of the N-S principal stress at the depth of 10km.

Fig. 27. Orientation of the E-W principal stress at the depth of 10km. (See Fig. 21 for detail).

Fig. 28. Magnitude of the E-W principal stress at the depth of 10km.

Fig. 29. Orientation of the axis of the near vertical principal stress at the depth of 10km. (See Fig. 21 for detail).

Fig. 30. Magnitude of the near vertical principal stress at the depth of 10km.

Fig. 31. Absolute error by the analytic method at  $(0, 0, -10 \text{ km})$  as a function of depth of the point force in the case of 30 km side length. Data for horizontal components are given only at peaks of the triangle and are interpolated linearly to be given at other nodes. Data for vertical components are directly given from theoretical solutions for the point surface.

Fig. 32. Maximum rational perturbation in the solution at  $(0, 0, -10 \text{ km})$  in the case of 30 km side length. Horizontal components and vertical components of data are perturbed separately. The ratio of perturbations in data are shown in %.

Fig. 33. Possible division of a conventional geodetic network which allows piecewise cubic interpolations in displacements.

Fig. 34. Possible division of a conventional geodetic network which allows piecewise quadratic interpolations in displacements.

Fig. 33. Possible division of a conventional geodetic network which allows piecewise cubic interpolations in displacements.

Fig. 34. Possible division of a conventional geodetic network which allows piecewise quadratic interpolations in displacements.

Fig. 35. Additional point in a center of a conventional geodetic network.

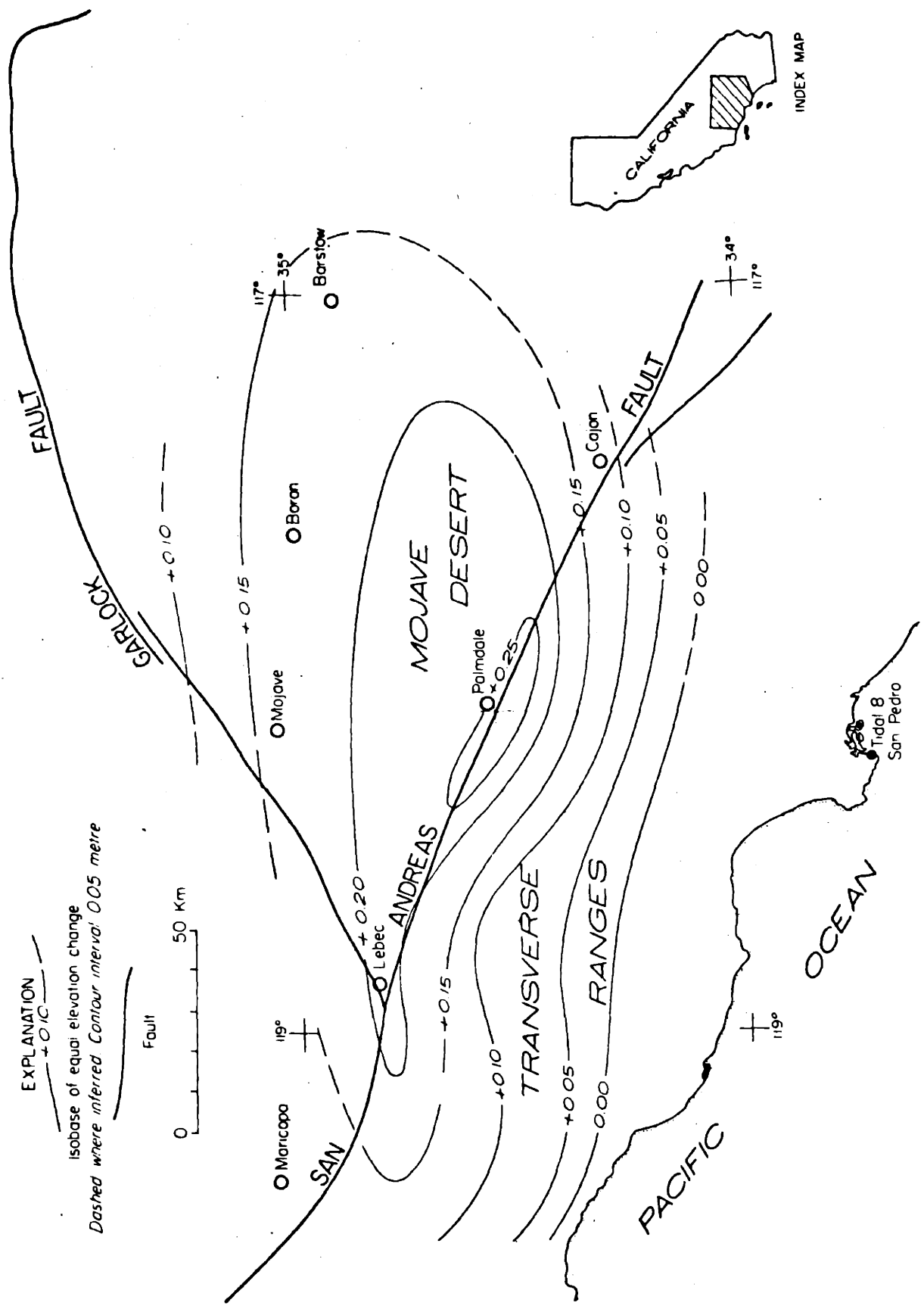


FIG. 16

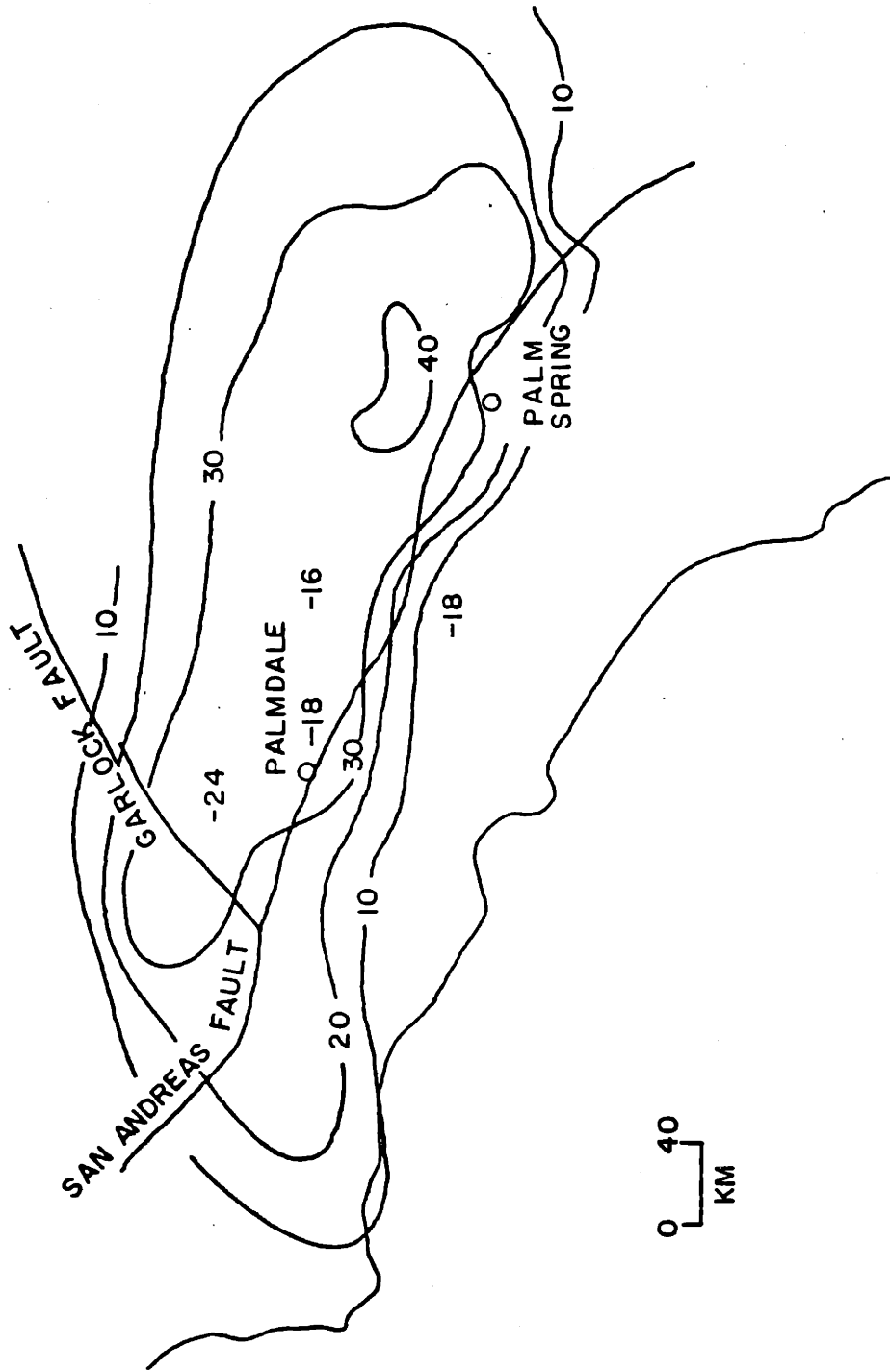


FIG. 17

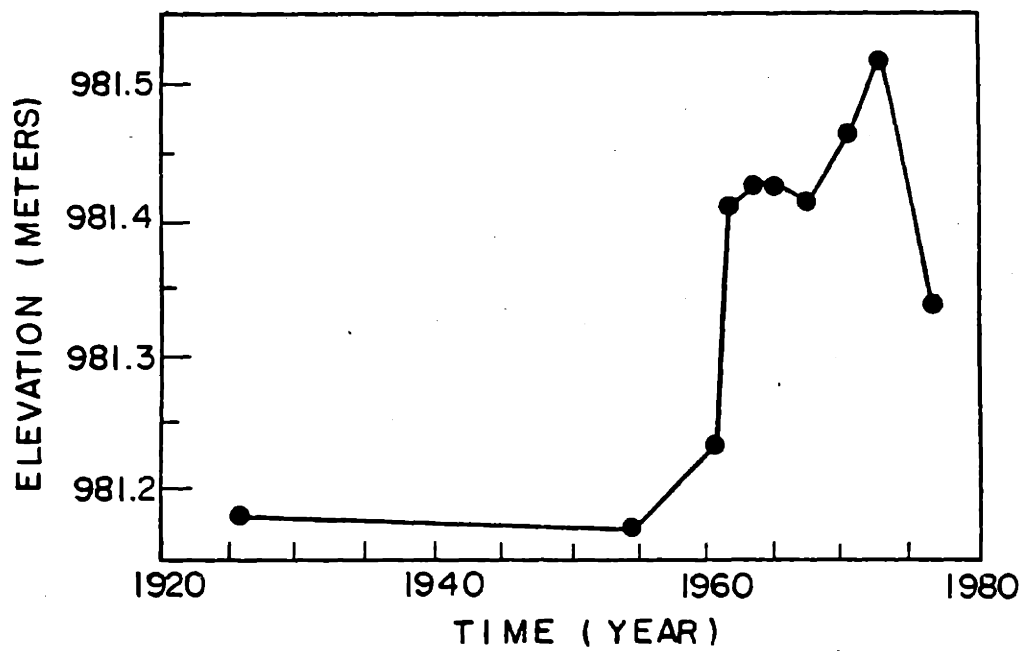
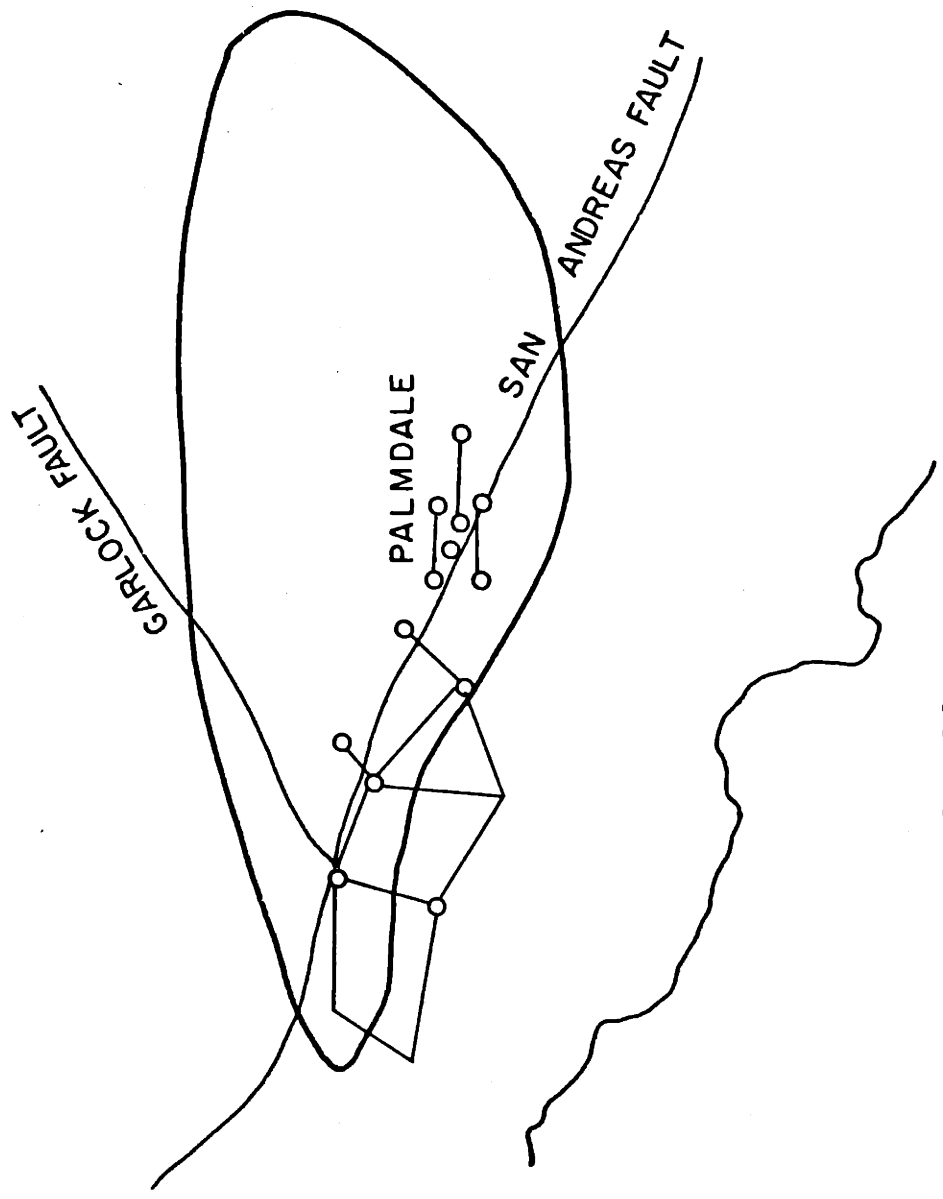


FIG.18





0 20  
KM




- 
 TRIANGULATION NETWORK  
USED BY THATCHER
- 
 GEODIMETER LINE USED  
BY SAVAGE
- 
 CONTOUR OF 15CM UPLIFT

FIG. 19

CONTOUR OF 15CM UPLIFT

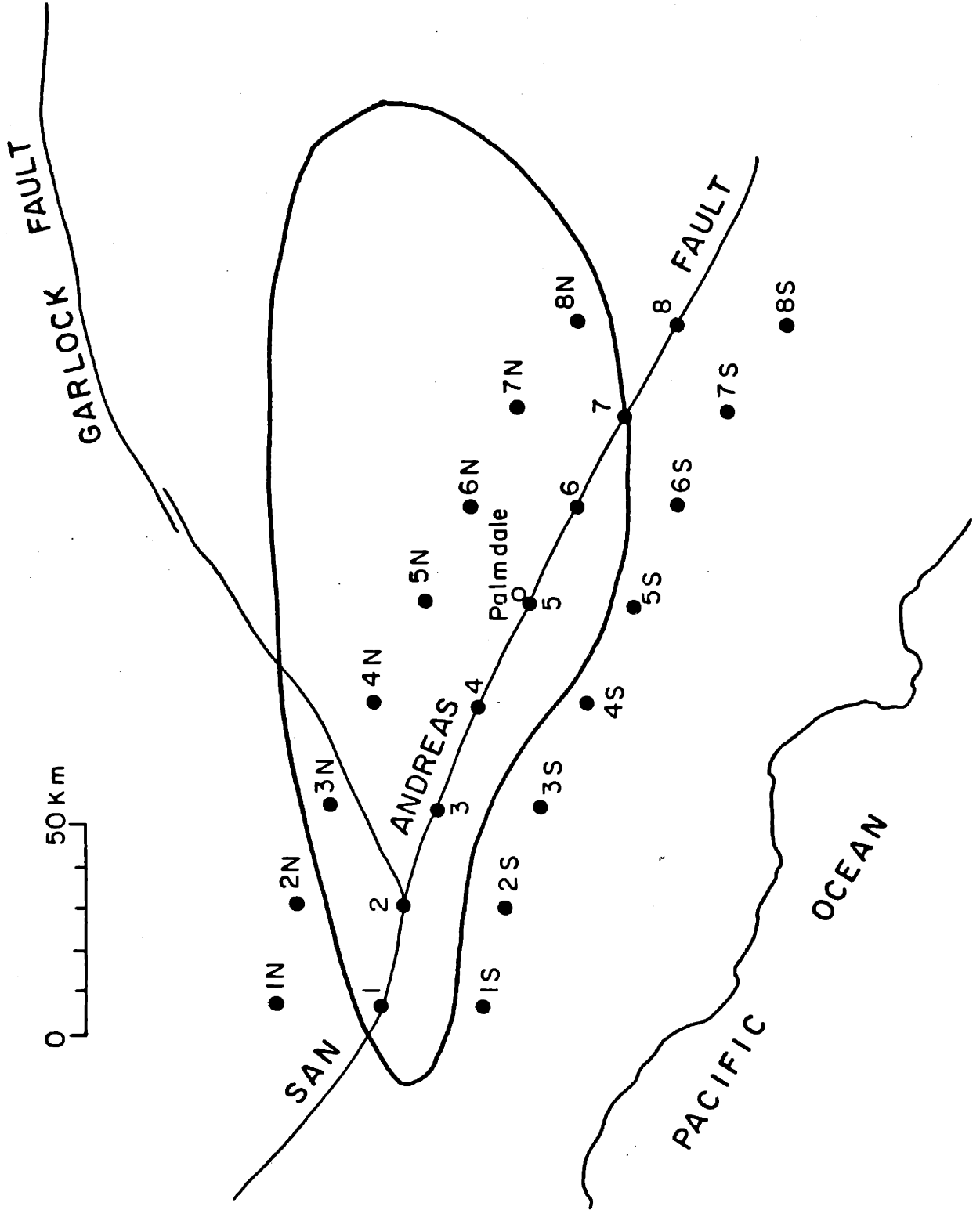


FIG. 20







~ CONTOUR OF 15CM UPLIFT

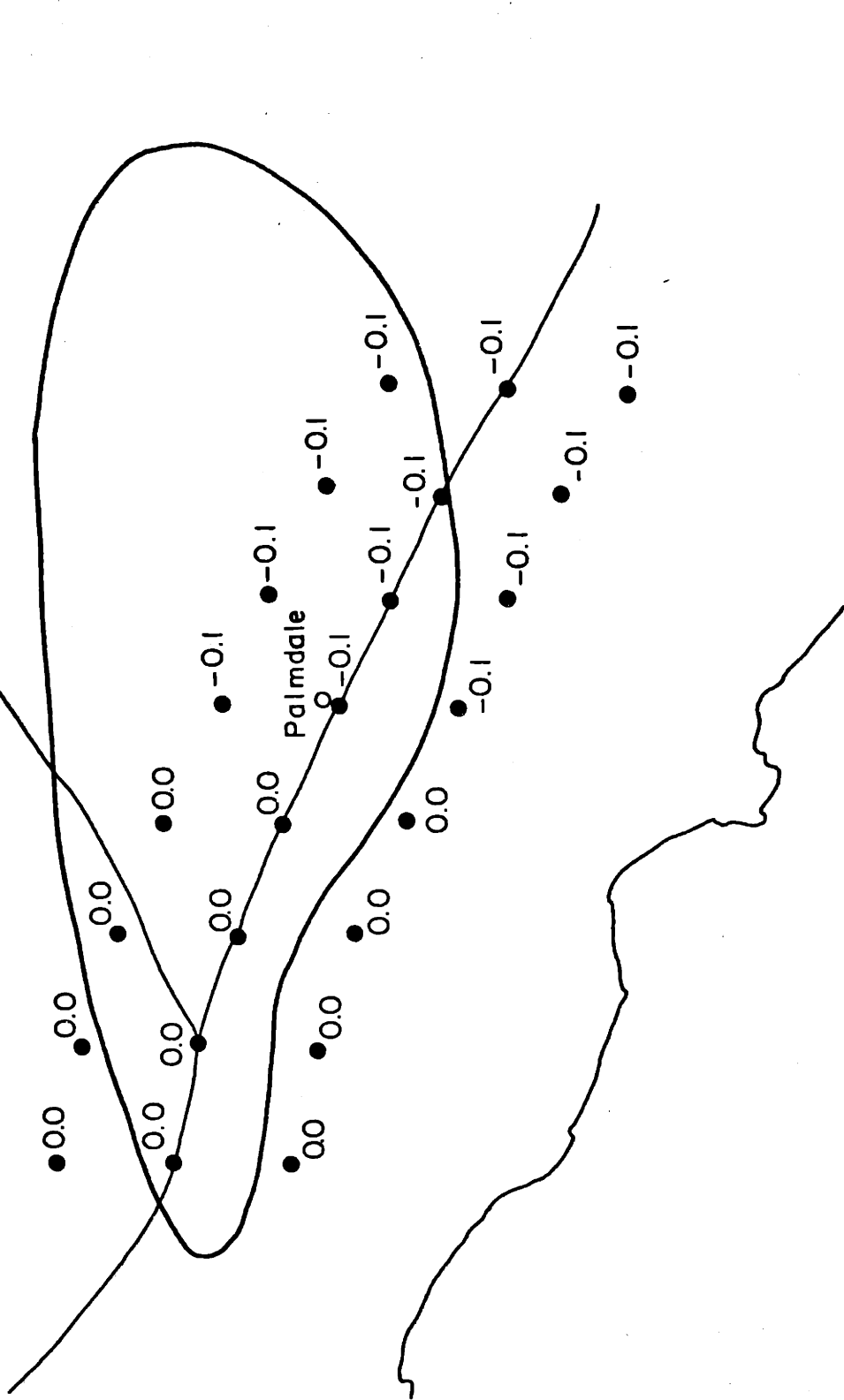


FIG. 24

CONTOUR OF 15 CM UPLIFT

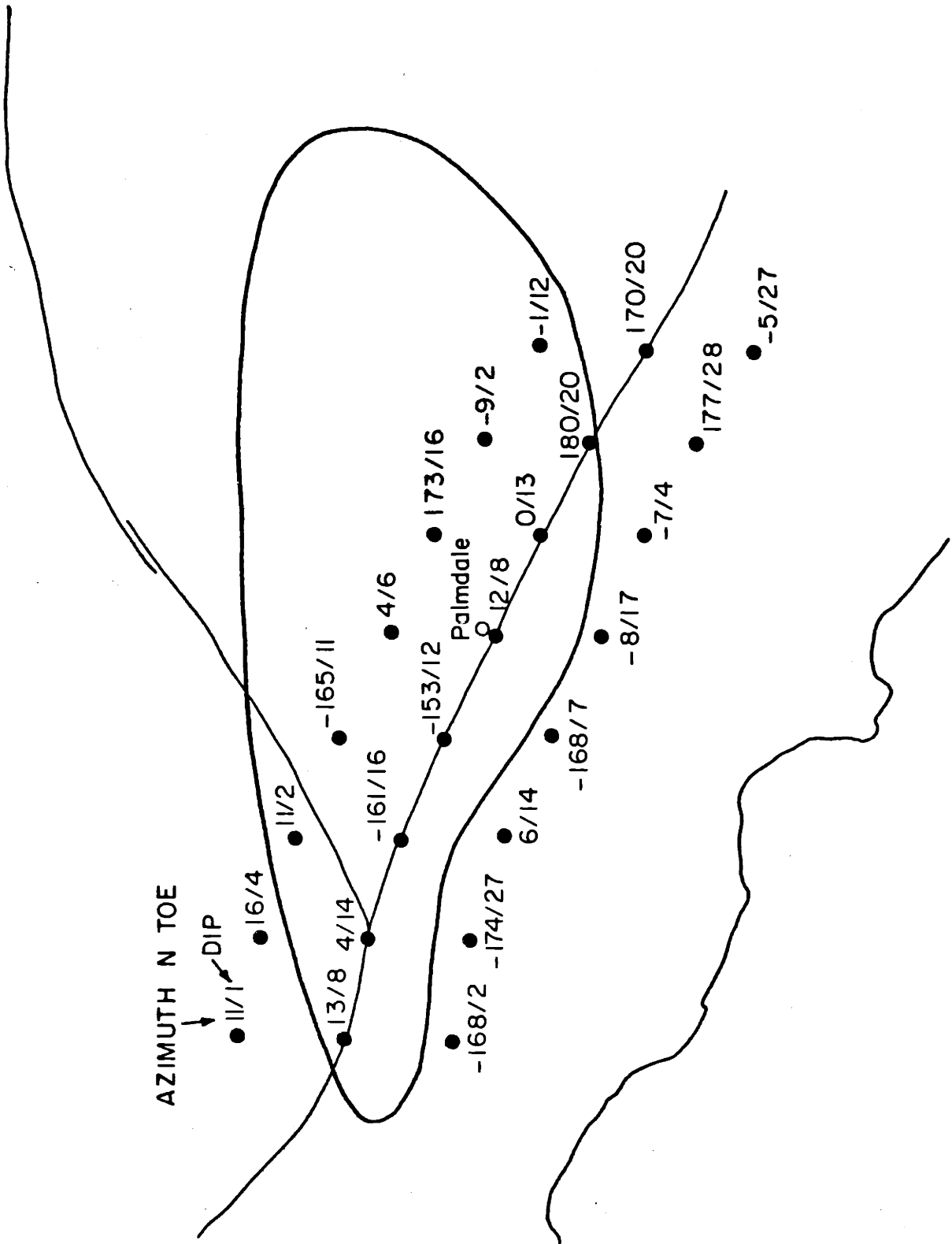


FIG. 25

CONTOUR OF 15 CM UPLIFT

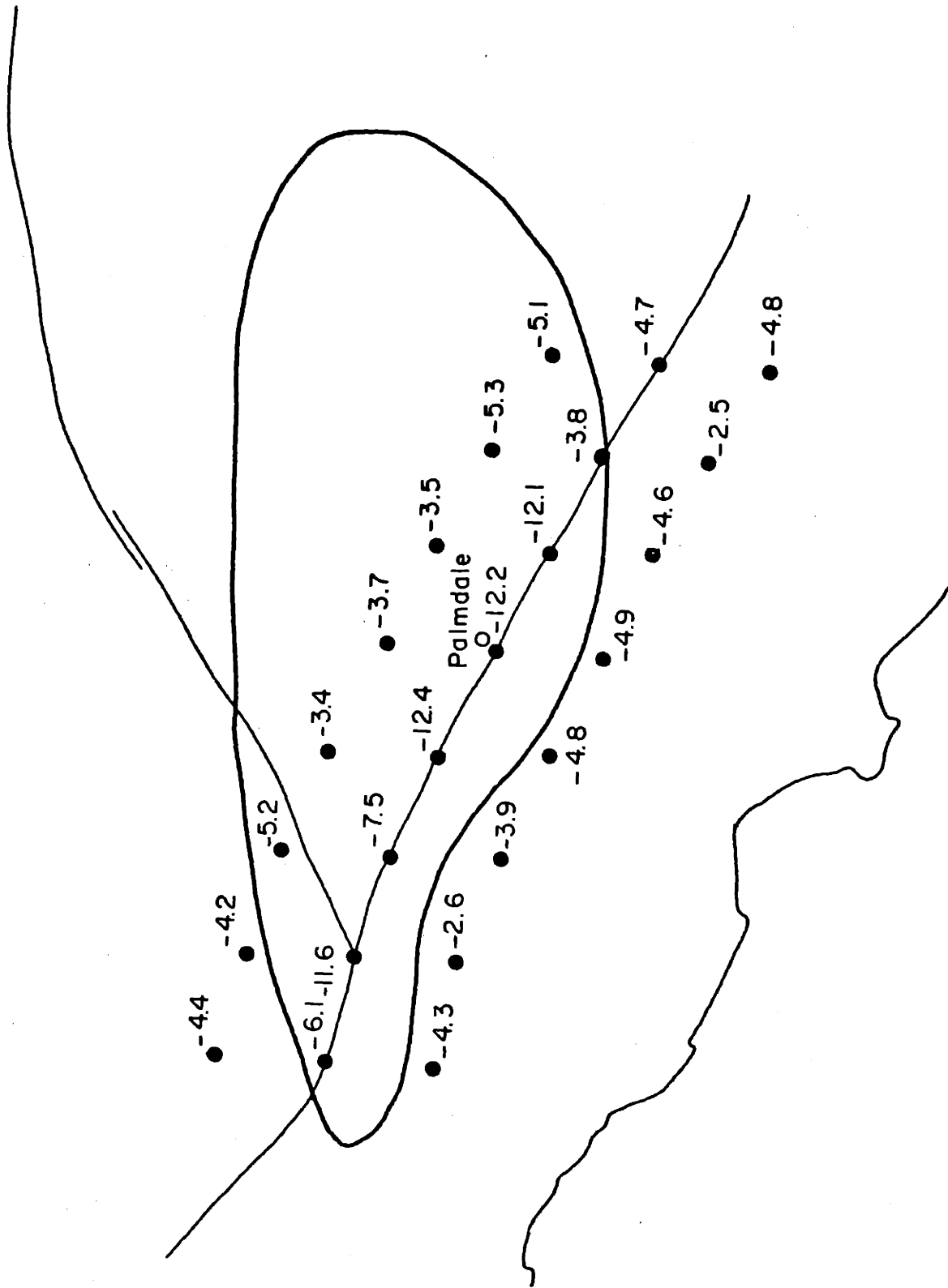


FIG. 26



CONTOUR OF 15CM UPLIFT

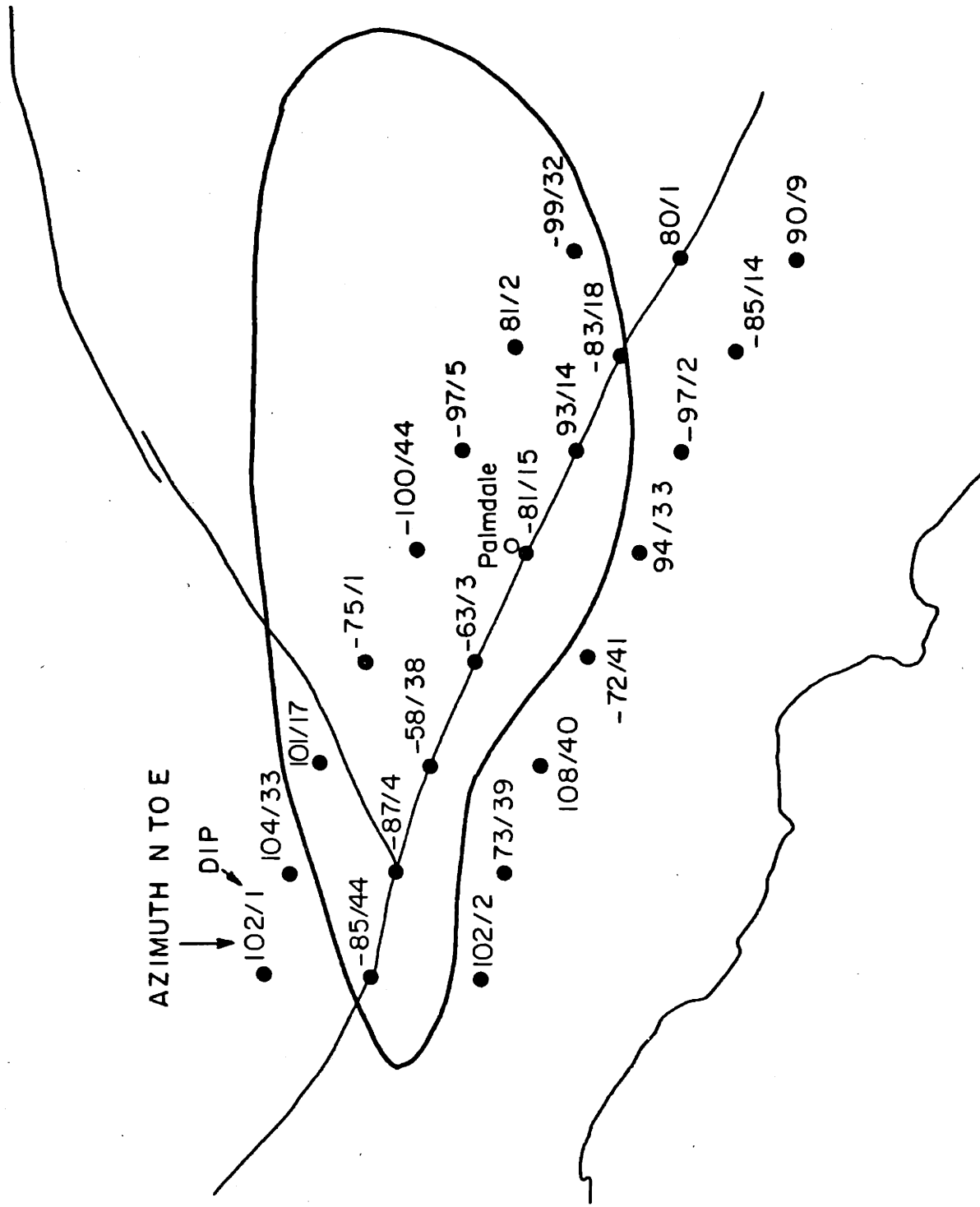


FIG. 27

CONTOUR OF 15 CM UPLIFT

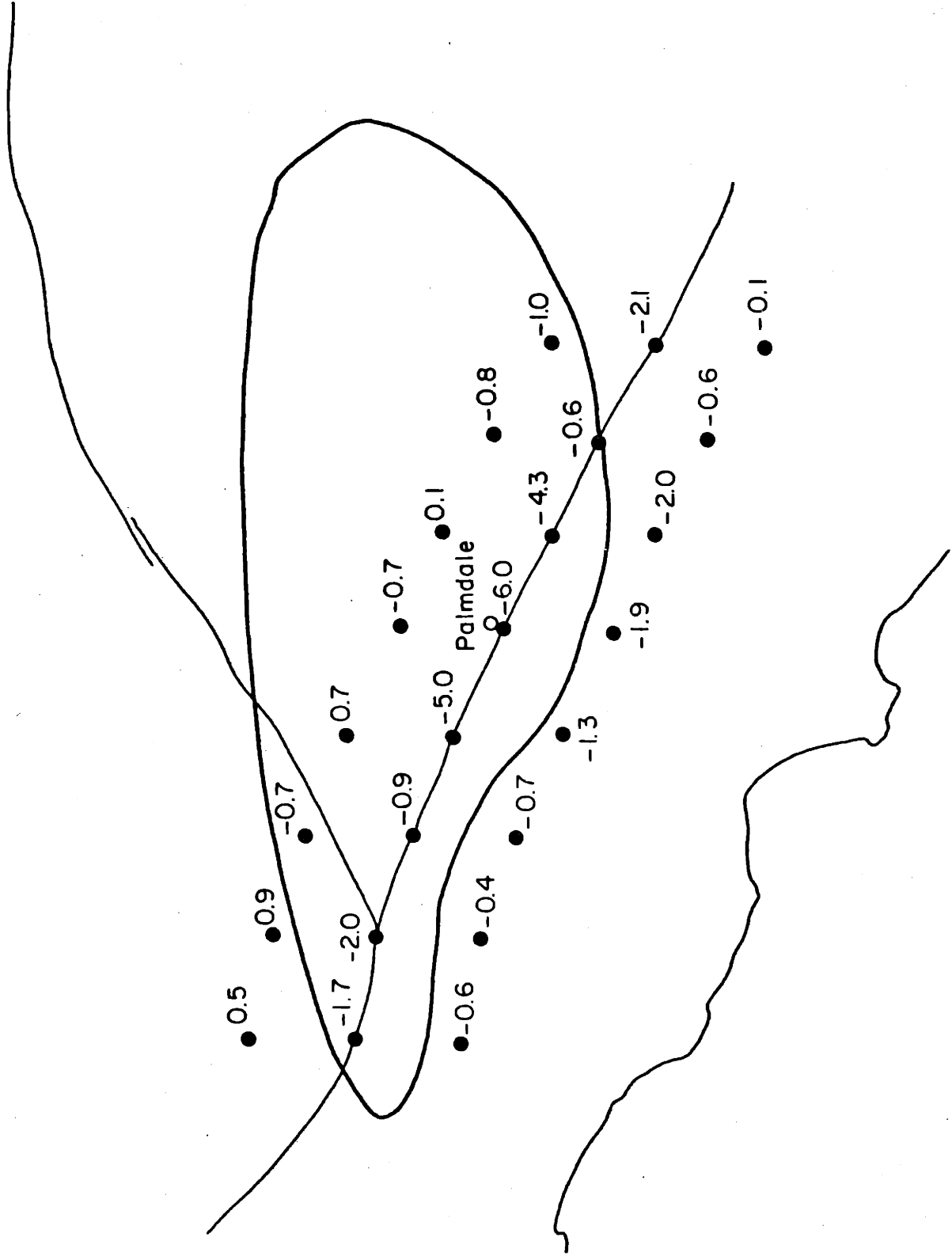


FIG. 28

CONTOUR OF 15 CM UPLIFT

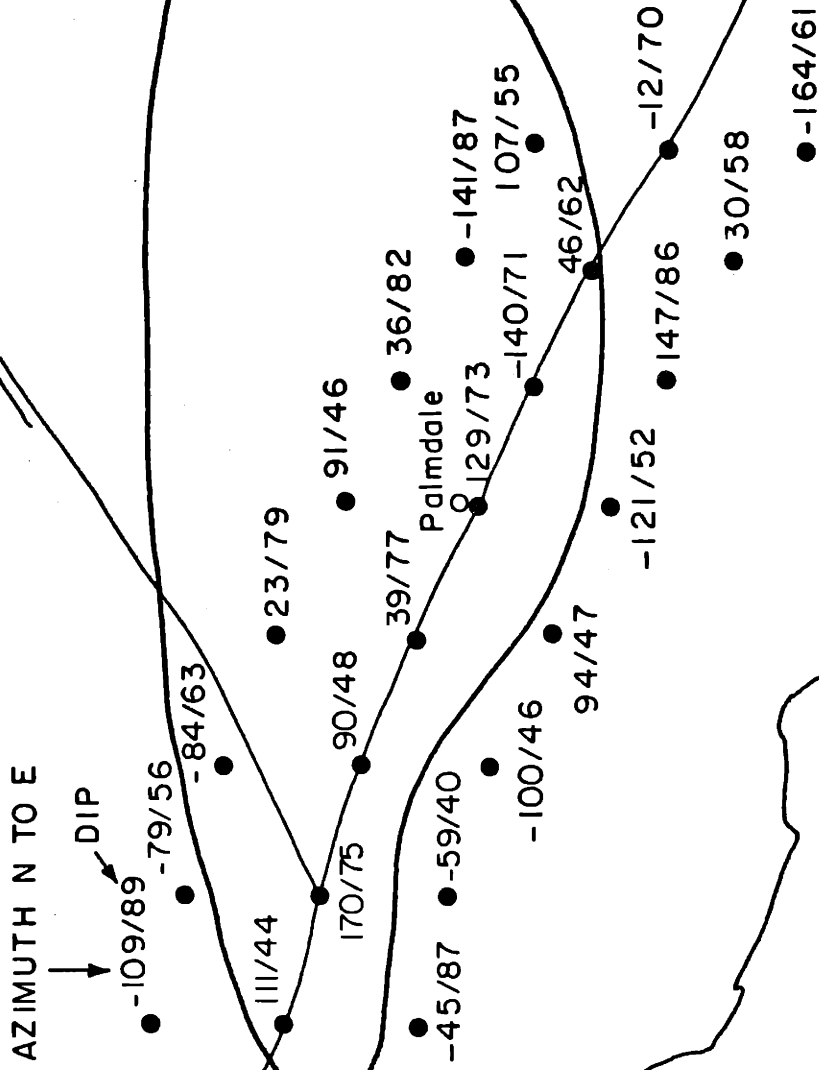


FIG. 29



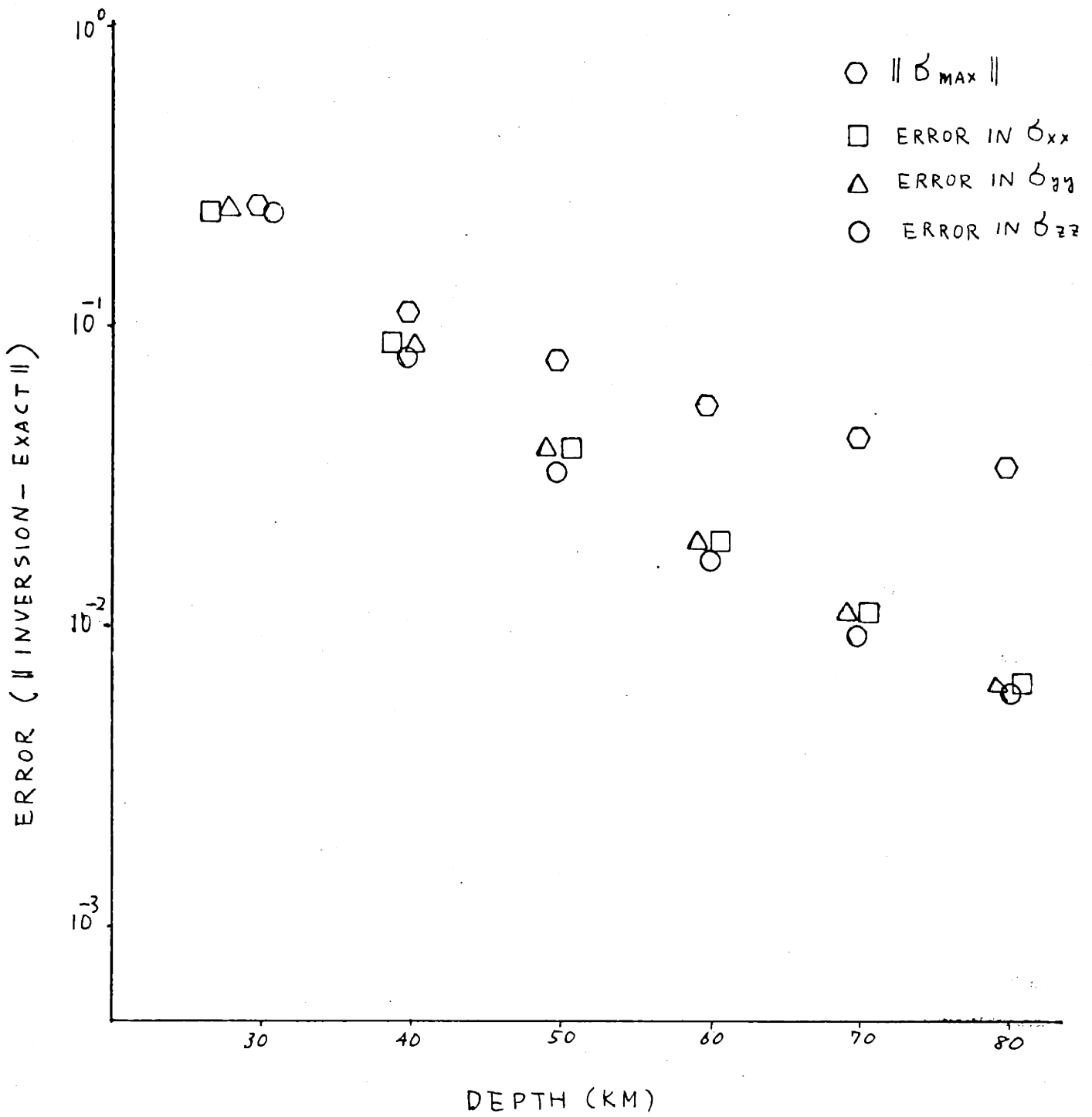


FIG. 31

□ PERTURBATION VERTICAL COMPONENT  
△ PERTURBATION HORIZONTAL COMPONENT

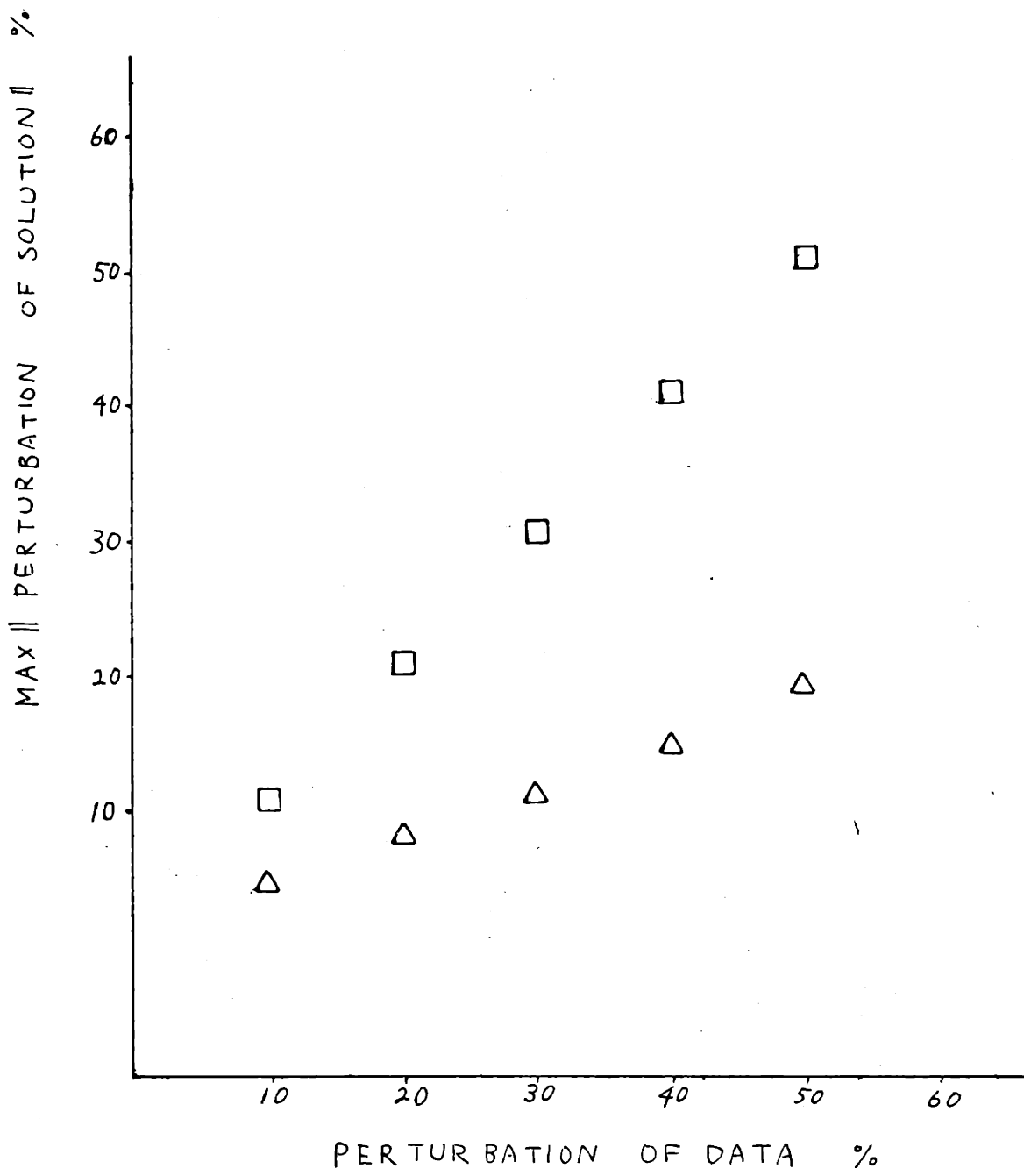


FIG. 32

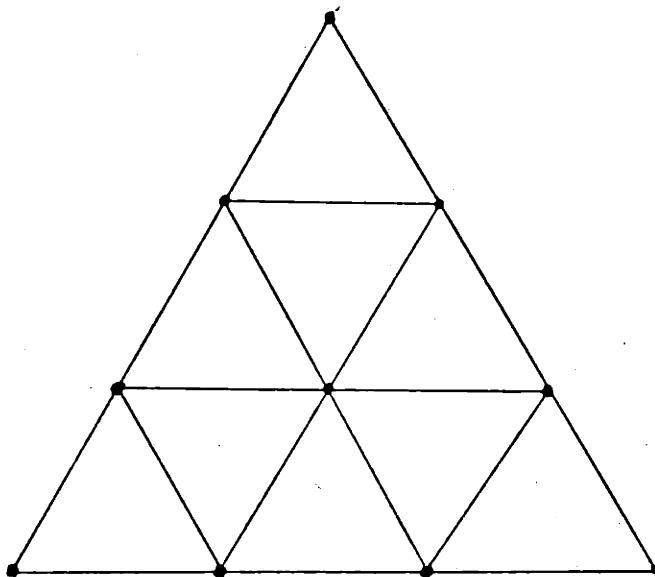


FIG. 33

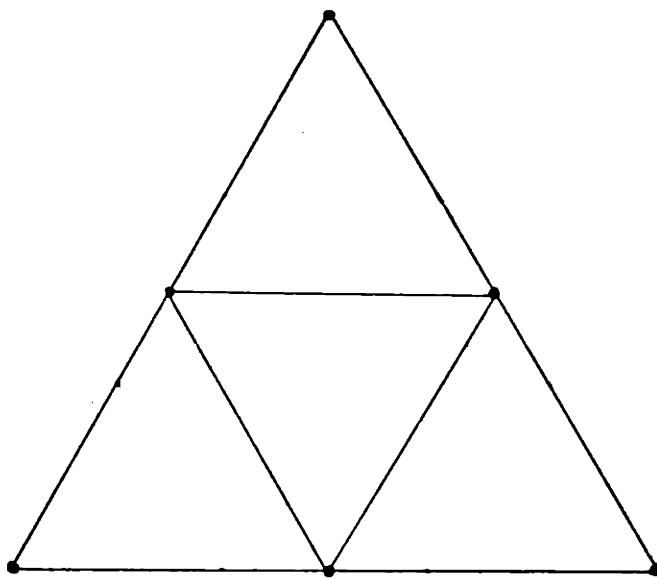


FIG. 34



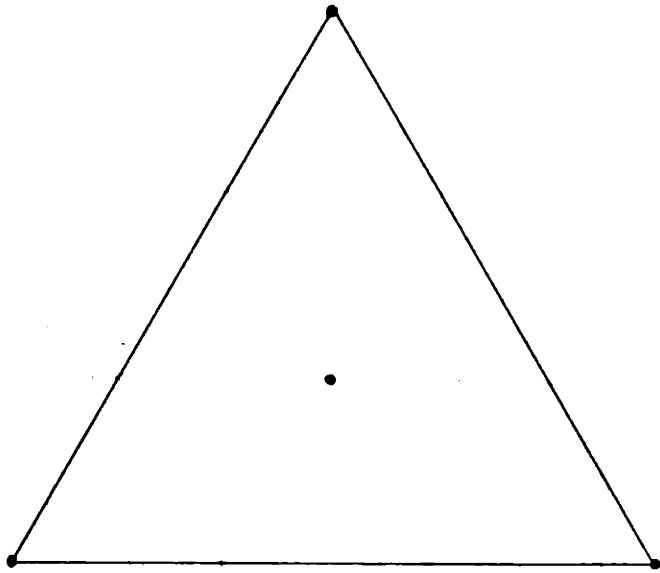


FIG. 35

## CHAPTER 6. CONCLUSIONS

We formulated our geodetic inverse problem for stress in the earth as an inverse boundary value problem in elasticity. This problem is mathematically equivalent to the Cauchy problem for elliptic equations which is known to be ill-posed.

We developed a general method to solve this problem based on the simultaneous use of eigenfunction expansion method and shooting method. We first applied it to the Cauchy problem for the Laplace equation to illustrate the essence of method by solving the simplest problem of all. The solution of the inverse problem obtained by this eigenfunction expansion-shooting method was shown to be exact if we can avoid the possibility of highly oscillating solutions beforehand.

Next, the eigenfunction expansion-shooting method was applied to the two-dimensional elastostatic inverse problems for which polynomial expansions of Airy's stress function give exact solutions for the inverse problems with boundary conditions expanded in the polynomial. Polynomial expansions up to fourth order are carried out to illustrate the technique. The three-dimensional elastostatic inverse problem was then solved by the same method where we had to use the Galerkin vector instead of the Airy's stress function. The exact solutions based on the eigenfunction expansion of the

Galerkin vector by polynomials up to fifth order are obtained.

We then discussed practical aspects of the application of our method to solving a geodetic inverse problem for stress in the earth. Because solutions obtained by the fifth order polynomial expansion require ten parameters to be specified for each component of displacement vector observed on the surface, an equal-sided triangular geodetic network with three data points on each side and one data point in the center was considered to be advantageous because current geodetic measurements are conducted along polygonal networks that can be split into triangles. To analyze the error due to truncating the eigenfunction expansion up to the fifth order, we used data generated by a buried point source and a strip of dislocation in half space. The solutions based on the eigenfunction expansion by polynomials up to the fifth order were shown to be superior to those obtained by the finite element method when inversion results are compared with the known true solution. The triangular network with side length of 30km gives an adequate accuracy as shown by comparison with the true solutions.

The inversion for stress using a triangular network with equal side length of 30km are then applied to geodetic data obtained by levelling and geodimeter measurement in southern California where anomalous uplift called Palmdale bulge is observed along the San Andreas fault. The principal stresses at 10km depth obtained by the inversion method showed significantly different patterns from those at the surface.

At the surface, the principal stresses are the nearly N-S horizontal compression of 3.5 to 4.5 bars, the nearly E-W horizontal compression with very small magnitude and vertical stress of zero magnitude. At 10km depth, the N-S compression reaches to 12 bars and the E-W compression reaches to 6 bars under the central region of the Palmdale bulge. Thus, the incremental shear stress along the fault at 10km depth near Palmdale is only slightly greater than at the surface, but the incremental normal compressional stress increases with depth considerably, suggesting a locking mechanism on the San Andreas fault during the period of Palmdale uplift. The result is consistent with the swarm of microearthquakes which occurred in this area during 1977 to 1978 when the uplift trend stopped and turned to downwarp.

The state of incremental stress at 10km depth under the Palmdale bulge during the uplift period may be summarized as an increased horizontal compression and increased vertical tension while the shear stress on the fault was only slightly greater than at the surface.

These results show the usefulness of our inversion scheme in earthquake prediction research. It gives a framework for tying geodetic data with other geophysical measurements on precursors by finding incremental stress at depth from geodetic data and then relating the incremental stress with the precursory phenomena which are believed to be stress dependent.

Our method requires data consisting of matched three

component displacement measured at the same geodetic network. These data are not available currently. New methods based on space technology, such as ARIES (MacDoran, 1973) would be useful for obtaining data needed for the application of our inversion scheme.

## REFERENCES

- Aki, K., Generation and propagation of G waves from Niigata earthquake of Jan. 16, 1964. Part 2. Estimation of earthquake moment, released energy, and stress-strain drop from the G wave spectrum, *Bull. Earthq. Res. Inst.*, 44, 73-88, 1966.
- Alewine, R.W. and T.H. Heaton, Tilts associated with the Pt. Mugu earthquake, in *Proceedings of the Conference on Tectonic Problems of the San Andreas Fault System*, Kovach, R.L. and A. Nur editor, 86-93, Stanford Univ., Publ., Geol. Sci., Vol. 13, Stanford, CA, 1973.
- Alewine, R.W. and T.H. Jordan, Generalized inversion of earthquake static displacement fields, *Geophys. J.R. astr. Soc.*, 35, 357-380, 1973.
- Atkinson, D. Analytic extrapolations and inverse problems, in *Applied inverse problems*. Sabatier, P.C. ed., Lecture Notes in Physics, Vol. 85, Springer, Berlin, 1978.
- Atwater, T. and P. Molnar, Relative motion of the Pacific and North American plates deduced from the sea floor spreading in the Atlantic, Indian and South Pacific Oceans, in *Proceedings of the Conference on Tectonic Problems on the San Andreas Fault System*, Kovach, R.L. and A. Nur, editor, 125-135, Stanford Univ. Publ., Geol. Sci., Vol. 13, Stanford, CA, 1973.

- Bakun, W.H., R.M. Stewart, and D. Tocher, Variations in  $V_p/V_s$  in Bear Valley in 1972, in Proceedings of the Conference on Tectonic Problems of the San Andreas Fault System, Kovach, R.L. and A. Nur edit., 453-462, Stanford Univ. Publ., Geol. Sci., Vol. 13, Stanford, CA, 1973.
- Bellman, R. Dynamic Programming, Princeton University Press, NJ, 1975.
- Bellman, R., H.H. Kagiwada, and R.E. Kalaba, Invariant imbedding and the numerical integration of boundary value problems for unstable systems of ordinary differential equations, *Comm. A.C.M.*, 10, 100-102, 1967.
- Bellman, R. and R.E. Kalaba, Quasilinearization and Nonlinear Boundary Value Problems, American Elsevier, New York, 1965.
- Bomford, G., Geodesy, 3rd ed., Clarendon Press, Oxford, 1971.
- Brace, W.F. and A.S. Orange, Electrical resistivity changes in saturated rocks during fracture and frictional sliding, *J. Geophys. Res.*, 73, 1433-1445, 1968a.
- Brune, J.N., T.L. Henyey, and R.F. Roy, Heat flow, stress, and rate of slip along the San Andreas Fault, California, *J. Geophys. Res.*, 74, 3821-3827, 1969.
- Castle, R.O., J.N. Alt, J.C. Savage, and E.I. Balazs, Elevation changes preceding the San Fernando earthquake of February 9, 1971, *Geology* 2, 61-66, 1974.
- Castle, R.O., J.P. Church, and M.R. Elliott, Aseismic uplift in southern California, *Science*, 192, 251-253, 1976.

- Chinnery, M.A., The stress changes that accompany strike-slip faulting, *Bull. Seism. Soc. Am.*, 53, 921-932, 1963.
- Collatz, L., The Numerical Treatment of Differential Equations 3rd ed., Springer, Berlin, 1966.
- Courant, R. and D. Hilbert, Method of Mathematical Physics, Interscience, Inc., New York, 1953.
- Danbara, T., Crustal movements before at and after the Niigata earthquake, Report of the coordinate committee for earthquake prediction, 9, 93-96, 1973 (in Japanese).
- Douglas, J. and T. Dupont, Collocation methods for parabolic equations in a single space variable, *Lecture Notes in Mathematics*, vol. 385, Springer, Berlin, 1974.
- Ewing, E.C. and M.M. Mitchel, Introduction to Geodesy, American Elsevier, New York, 1970.
- Forsyth, D. and S. Uyeda, On the relative importance of the driving forces of plate motion, *Geophys. J. Roy. Astron. Soc.*, 43, 163-200, 1975.
- Franklin, J., Well-posed stochastic extensions of ill-posed linear problems, *J. Math. Anal. Appl.*, 21, 682-716, 1970.
- Fung, Y.C., Foundations of Solid Mechanics, Prentice-Hall, NJ, 1965.
- Garabedian, P.R., Stability of Cauchy's problem in space for analytic systems of arbitrary type, *J. Math. Mech.*, 9, 905-914, 1960.
- Garabedian, P.R. and H.M. Lieberstein, On the numerical calculation of detached bow shock waves in hypersonic flow, *J. Aero. Sci.*, 25, 109-118, 1958.



- Hadamard, J., Lecture on Cauchy's Problem in Linear Partial Differential Equations, Dover, New York, 1952.
- Hadley, K.,  $V_p/V_s$  anomalies in dilatant rock samples, *Pure Appl. Geophys.*, 113, 1-23, 1975.
- Hanks, T.C., Earthquake stress drops, ambient tectonic stress, and stresses that drive plate motions, *Pageoph.*, 115, 441-458, 1977.
- Ikeda, K., Three dimensional geodetic inversion method for stress modelling in the lithosphere, Ms Thesis, M.I.T., 1980.
- Jackson, D.D. and Lee, W.B., The Palmdale bulge -an alternate interpretation (Abstract), *EOS (Trans. Am. Geophys. Un.)*, 60, 810, 1979.
- Johnston, M.J.S., Local magnetic field variations and stress changes near a slip discontinuity on the San Andreas fault, *J. Geomag. Geoelectr.*, 30, 511-522, 1978.
- Johnston, M.J.S., F.J. Williams, J. McWhister, and B.E. Williams, Tectonomagnetic anomaly during the southern California downwarp, *J. Geophys. Res.*, 84, 6026-6030, 1979.
- Jungles, P.H. and G.A. Frazier, Finite element analysis of the residual displacements for an earthquake rupture: Source parameters for the San Fernando earthquake, *J. Geophys. Res.*, 78, 5062-5083, 1973.
- Keller, H.B., Numerical Methods for Two-point Boundary Value Problems: Shooting Method, American Elsevier, New York, 1972.

- Knops, R.J., Logarithmic convexity and other techniques applied to problems in continuum mechanics, in Symposium on non-well posed problems and logarithmic convexity, Knops, R.J. ed., Lecture Notes in Mathematics, Vol. 316, Springer, Berlin, 1973.
- Lachenbruch, A.H. and J.H. Sass, Thermo-mechanical aspects of the San Andreas fault system, in Proceedings of Conference on Tectonic Problems of the San Andreas Fault System, Kovach, R.L. and A. Nur, edit., Stanford Univ. Publ., Geol. Sci., Vol. 13, Stanford, CA, 1973.
- Lattes, R. and Lions, J.L., The Method of Quasireversability, American Elsevier, New York, 1969.
- Lavrentiev, M.M., Some Improperly Posed Problems of Mathematical Physics, Springer, Berlin, 1967.
- Levenberg, K., A method for the solution of certain non-linear problems in least squares, Earthq. Quart. Appl. Math., 2, 164-168, 1944.
- Lieberstein, H.M., Theory of Partial Differential Equations, Academic Press, New York, 1972.
- Lions, J.L., Remarks on the theory of optimal control of distributed systems, in Control Theory of Systems Governed by Partial Differential Equations, A.K. Aziz, J.W. Wingate, M.J. Balas ed., Academic Press, New York, 1977.

- MacDoran, P.F., Radio interferometry for study of the earthquake mechanism in Proceedings of the Conference on Tectonic Problems of the San Andreas Fault System, Kovach, R.L. and A. Nur, ed., 104-123, Stanford Univ. Publ., Geol. Sci., Vol. 13, Stanford, CA, 1973.
- Matsu'ura, M., Inversion of geodetic data, Part I., Mathematical formulation, J. Phys. Earth, 25, 69-90, 1977.
- Mazzella, A., and H.F. Morrison, Electrical resistivity variations associated with earthquakes on the San Andreas fault, Science, 185, 855-857, 1974.
- McCowan, D.W., P. Glover, S.S. Alexander, A static and California earthquake, Geophys. J. R. Astr. Soc., 48, 163-185, 1977.
- McNally, K.C., H. Kanamori, J. Pechmann, and G. Enis, Seismicity increase along the San Andreas fault, southern California, Science, 201, 81 -81 , 1978.
- Meyer, G.H., Initial value methods for boundary value problems: theory and application of invariant imbedding, Academic Press, New York, 1973.
- Mindlin, R.D., Force at a point in the interior of a semi-infinite solid, Physics, 7, 195-202, 1936.
- Morse, P.M. and H. Feshbach, Methods of Theoretical Physics, McGraw-Hill, NY, 1953.
- Nur, A., and G. Simmons, The effect of saturation on velocity in low porosity rocks, Earth Planet. Sci. Lett., 7, 183-193, 1969.

- Payne, L.E., Improperly Posed Problems in Partial Differential Equations, SIAM, Pennsylvania, 1975.
- Prenter, P.M., Splines and variational methods, John Wiley & Sons, New York, 1975.
- Prescott, W.H. and J.C. Savage, Strain accumulation on the San Andreas fault near Palmdale, California, *J. Geophys. Res.*, 81, 4901-4908, 1976.
- Raleigh, B., G. Bennet, H. Craig, T. Hanks, P. Molnar, A. Nur, J. Savage, C. Scholz, R. Turner, and F. Wu, Prediction of the Haicheng earthquake, *EOS (Trans. Am. Geophys. Un.)*, 58, 236-272, 1977.
- Reid, H.F., Permanent displacement of the ground, in the California earthquake of April 18, 1906, Report of the State of Earthquake Investigation Commission, Vol. 2, 16-28, Carnegie Institution of Washington, Washington, DC, 1910.
- Richardson, R.M. and S.C. Solomon, Apparent stress and stress drop for interplate earthquakes and tectonic stress in the plates, *Pure Appl. Geophys.*, 115, 317-331, 1977.
- Richardson, R.M., Finite element modeling of stress in the Nazca plate: Driving forces and plate boundary earthquakes, *Tectonophysics*, 50, 223-248, 1978.
- Rikitake, T., Precursors to the 1978 near Izu-Oshima island, Japan, earthquake of magnitude 7.0 in *Current Research in Earthquake Prediction I.*, T. Rikitake ed., Japan Scientific Societies Press, Tokyo, in press.
- Sassa, K. and E. Nishimura, On phenomena forerunning earthquakes, *Trans. Am. Geophys. Un.*, 32, 1-6, 1951.

Savage, J.C., W.H. Prescott, and W.T. Kinoshita, Geodimeter measurements along the San Andreas fault, in Proceedings of the Conference on Tectonic Problems of the San Andreas Fault System, Kovach, R.L. and A. Nur, ed., 44-53, Stanford Univ. Publ., Geol. Sci., Vol. 13, Stanford, CA, 1973.

Savage, J.C., W.H. Prescott, M. Lisowski, and N. King, Strain in southern California: Measured uniaxial north-south regional contraction, *Science*, 202, 883-885, 1978.

Savage, J.C. and W.H. Prescott, Geodimeter measurements of strain during the southern California uplift, *J. Geophys. Res.*, 84, 171-177, 1979.

Scott, M.R., Invariant Imbedding and its Applications to Ordinary Differential Equations, Addison-Wesley Publishing Co., MA, 1973.

Semenov, A.M., Variations in the travel-time of transverse and longitudinal waves before violent earthquakes, *Izv. Acad. Sci. USSR, Physics of Solid Earth*, 4, 245-, 1969.

Smith, A.T., Time-dependent strain accumulation and release at island arcs: Implications for 1946 Nankaido earthquake, Ph.D. Thesis, M.I.T., 1974.

Sokolnikoff, I.S., Mathematical Theory of Elasticity, 2nd ed., McGraw-Hill, New York, 1956.

Sommerfeld, A.J.W., Partial Differential Equations in Physics, Academic Press, New York, 1949.

Stesky, R.M., The mechanical behavior of faulted rock at high temperature and pressure, Ph.D. Thesis, M.I.T., 1975.

Stesky, R.M. and W.F. Brace, Estimation of frictional stress on the San Andreas fault from laboratory measurements, in Proceedings of the Conference on Tectonic Problems of the San Andreas Fault System, Kovach, R.L. and A. Nur, ed., 206-214, Stanford Univ. Publ., Geol. Sci., Vol. 13, Stanford, CA, 1973.

Stewart, G.S., Prediction of the Pt. Mugu earthquake by two methods in Proceedings of the Conference on Tectonic Problem of the San Andreas Fault System, Kovach, R.L. and A. Nur, ed., Stanford Univ. Pub., Geol. Sci., Vol. 13, Stanford, CA, 1973.

Tikonov, A.N., Solutions of Incorrectly Formulated Problems and the Regularization Method, Soviet Math. Dokl. 4, 1035-1038, 1963.

Timoshenko, S. and N. Goodier, Theory of Elasticity, McGraw-Hill, New York, 1970.

Treves, F., Basic Linear Partial Differential Equations, Academic Press, New York, 1975.

Tsumura, K., Anomalous crustal activity in the Izu Peninsula and earthquake prediction, Earthquake Prediction Symposium, 46-55, 1976 (in Japanese).

Thatcher, W., Episodic strain accumulation in southern California, Science, 194, 691-695, 1976.

Whitcomb, J.H., J.D. Garmany, and D.L. Anderson, Earthquake prediction: Variation of seismic velocities before the San Fernando earthquake, Science, 180, 632-635, 1973.

- Wyss, M., Stress estimates of South American shallow and deep earthquakes, *J. Geophys. Res.*, 75, 1529-1544, 1970.
- Wyss, M., Interpretation of the Southern California uplift in terms of the dilatancy hypothesis, *Nature*, 266, 1977.
- Wyss, M., and P. Molnar, Efficiency, stress drop, apparent stress, effective stress and frictional stress of Denver, Colorado earthquakes, *J. Geophys. Res.*, 77, 1433-1438, 1972.
- Zienkiewicz, O.C., The Finite Element Method in Engineering Science, McGraw-Hill, New York, 1971.
- Zlamal, M., On the finite element method, *Numer. Math.*, 12, 394-409, 1968.